

2015

# Novel BODIPY Dyes for Dye-sensitized Solar Cells

Hafsah Klfout

*Eastern Illinois University*

This research is a product of the graduate program in [Chemistry](#) at Eastern Illinois University. [Find out more](#) about the program.

---

## Recommended Citation

Klfout, Hafsah, "Novel BODIPY Dyes for Dye-sensitized Solar Cells" (2015). *Masters Theses*. 2377.  
<https://thekeep.eiu.edu/theses/2377>

This is brought to you for free and open access by the Student Theses & Publications at The Keep. It has been accepted for inclusion in Masters Theses by an authorized administrator of The Keep. For more information, please contact [tabruns@eiu.edu](mailto:tabruns@eiu.edu).

  
**The Graduate School**  
EASTERN ILLINOIS UNIVERSITY™  
**Thesis Maintenance and Reproduction Certificate**

FOR: Graduate Candidates Completing Theses in Partial Fulfillment of the Degree  
Graduate Faculty Advisors Directing the Theses

RE: Preservation, Reproduction, and Distribution of Thesis Research

---

Preserving, reproducing, and distributing thesis research is an important part of Booth Library's responsibility to provide access to scholarship. In order to further this goal, Booth Library makes all graduate theses completed as part of a degree program at Eastern Illinois University available for personal study, research, and other not-for-profit educational purposes. Under 17 U.S.C. § 108, the library may reproduce and distribute a copy without infringing on copyright; however, professional courtesy dictates that permission be requested from the author before doing so.

Your signatures affirm the following:

- The graduate candidate is the author of this thesis.
- The graduate candidate retains the copyright and intellectual property rights associated with the original research, creative activity, and intellectual or artistic content of the thesis.
- The graduate candidate certifies her/his compliance with federal copyright law (Title 17 of the U. S. Code) and her/his right to authorize reproduction and distribution of all copyrighted materials included in this thesis.
- The graduate candidate in consultation with the faculty advisor grants Booth Library the non-exclusive, perpetual right to make copies of the thesis freely and publicly available without restriction, by means of any current or successive technology, including by not limited to photocopying, microfilm, digitization, or internet.
- The graduate candidate acknowledges that by depositing her/his thesis with Booth Library, her/his work is available for viewing by the public and may be borrowed through the library's circulation and interlibrary loan departments, or accessed electronically.
- The graduate candidate waives the confidentiality provisions of the Family Educational Rights and Privacy Act (FERPA) (20 U. S. C. § 1232g; 34 CFR Part 99) with respect to the contents of the thesis and with respect to information concerning authorship of the thesis, including name and status as a student at Eastern Illinois University.

I have conferred with my graduate faculty advisor. My signature below indicates that I have read and agree with the above statements, and hereby give my permission to allow Booth Library to reproduce and distribute my thesis. My adviser's signature indicates concurrence to reproduce and distribute the thesis.

\_\_\_\_\_  
Graduate Candidate Signature

Hafsah Kifout  
Printed Name

Chemistry  
Graduate Degree Program

\_\_\_\_\_  
Faculty Adviser Signature

HONGSHAN HE  
Printed Name

8/21/15  
Date

*Please submit in duplicate.*

**Novel BODIPY Dyes for Dye-sensitized Solar Cells**

(TITLE)

BY

**Hafsah Klfout**

**THESIS**

SUBMITTED IN PARTIAL FULLMENT OF THE REQUIREMENTS  
FOR THE DEGREE OF

**Master of Science in Chemistry**

IN THE GRADUATE SCHOOL, EASTERN ILLINOIS UNIVERSITY  
CHARLESTON, IL

**2015**

YEAR

I HEREBY RECOMMEND THAT THIS THESIS BE ACCEPTED AS FULFILLING  
THIS PART OF THE GRADUATE DEGREE CITED ABOVE



THESIS COMMITTEE CHAIR

8/21/15

DATE

8/21/15

DEPARTMENT SCHOOL CHAIR

DATE

THESIS COMMITTEE MEMBER

8/21/15

DATE

THESIS COMMITTEE MEMBER

8/21/2015

DATE

THESIS COMMITTEE MEMBER

8/21/15

DATE

THESIS COMMITTEE MEMBER

DATE

# **Novel BODIPY Dyes for Dye-sensitized Solar Cells**

**HAFSAH KLFOUT**

**Research Advisor: Dr. Hongshan He**

**Eastern Illinois University**

**Chemistry Department**



## TABLE OF CONTENTS

TABLE OF CONTENTS.....	v
ABBREVIATION.....	ix
ABSTRACT.....	x
ACKNOWLEDGEMENT .....	xii
LIST OF FIGURES.....	xiii
LIST OF TABLES.....	xvi
CHAPTER 1 INTRODUCTION.....	1
<b>1.1. Background</b> .....	1
<b>1.2. Previous work</b> .....	4
1.2.1. Ruthenium Dyes.....	4
1.2.2. Porphyrin Dyes.....	5
1.2.3. BODIPY Dyes.....	8
<b>1.3. Motivation</b> .....	18
<b>1.4. Objectives</b> .....	18
CHAPTER 2 SYNTHESIS & MEASUREMENTS .....	19
<b>2.1. Materials</b> .....	19
<b>2.2. Instrument</b> .....	19
<b>2.3. Synthesis of Dyes</b> .....	20
<b>2.3.1. Synthesis of HHK1</b> .....	20

2.3.1. a. Synthesis of PB.....	21
2.3.1. b. Synthesis of PBI.....	23
2.3.1. c. Synthesis of PBI <sub>2</sub> .....	24
2.3.1. d. Synthesis of DPB.....	25
2.3.1. e. Synthesis of DPBI.....	26
2.3.1. f. Synthesis of HHK1.....	27
<b>2.3.2 Synthesis of HHK2.....</b>	<b>28</b>
2.3.2. a. Synthesis of C <sub>6</sub> PB.....	29
2.3.2. b. Synthesis of C <sub>6</sub> PBI <sub>2</sub> .....	30
2.3.2. c. Synthesis of C <sub>6</sub> DPBI.....	31
2.3.2. d. Synthesis of HHK2.....	32
<b>2.4. Measurements.....</b>	<b>33</b>
2.4.1. UV-Vis Absorption Spectroscopy in Solution.....	34
2.4.2. UV-Vis Absorption Spectroscopy in TiO <sub>2</sub> Film .....	34
2.4.3. Calibration Curve Measurements .....	35
2.4.4. Dye Loading Density in TiO <sub>2</sub> .....	35
2.4.5. Fluorescence Spectroscopy (FL).....	35
2.4.6. Nuclear Magnetic Resonance (NMR) Spectroscopy .....	40
2.4.7. Elemental Analysis (EA) & Mass Spectrometry (MS).....	40
2.4.8. Fabrication and Photovoltaic Characterization of DSCs .....	40
<b>CHAPTER 3 CHARACTERIZATION &amp; PHYSICAL MEASUREMENTS .....</b>	<b>41</b>
<b>3.1. Characterization.....</b>	<b>41</b>
3.1.1. NMR.....	41

3.1.1.a. PB.....	41
3.1.1.b. PBI.....	42
3.1.1.c. PBI <sub>2</sub> .....	43
3.1.1.d. DPB.....	44
3.1.1.e. DPBI.....	45
3.1.1.f. HHK1.....	45
3.1.1.g. C <sub>6</sub> PBI <sub>2</sub> .....	46
3.1.1.h. C <sub>6</sub> DPBI.....	47
3.1.1.i. HHK2.....	47
3.1.2. Elemental Analysis (EA) & Mass Spectrometry (MS).....	50
3.1.3. X-ray Diffraction.....	57
<b>3.2. Photophysical Properties.....</b>	<b>60</b>
3.2.1. UV-Vis Absorption in Solution.....	60
3.2.1.a. UV-Vis Absorption in Solution ofHHK1 dyes.....	60
3.2.1.b. UV-Vis Absorption in Solution of HHK2dyes.....	61
3.2.2. UV-Vis Absorption in TiO <sub>2</sub> .....	64
3.2.3. Calibration Curve Measurement.....	66
3.2.4. Dye-loading Density on TiO <sub>2</sub> .....	66
3.2.5. Fluorescence (FL).....	66
<b>CHAPTER 4 PHOTOVOLTAIC PROPERTIES.....</b>	<b>69</b>
<b>4.1. J-V Curves.....</b>	<b>69</b>
<b>CHAPTER 5 CONCLUSION.....</b>	<b>72</b>

<b>REFERENCES.....</b>	<b>74</b>
<b>APPENDICES.....</b>	<b>78</b>

## Abbreviation

1. BODIPY= Boron-dipyrromethene.
2. PB= BODIPY without any substituent
3. PBI= BODIPY with one iodine atom in C2 position
4. PBI<sub>2</sub>= BODIPY with two iodine atoms in C2 and C6 positions
5. PBD= BODIPY with 4-ethynyl-N, N-dimethylaniline group in C6 position
6. DPBI= BODIPY conjugated with 4-ethynyl-N, N-dimethylaniline group in C6 and iodine atom in C2 position
7. C<sub>6</sub>PB, C<sub>6</sub>PBI<sub>2</sub>, and C<sub>6</sub>DPBI mean the same as PB, PBI<sub>2</sub>, and DPBI but they are attached to 2,6-bis(hexyloxy)benzene group instead of to mesityl group.
8. DMF= Dimethylformamide
9. THF= Tetrahydrofuran
10. TEA= Triethylamine
11. FTO= Fluorine doped Tin Oxide (FTO) Coated Glass
12. DSCs= Dye-sensitized solar cells
13. TLC= Thin Layer Chromatography

## ABSTRACT

Dyes-sensitized solar cells (DSCs) are of importance to efficient conversion of solar energy to electricity. The modern version of a DSC is a titanium dioxide nanoparticles-based electrochemical device, in which solar energy is absorbed by dye molecules and electrons from excited dye molecules are injected into the conduction band of titanium dioxide nanoparticle. The electrons are then transported through a network of interconnected TiO<sub>2</sub> particles to the fluorine- tin -oxide layer to the external circuit. In this process dye molecules are crucial to the device's energy conversion efficiency.

Boron-dipyrromethenes, known as BODIPY dyes, show strong absorption in the visible light region. They have high fluorescence quantum yields and are soluble in most organic solvents. They also exhibit strong photostability making them suitable for DSC applications. The *meso*-substituted BODIPY dyes showed poor photovoltaic performance. However, several studies have shown the promise of 2- or 6-position substituted BODIPY dyes for DSCs.

Two BODIPY dyes, HHK1 and HHK2, with a premium donor- $\pi$ -acceptor molecular configuration were successfully synthesized using Sonogashira coupling reactions. The yields were with 90 % yield for HHK1 and the yield for HHK2 was not determined. Two dyes were also characterized by NMR, MS, UV-Vis spectrum, and fluorescence spectroscopy. The absorption peak for HHK1 was red shifted from 503 nm in PB without any substituent in 2 and 6 positions to 575 nm. For HHK2 dye the absorption was red shifted to 576 nm due to the bulky hexyloxy group on the aldehyde. This hexyloxy group on the benzene group in the *meso* position. Fluorescence spectra showed emission peaks at 592 nm and 670 nm for HHK1 and HHK2, respectively. The absorption spectra of HHK1 and HHK2 on TiO<sub>2</sub> film were blue shifted and the peaks became narrower.

The photovoltaic performance of HHK1 and HHK2 sensitized solar cells exhibited efficiency of 0.87% and 0.57%, respectively.

## ACKNOWLEDGEMENTS

I would like to express my deepest gratitude to Dr. Hongshan He, without whose endless patience and help this thesis would be much harder. I also want to thank him for providing me the opportunity to work as a team member in his group and providing me continual support, advice and suggestions during my study at Eastern Illinois University. I would also like to thank him for spending lots of time in the lab while I did experiments. In addition, I would especially thank him for his help with thesis writing, as his comments on the drafts were helpful and valuable.

I would like also to acknowledge the Saudi Arabian Cultural Mission for funding my graduate study. I wouldn't have had the opportunity to come EIU to continue my graduate study without the support.

I would like to thank Eastern Illinois University, especially the Chemistry Department, the Graduate School, and the College of Sciences, the EIU President's Fund for Research and Creative Activity, the Extreme Science and Engineering Discovery Environment (XSEDE), as well as the Chemistry stockroom for the support of this work. Also, I would like to thank my thesis committee; Dr. Daniel Sheeran, Dr. Mark E. McGuire, and Dr. Zhiqing Yan for their assistance, patience, support, and guidance throughout this work.

I also would like to thank Dr. Sheeran and Dr. Lawrence for helping me with NMR spectra. I also wanted to express my great thanks to Dr. Kraig Wheeler for X-ray diffraction analysis and Dr. Radu Semeniuc for the use his glovebox facility in his lab, and Dr. Xiangli Wang for her reaction setup in glovebox. Last but not least I would like to thank my husband, family and friends for all their love and support.



## LIST OF FIGURES

Figure 1.1. Cross-view of a Grätzel type DSC .....	3
Figure 1.2. Molecular structures of BET dye in the left and LH3 dye in the right .....	4
Figure 1-3. Structures of the ruthenium-based dye N3.....	5
Figure 1.4. Porphyrin ring with four <i>meso</i> - and eight $\beta$ - positions.....	6
Figure 1.5. Aggregation of porphyrin dyes on TiO <sub>2</sub> . H-type aggregation dyes arranged face-to-face (left), J-type aggregation dyes arranged side-by-side (right).....	7
Figure 1.6. Chemical Structure of YD2 Porphyrin dye with D- $\pi$ -A structure.....	8
Figure 1.7. Chemical structure of boron-dipyrromethene (BODIPY) core .....	10
Figure 2.1. The chemical structure of HHK1.....	20
Figure 2.2. The synthetic route for HHK1 dyes .....	21
Figure 2.3. Synthesis of PB.....	22
Figure 2.4. Synthesis of PBI.....	23
Figure 2.5. Synthesis of PBI <sub>2</sub> .....	24
Figure 2.6. Synthesis of DPB.....	25
Figure 2.7. Synthesis of DPBI.....	25
Figure 2.8. Synthesis of HHK1 .....	26
Figure 2.9. The chemical structure of HHK2.....	27
Figure 2.10. The synthetic route for HHK2 dyes .....	28

Figure 2.11. Synthesis of C <sub>6</sub> PB.....	29
Figure 2.12. Synthesis of C <sub>6</sub> PBI <sub>2</sub> .....	30
Figure 2.13. Synthesis of C <sub>6</sub> DPBI.....	31
Figure 2.14. Synthesis of HHK2.....	33
Figure 2.15. TiO <sub>2</sub> coated slide inside a cuvette contains 3 mL of methanol.....	36
Figure 2.16. A cross-view diagram of DSC.....	37
Figure 2.17. Half covered FTO glass with 3 M magic tape.....	38
Figure 2.18. Top view of assembled cell.....	39
Figure 2.19. Experimental setup of I-V measurement.....	49
Figure 3.14 .Mass spectra of HHK1 in the negative ion mode.....	49
Figure 3.15. Mass spectra of HHK1 in the positive ion mode.....	51
Figure 3.16. ORTEP diagram of PBI with 50% thermal ellipsoid probability. Hydrogen atoms were omitted for clarity.....	52
Figure 3.17. ORTEP diagrams of DPB with 50% thermal ellipsoid probability. Hydrogen atoms were omitted for clarity.....	52
Figure 3.18. ORTEP diagram of C <sub>6</sub> PBI <sub>2</sub> with 50% thermal ellipsoid probability. Hydrogen atoms were omitted for clarity.....	53
Figure 3.19. ORTEP diagram of C <sub>6</sub> DPBI with 50% thermal ellipsoid probability. Hydrogen atoms were omitted for clarity.....	54

Figure 3.20. Absorption spectra of dyes PB, PBI, PBI <sub>2</sub> , DPBI, and HHK1 in CHCl <sub>3</sub> solution at room temperature.....	58
Figure 3.21. Absorption spectra of dyes C <sub>6</sub> PB, C <sub>6</sub> PBI <sub>2</sub> , C <sub>6</sub> DPBI, and HHK2 in CHCl <sub>3</sub> solution at room temperature.....	59
Figure 3.22. Absorption spectrum of HHK1 on TiO <sub>2</sub> film.....	60
Figure 3.23. Absorption spectrum of HHK2 on TiO <sub>2</sub> film.....	60
Figure 3.24. Calibration curve of HHK1 in 0.1 M NaOH (DMF/H <sub>2</sub> O) solution.....	62
Figure 3.25. Calibration curve of HHK2 in 0.1 M NaOH (DMF/H <sub>2</sub> O) solution.....	63
Figure 3.26. Absorption of HHK1 in TiO <sub>2</sub> and in & 0.1 M of NaOH (DMF/H <sub>2</sub> O) as a solution (dye loading) .....	65
Figure 3.27. Absorption of HHK2 in TiO <sub>2</sub> and in & 0.1 M of NaOH (DMF/H <sub>2</sub> O) as a solution (dye loading).....	65
Figure 3.28. Fluorescence spectrum of HHK1 in CHCl <sub>3</sub> solution.....	67
Figure 3.29. Fluorescence spectrum of HHK2 in CHCl <sub>3</sub> solution.....	67
Figure 4.1. Optical image of dye-coated TiO <sub>2</sub> film and assembled DSCs.....	70
Figure 4.2. J–V curve of HHK1 BODIPY dye-sensitized solar cells (dye loading time 4 h).....	70
Figure 4.3. J–V curve of HHK2 BODIPY dye-sensitized solar cells (dye loading time 4h).....	71

## LIST OF TABLES

Table 1.1. Summary of the efficiency and maximum wavelengths of BODIPY dyes for DSCs.....	13
Table 3.1. Structural parameters for PBI, DPB, C <sub>6</sub> PBI <sub>2</sub> , and C <sub>6</sub> DPBI.....	55
Table 3.2. Selected bond length and bond angles for PBI, DPB, C <sub>6</sub> PBI <sub>2</sub> , and C <sub>6</sub> DPBI.....	56
Table 3.3. The concentrations, volume, absorption maximum and absorption coefficients of PB, PBI, PBI <sub>2</sub> , DPBI, and HHK1 dyes in CHCl <sub>3</sub> at room temperature.....	58
Table 3.4. The concentrations, volume, absorption maximum and absorption coefficient data of C <sub>6</sub> PB, C <sub>6</sub> PBI <sub>2</sub> , C <sub>6</sub> DPBI and HHK2 dyes in CHCl <sub>3</sub> at room temperature.....	59
Table 3.5. Concentration, volume and maximum wavelength data of calibration curve measurement of HHK1.....	63
Table 3.6. Concentration, volume and maximum wavelength data of calibration curve measurement of HHK2.....	65
Table 3.7. The results of dye loading density measurements.....	66
Table 3.8. The fluorescence data of HHK1 and HHK2 dyes in CHCl <sub>3</sub> .....	68
Table 4.1. Photovoltaic data of HHK1 and HHK2 dyes sensitized solar cells (dye loading time 4h).....	71

# CHAPTER 1

## INTRODUCTION

### 1.1. Background

The use of energy has been increasing generation after generation; therefore there must be new sources of energy to match the needs of human being without costing them more.<sup>(1)</sup> Renewable energy is the energy that comes from natural energy sources that do not degrade, for example, sunlight, wind, etc. They are friendly to the environment. Solar energy is being considered as a renewable energy because it supplies energy from the Sun. In fact, solar energy is the most important alternative energy source that is abundant and renewable. It has shown a remarkable contribution to solving the energy shortage problems in the world.<sup>(1)</sup> In 1839, Alexandre Edmond discovered that some materials produced a tiny amount of electric. When exposed to light.<sup>(2)</sup> In 1876, William Grylls Adams and Richard Evans discovered that selenium, which is a solid material, produced electricity when exposed to light. Solar cells are used to convert solar energy to electricity. It is the best way to use the solar energy from the Sun with low cost.<sup>(1)</sup> Solar cells have been developed through three generations. The first generation crystalline silicon (c-Si) achieved up to 25% of high energy conversion efficiency.<sup>(1, 3)</sup> However, silicon-based cells have some issues such as they need pure silicon, and the cost of the production is high.<sup>(1, 3, 4)</sup> Several other alternative devices were also developed with either high manufacture cost or poor efficiency; therefore other cost-effective technologies are being sought to meet this challenge.

Dye-sensitized solar cells (DSCs) are lightweight devices made from low-cost materials with less impact to environment. This cell classified as a thin-film solar cell. It is based on

mesoporous titanium dioxide nanoparticles that are coated with organic or inorganic light-harvesting materials. This technique has shown promising high efficiency for converting solar energy into electricity. Dyes-sensitized solar cells have been of interest to scientists and researchers and have been well studied in the last twenty years. There were a lot of publications from 1991-2015 about how to engineer low-cost and high efficiency dye-sensitized solar cells. (1, 3, 4)

The Grätzel cell is the modern version of a DSC. It is a titanium dioxide nanoparticle ( $\text{TiO}_2$  NP)-based electrochemical device, in which dye-coated and interconnected  $\text{TiO}_2$  NPs in the anatase phase are randomly packed on a substrate, such as fluorine-tin-oxide (FTO)-coated transparent conducting glass (TCO glass). (4) A cross-view of the cell was shown in Figure 1.1. The cell has three major components: a photoelectrode, a counterelectrode, and an electrolyte. The photoelectrode is a dye-coated  $\text{TiO}_2$  nanoparticle film with a thickness of  $\sim 15 \mu\text{m}$ . The counterelectrode is a Pt-coated FTO glass. The electrolyte is a solution that contains a redox couple. The commonly used redox couple is  $\text{I}^-/\text{I}_3^-$ . Under sunlight, the photons are adsorbed by a sensitizer, which is anchored to the surface of a wide band semiconductor, such as  $\text{TiO}_2$  NPs. Charge then separated by photo-induced electron injection from the excited state of the dye into the conduction band of the semiconductor. Electrons are then migrated from the conduction band of the semiconductor to the charge collector. The state-of-the-art DSC is a titanium dioxide nanoparticles ( $\text{TiO}_2$  NPs)-based electrochemical device, in which interconnected  $\text{TiO}_2$  NPs in the anatase phase are randomly arranged on a substrate, such as fluorine-tin-oxide (FTO)-coated transparent conducting glass (TCO glass). (3, 4)

Dyes play important roles in DSCs. Beside several other factors, one major responsibility of dye molecules is to harvest sunlight as much as possible. Ruthenium-based dyes

have been studied extensively in the past twenty years. Ruthenium dye complexes have achieved 11% efficiency to convert the light into electricity. <sup>(6)</sup> However, there are still disadvantages with these complexes. Ruthenium is a rare metal that makes ruthenium complexes too expensive. Also, it lacks absorption in the red region of the visible spectrum, where the light-harvesting process is at a maximum. <sup>(3,5,6)</sup>

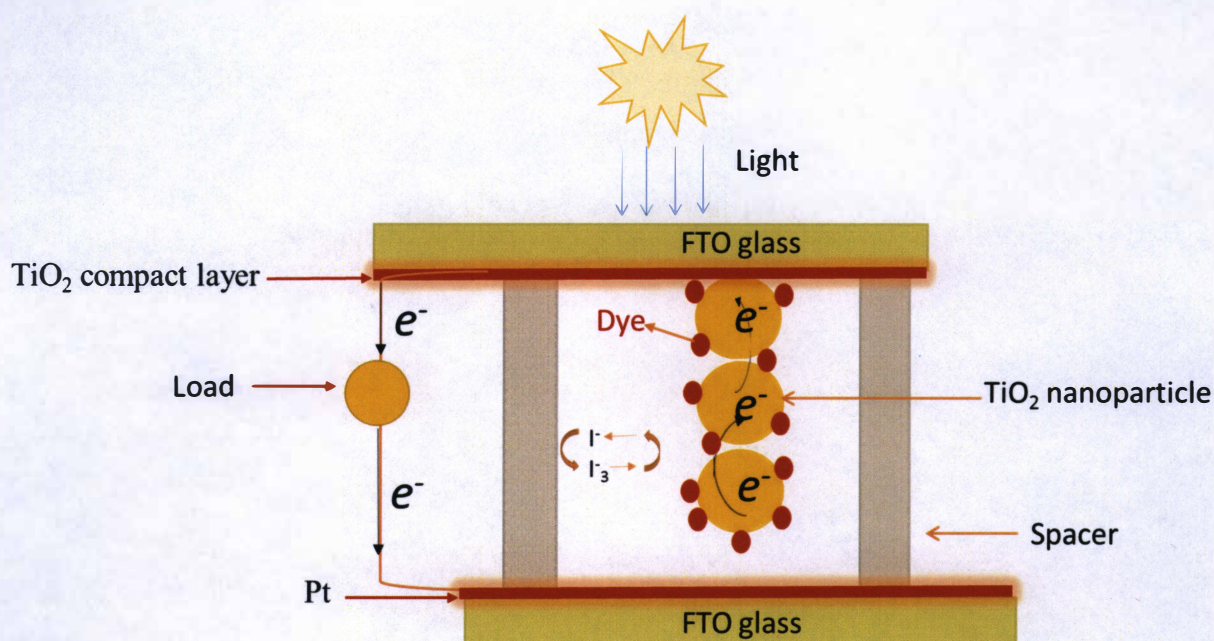


Figure 1.1. Cross-view of a Grätzel type DSC

Porphyrin dyes have shown a great promise for DSCs. Porphyrin dyes have achieved 13% efficiency in 2014. <sup>(7)</sup> However, there is still a need to develop other organic dyes that have strong absorption in the visible light region to achieve high efficiency. <sup>(8,9,10,11)</sup> Boron-dipyrrromethenes, known as BODIPY dyes, were first discovered in 1968 by Treibs and Kreuzer. <sup>(12)</sup> These dyes have good quantum yield, high absorption coefficient, fluorescence, and good photochemical stability, and are excellent candidates for DSCs. <sup>(13,14,15)</sup> In 2012, He *et al* found BODIPY dye BET can act as co-sensitizer. Its absorption spectrum is complementary to that of



porphyrin dye.<sup>(13)</sup> It was found that the conversion efficiency of TMPZn increased from 1.09% to 2.90%, and from 6.65% to 7.60% for LD12.<sup>(6, 13)</sup> Conjugation of BODIPY dyes to porphyrin can also enhance the energy conversion efficiency. An example (LH3) was reported in 2010 by Hupp and co-workers as shown in Figure 1.2.<sup>(15)</sup> For these reasons researchers tried hard to study and investigate BODIPY dyes. Recent study showed that BODIPY dyes can be used as a standalone dye for DSCs.<sup>(16)</sup> This can be achieved by synthesizing novel BODIPY dyes with donor- $\pi$ -acceptor system.

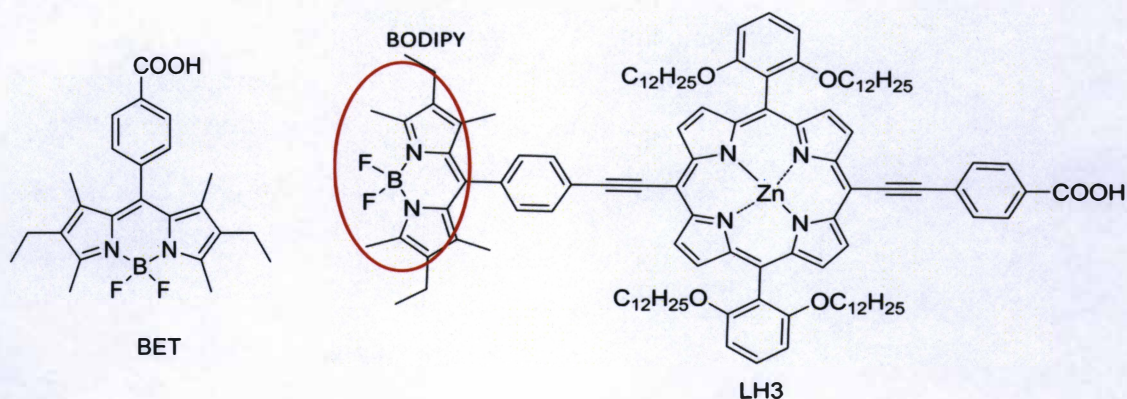


Figure 1.2. Molecular structures of BET dye in the left and LH3 dye in the right.

## 1.2. Previous work

### 1.2.1 Ruthenium Dyes

In the past twenty years, ruthenium-based dyes have been studied extensively. The first dye-sensitized solar cell with a ruthenium complex as a dye was reported in 1991 by Michael Grätzel and coworkers.<sup>(4)</sup> Three representative ruthenium-based dyes, i.e. N3, N719, and N794 have been studied extensively.<sup>(6, 17)</sup> The N3 dye, shown in Figure 1.3, was usually prepared from a 'one-pot' reaction from a dichloro(*p*-cymene)ruthenium(II) dimer, 4,4'-dicarboxy-2,2'-bipyridine, and ammonium thiocyanate in DMF at elevated temperature under N<sub>2</sub> atmosphere.



The obtained compound had a dark reddish color. Deprotonation and ion exchange between H and TBA gave the desired dye N719. It was extremely difficult to obtain pure dye; therefore those dyes were quite expensive. Although ruthenium-based dyes have been used as sensitizers and have achieved more than 11% efficiency, there are some disadvantages with these complexes. Ruthenium is a rare metal that makes ruthenium complexes too expensive. Moreover, there is also a lack of absorption in the red region of the visible spectrum, where the light-harvesting process is maximal. (4, 6, 17)

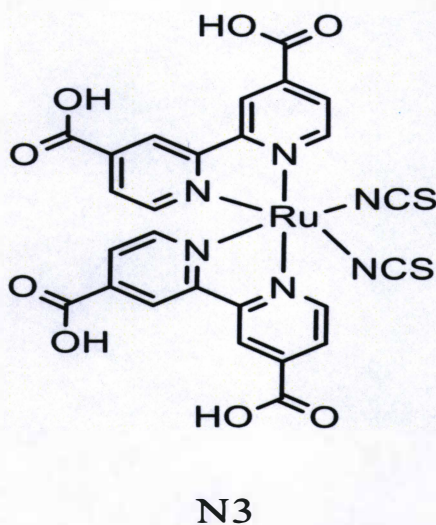


Figure 1.3. Structure of the ruthenium-based dye N3

### 1.2.2. Porphyrin dyes

Porphyrins are aromatic organic compounds that occur in nature. The most common example of porphyrins is heme protein, the pigment in red blood cells. It is a cofactor of the protein hemoglobin. (18, 19, 20) The porphyrin has four pyrrole subunits connected through methene groups. (18, 19, 20, 21, 22) It has four *meso*- and eight  $\beta$ - positions available for functionalization as shown in Figure 1.4. If porphyrin is not bound to metal, it is called a free base. However,

porphyrins are easy to bind to metal ions. The most common metal is zinc. The resulting compounds are zinc porphyrin complexes. <sup>(21, 22, 23, 24, 25)</sup> Porphyrin dyes are environmentally friendly because zinc metal has less impact on the environment compared to other transition metals such as Ru. The porphyrin have extremely high absorption coefficient due to its highly conjugated electron delocalized structure. <sup>(26, 27, 28, 29, 30, 31)</sup> The heterocyclic macrocycle has 18 electrons to delocalize; it has two absorption bands in the UV-vis spectrum. The intense Soret band is usually between 400-450 nm and the second moderate Q band between at 500-650 nm. <sup>(29)</sup>

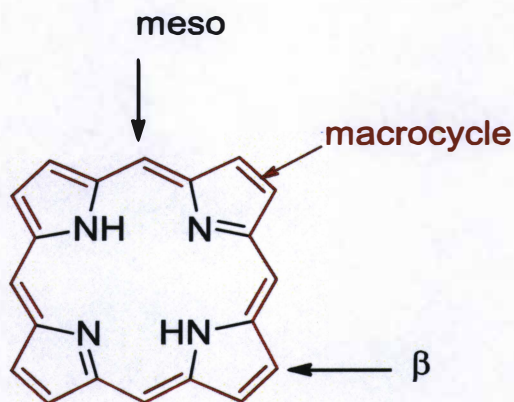


Figure 1.4. Porphyrin ring with four *meso*- and eight  $\beta$ - positions

Porphyrin dyes have been extensively studied in the past for dye-sensitized solar cell. Porphyrin dyes as excellent "nature" pigments are promising for dye-sensitized solar cells (DSCs). <sup>(26, 27, 28, 29)</sup> Early studies used 5,10,15,20-tetraphenylporphyrin zinc derivatives as dyes and the resulting photoelectrodes showed a deep purple color. The energy conversion efficiency was less than 2%. In 2007, Grätzel et al. conjugated a malonic acid group to b-pyrrolic positions of the porphyrin ring. The photoelectrode exhibited a green color and the resulting device produced energy conversion of 7.1% under AM 1.5G conditions. Since then, a variety of



porphyrins have been synthesized and their photovoltaic performance has been evaluated. The results revealed that high efficiency can be achieved by adding donor groups, attaching bulky substituents, or elongating the  $\pi$ -conjugation through double or triple bonds between the porphyrin ring and an anchoring carboxylic acid group. Up to now, a donor-p-acceptor structure has emerged as a premium model for constructing high performance dyes. In 2010, YD2 dye achieved high efficiency at 11 % and absorption on  $\text{TiO}_2$  at 720 nm as shown in Figure 1.5. Recently, the highest energy conversion efficiency of 13% was reported by Grätzel *et al.* when a functionalized porphyrin dye and a cobalt-based redox couple were used. <sup>(21, 27)</sup>

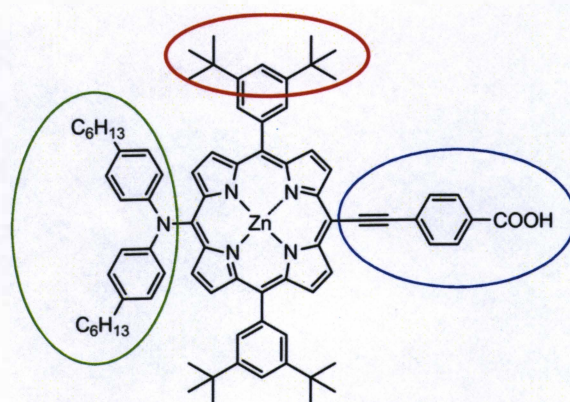


Figure 1.5. Chemical Structure of YD2 Porphyrin dye with D- $\pi$ -A structure

Although porphyrin has many advantages in DSC's environment, there are still some disadvantages of porphyrin as dyes for DSCs, such as the tendency to aggregate on the  $\text{TiO}_2$  surface, which is considered the main issue reason for poor charge collection efficiency in porphyrin dyes. <sup>(30, 31)</sup> The planar structure of the porphyrin dye, which can occur when porphyrin molecules are close to each other, causes interactions between them that can inhibit the electron injection and incite electron recombination. <sup>(32)</sup> Porphyrin dyes are easy to aggregate. There are two types of aggregation which are J-type and H-type. J-type has the monolayer of dyes molecules arranged side-by-side which leading to a narrower red-shifted

absorption band. In this case, the transition moments are parallel as shown in Figure 1.6. On the other hand, H-type aggregation is defined when the dyes molecules are arranged face-to-face, in which case the absorption band will be blue shifted. <sup>(30, 31)</sup> Research shows that the efficiency of porphyrin-sensitized solar cells can be increased by adding donor groups to porphyrin ring, attaching bulky substituents to the phenyl groups by introducing double or triple bonds between the porphyrin ring and adding the anchoring carboxylic group (COOH) in a donor- $\pi$ -accepter system. <sup>(8, 7)</sup> This new type of dye is expected to have broader the absorption capability to have reduced the aggregation. <sup>(7)</sup>

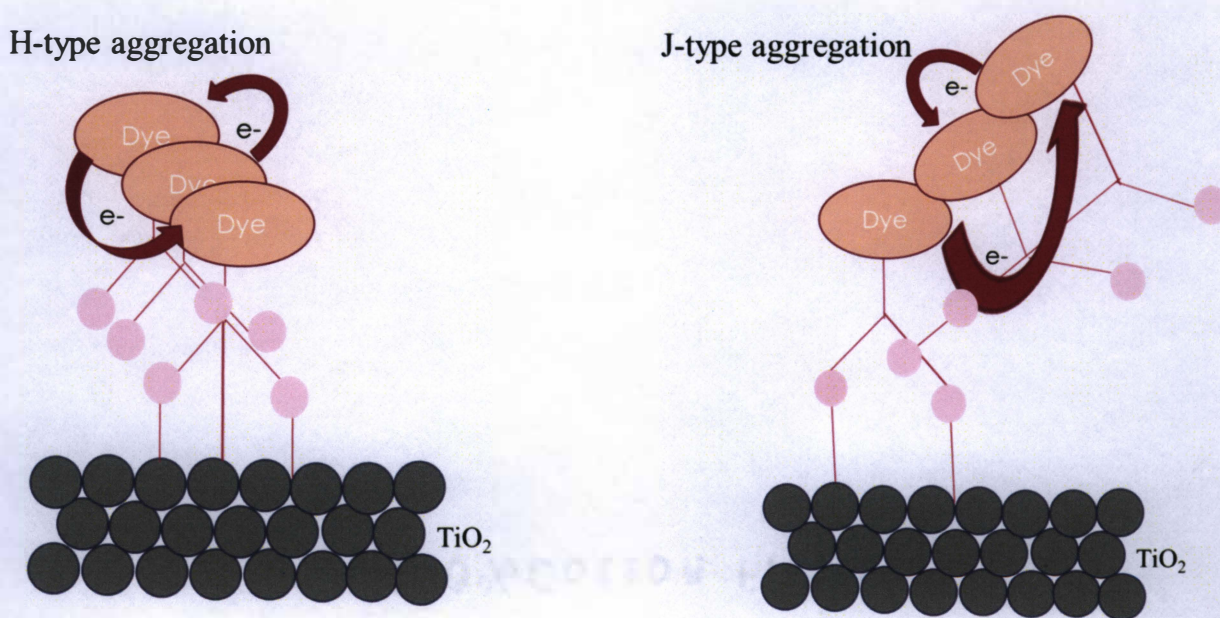


Figure 1.6. Aggregation of porphyrin dyes on TiO<sub>2</sub>. H-type aggregation dyes arranged face-to-face (left), J-type aggregation dyes arranged side-by-side (right).

### 1.2.3. BODIPY dye

Boron-dipyrromethene dyes, most commonly known as BODIPY dyes, have been recognized for their excellent optical properties such as strong absorption at 500 nm, in a region

where porphyrin dyes show weak absorption.<sup>(16)</sup> They have emerged as potential dyes for DCS for several reasons: high fluorescent, quantum yields and high solubility in most organic solvents. They exhibit strong photostability making them suitable for DSC applications.<sup>(34, 35)</sup> The chemical structure of BODIPY dye is shown in Figure 1.7. It composed of dipyrromethene complexed to a boron atom. The boron atom is further coordinated by two F anion. BODIPY dye has a narrow absorption in the visible region making it unsuitable for DSCs. Hupp *et al.* conjugated BODIPY with porphyrin and found the efficiency almost doubled.<sup>(18)</sup> He *et al.* found that BODIPY dye can act as a complementary dye for porphyrin dyes to enhance the energy conversion efficiency.<sup>(6, 14)</sup>

BODIPY dyes have been used for many chemical and biological applications. They have a broad range of applications in biomolecule labelling as well as fluorescence imaging.<sup>(16)</sup> The photostability of BODIPY's dyes is considered to be much better than many other proposed sensitizers.<sup>(14,16)</sup> Researchers found that when the charge is redistributed by exciting an electron from  $S_0$  to  $S_1$  energy level, the charge density on the *meso*-carbon increased; however, it was decreased on the other positions.<sup>(16)</sup> Studies on (C8) *meso* substituted BODIPY dyes showed poor photovoltaic performance. Several studies have shown that 2 or 6-position substituted BODIPY dyes show for promising performance for DSCs.<sup>(16)</sup>

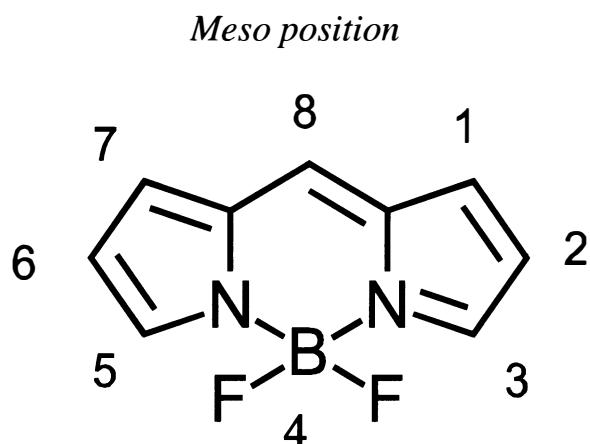


Figure 1.7. Chemical structure of boron-dipyrromethene (BODIPY) core

### **BODIPY as a Sensitizer for DSCs.**

The first BODIPY dye that was synthesized as a photosensitizer for DSCs was investigated by Fukuzumi *et al.* In their study, the BODIPY molecule was treated as a donor-acceptor system, in which a 2,4,5-trimethoxyphenyl group in *meso* position acted as a donor, and with the BODIPY core as an acceptor. The photoexcitation of this dye exhibited an electron transfer from the donor, which was from C-8 to the BODIPY core acceptor. The lifetime of the charge-separated state was 59 ps, at 298 K. Compared to porphyrin dyes, research on BODIPY-sensitized solar cells are scarce. The overall energy conversion efficiency was also much lower than the one from the state-of-the-art dyes. Table 1.1 listed several important BODIPY dyes reported in the literature. <sup>(35, 36, 37, 38, 39, 40)</sup>

Dye 1 was synthesized with a donor group attached on C-8; however, dye 2 was synthesized without an electron donating groups. It had a phenyl group on C-8 position and two carboxylic groups on C2 and C6 positions, respectively. The photovoltaic studies showed that the efficiency of dye 1 and dye 2 was 0.13 and 0.16%, respectively. <sup>(36)</sup> This study indicated the



position of donor groups that are attached to different position in dye 1 and dye 2 did not affect the efficiency too much. These results indicated that the low-efficiency values were not attributable to dye aggregation on the TiO<sub>2</sub> surface.<sup>(36)</sup> However, in another study, dye 3 was synthesized with a cyanoacrylic acid as an anchoring group and 4-(diphenylamino)phenyl as a donor group as shown in Table 1.1. The overall efficiency of dye 3 was 1.66%. The increased efficiency came from two factors. The first one is the conjugation of two 4-N,N-diphenylbenzene groups to its C3 position through a double bond, which broadened the absorption spectrum. The second one is the use of cyanoacetic acid instead of benzoic acid, which provided strong electron withdrawing force for the electron injection.<sup>(35)</sup>

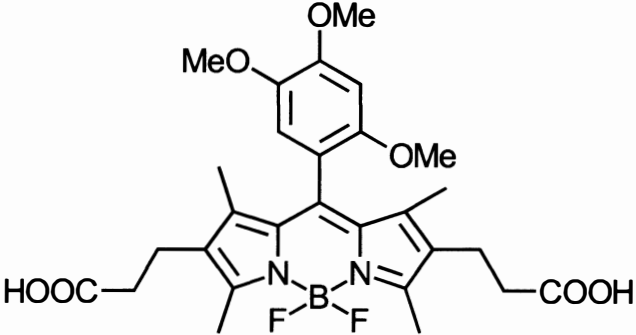
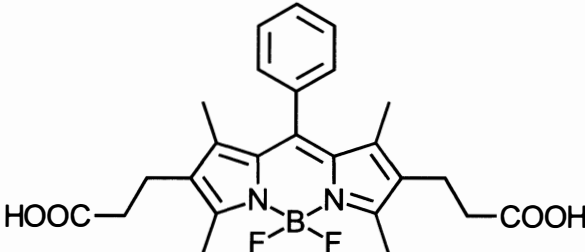
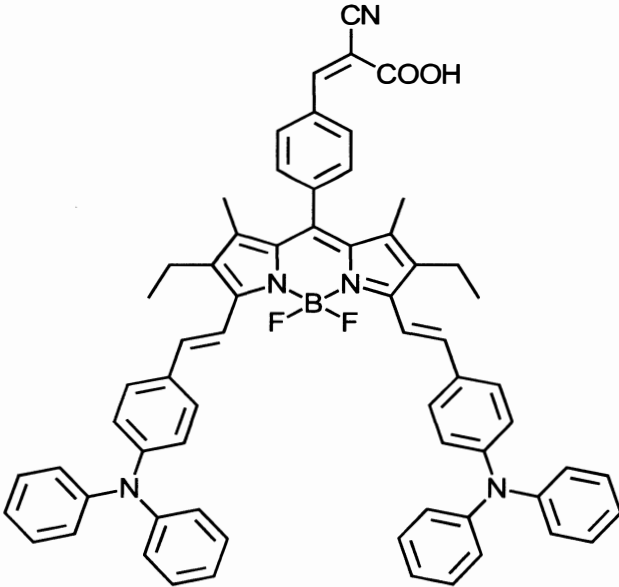
Akkaya *et al.* reported a series of novel BODIPY dyes that have broader absorption and higher efficiency for DSCs.<sup>(38)</sup> These dyes exhibited broader absorption with onsets between 650 and 760 nm. Dye 4 showed the highest efficiency of 1.88%. The high efficiency was due to the absence of methyl groups in 1 and 7 positions, which helped the BODIPY core form a plane with the phenyl group in the *meso* position. This planarity is quite favorable to the electron transfer from the donor to the acceptor. The efficiency increased when a co-adsorber chenodeoxycholic acid was added. In dye 5 the absorption was red shifted after a methoxy group was added to the donor; unfortunately, there was no improvement in the efficiency. Dye 6, containing two iodine atoms due to the heavy-atom-effect that was related to spin-orbit coupling. This caused efficient intersystem crossing for electron transfer to triplet state. Dye 7 showed efficiency similar to dye 4 that has long alkyl chains, which prevented the dye aggregation on TiO<sub>2</sub> surface. Dye 8 with a decyl chain also showed good efficiency, but was not as high as in dyes 4, 5 and 7. Dye 9 has a similar structure to dye 8, but has a different anchoring group. It gave similar energy conversion efficiency to dye 8.

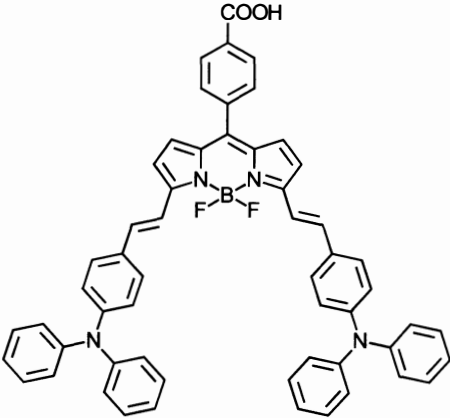
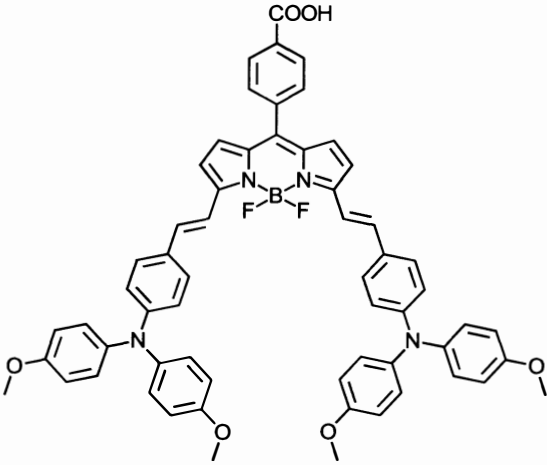
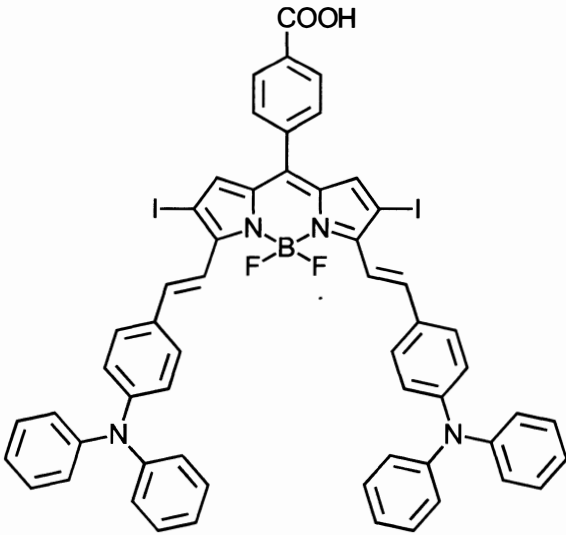
Recently, several new BODIPY dyes with different substituents have been studied for dye-sensitized solar cells. The donor- $\pi$ -acceptor structure was studied by Song and his group by adding donor and acceptor groups on C-6 and C-2 only to obtain D- $\pi$ -A structure.<sup>(16)</sup> Four dyes, i.e. dye 12, 13, 14, and 15 were synthesized. The results were also shown in Table 1.1. Dye 15 showed better efficiency than dyes 12, 13, 14. This is due to conjugation to thiophene residue, which enhanced the conjugation.<sup>(16)</sup> New BODIPY dyes 22, 23, and 24 were synthesized by Kubo and his group.<sup>(40)</sup> Dye 22 and 23 with two anchoring groups, are regioisomers. Dye 24 was synthesized with only one anchoring group. The absorption wavelengths were 647 nm for dye 22, 660 nm for dye 23, and 644 nm for dye 24. When incorporated into dye-sensitized solar cell, the efficiency of 5.24%, 6.06%, and 5.48% was obtained, respectively. The high efficiency came from adding more anchoring substituted groups that prevent the conjugation.

Dye-sensitized solar cells have been studied in the past twenty years and significant improvement in energy conversion efficiency has been achieved 11% of ruthenium-based dyes, 13% of porphyrin dyes and 6.06% of BODIPY dyes. Environmental issues of ruthenium complexes lead to find a replacement such as organic dyes. Organic dyes, such as porphyrin and BODIPY dyes shown a great promise for dye synthesized solar cell. Also, the lack absorption of porphyrin dyes and the aggregation on TiO<sub>2</sub> surface open the gate for BODIPY dyes to synthesize as complementary dyes or as standard dyes for dye synthesized solar cell since it has strong absorption in visible light.



Table 1.1. Summary of the efficiency and maximum wavelengths of BODIPY dyes for DSCs

Dye	Structure	$\eta$ (%)	$\lambda_{\max}$ (nm)	Ref
1		0.13	524 in CH <sub>3</sub> CN	36
2		0.16	520 in CH <sub>3</sub> CN	36
3		1.66	700 in CHCl <sub>3</sub>	35

Dye	Structure	$\eta$ (%)	$\lambda_{\text{max}}$ (nm)	Ref
4		1.88	724 in $\text{CHCl}_3$	37
5		1.32	746 in $\text{CHCl}_3$	37-38
6		0.23	761 in $\text{CHCl}_3$	37

Dye	Structure	$\eta$ (%)	$\lambda_{\max}$ (nm)	Ref
7		1.81	668 in CHCl <sub>3</sub>	37
8		1.40	707 in CHCl <sub>3</sub>	37
9		0.75	695 in CHCl <sub>3</sub>	37-38

Dye	Structure	$\eta$ (%)	$\lambda_{\max}$ (nm)	Ref
10		0.20	730 in $\text{CHCl}_3$	37
12		0.33	532 in $\text{CHCl}_3$	39
13		0.33	532 in $\text{CHCl}_3$	39
14		0.92	532 in $\text{CHCl}_3$	39
15		1.30	532 in $\text{CHCl}_3$	39

Dye	Structure	$\eta$ (%)	$\lambda_{\max}$ (nm)	Ref
22		5.24	647, 457, 371 in THF	40
23		6.06	660, 406, 369 in THF	40
24		5.48	644, 371 in THF	40

### **1.3. Motivation**

There is a need for developing new BODIPY dyes with broader light absorption capability and stronger binding strength on the TiO<sub>2</sub> surface for efficient and stable DSCs.

### **1.4. Objectives**

- Synthesize BODIPY dyes with a donor- $\pi$ -accepter configuration
- Characterize the synthesized dyes
- Determine absorption and fluorescence properties
- Determine the dye loading density on TiO<sub>2</sub>
- Fabricate solar cells and determine energy conversion efficiency

## CHAPTER 2

### SYNTHESIS & MEASUREMENTS

#### 2.1. Materials

All reagents and solvents were obtained from commercial sources and used without further purification unless otherwise noted. Other chemicals were analytical grade and used as received. Hexanes, methanol (CH<sub>3</sub>OH), dichloromethane (CH<sub>2</sub>Cl<sub>2</sub>), chloroform (CHCl<sub>3</sub>), triethylamine (Et<sub>3</sub>N), and NaOH were obtained from Fisher Chemical Scientific and used without further purification. Tetrahydrofuran (THF), dimethylformamide (DMF), CDCl<sub>3</sub> (solvent for NMR), N-iodosuccinimide (NIS), copper (I) iodide (CuI), tetrakis (triphenylphosphine) palladium(0) Pd(PPh<sub>3</sub>)<sub>4</sub>, boron trifluoride diethyl etherate (BF<sub>3</sub>OEt<sub>2</sub>), 2,4-dimethylpyrrole, and mesitaldehyde were obtained from ACROS Organics. Nitrogen gas and Argon gas were supplied by Geno Welding (Mattoon, Illinois). 2,3-Dichloro-5,6-dicyano-1,4-benzoquinone (DDQ) was obtained from Biosynth International, Inc. Silica gel was obtained from Dynamic Adsorbents, Inc. TiO<sub>2</sub> paste DSL (18 NR-T) was obtained from DYESOL. 2,6-Bis(hexyloxy)benzaldehyde was prepared by Dr. Lianzhi Zhang from South Dakota State University.

#### 2.2. Instrument

Column chromatography was performed using 200 mesh or 230-400 mesh silica gel. NMR spectra were obtained on a 400 MHz Bruker Avance II-NMR spectrometer, using ACROS Organics chloroform-d 99.8% D, containing 0.03% (v/v) TMS. <sup>1</sup>H NMR signals were referenced to TMS, while <sup>13</sup>C NMR signals were referred to the residual solvent peak. NMR spectra were processed using Bruker's TopSpin software. UV-Vis absorption spectra were performed on a

Cary 100 Series UV-Vis Dual Beam Spectrophotometer over a range of 200-800 nm. Single-crystal X-ray crystallography was analyzed using Bruker APEX II CCD diffractometer.

Fluorescence spectra were obtained on a MINCO Bowman Series 2 Luminescence Spectrometer.

Glovebox was supplied by MBRAun. Spincoater was supplied by Laurell and MODEL is WS-400B-6NPP/LITE. Current-voltage (I-V) measurements of dye sensitized solar cells were carried out on ORIEL photovoltaic measurement unit using LCS-100, as a light source.

## 2.3. Synthesis of Dyes

### 2.3.1. Synthesis of HHK1

The first task was to synthesis dye HHK1 with a mesityl group in *meso* position of BODIPY core, 4-ethynyl-N,N-dimethylbenzamino as a donor and 4-ethynylbenzoic acid as an anchoring group. The chemical structure of this dye was shown in Figure 2.1 and its synthetic route was described in Figure 2.2. The details will be presented in the following sections.

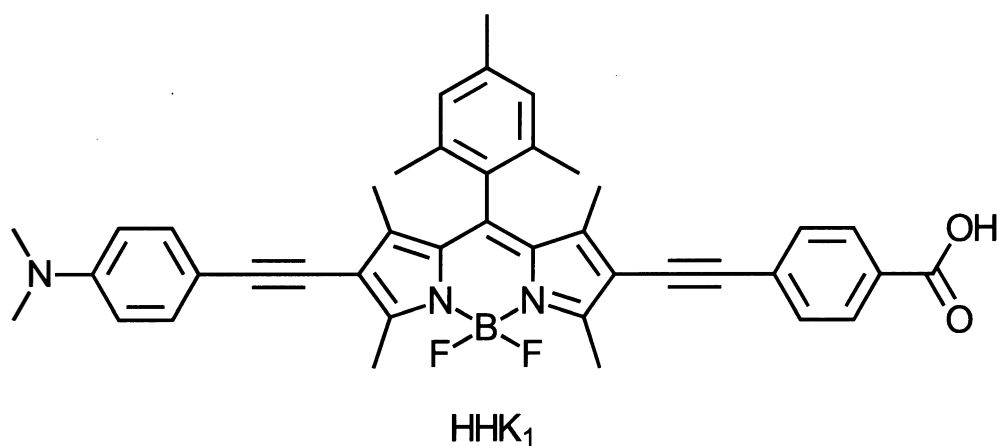


Figure 2.1. The chemical structure of HHK1



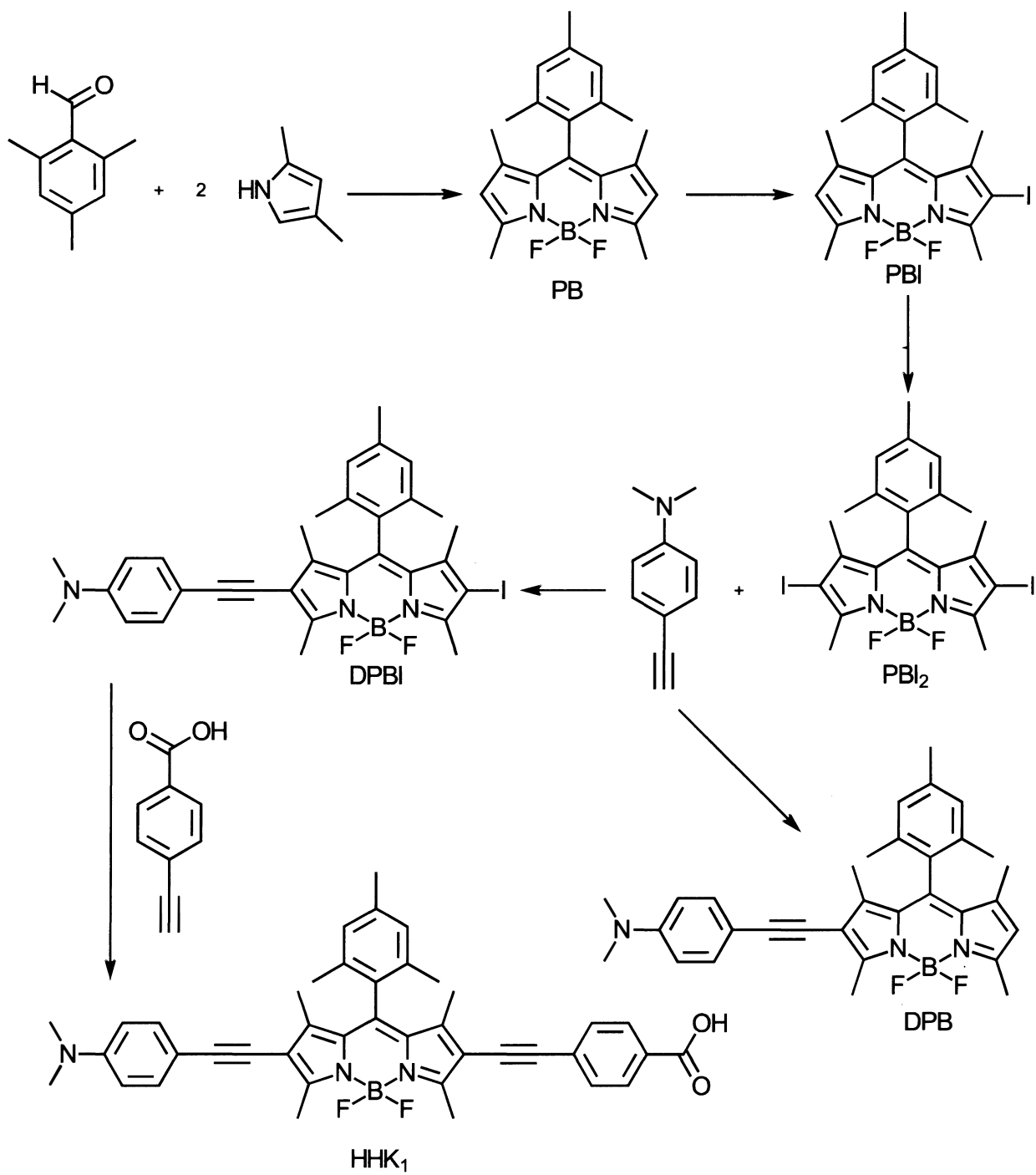


Figure 2.2. The synthetic route for HHK1 dyes

### 2.3.1. a. Synthesis of PB <sup>(41)</sup>

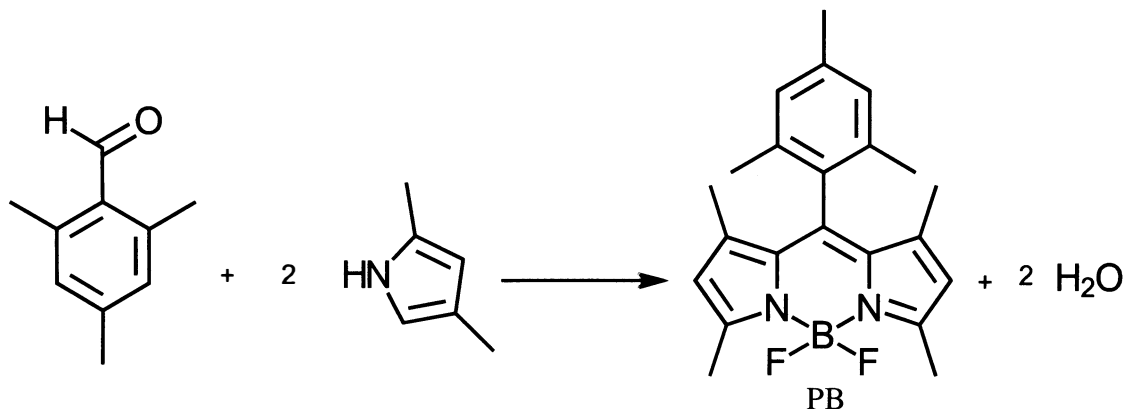


Figure 2.3. Synthesis of PB

To a 250 mL two neck round- bottom flask was added 200 mL of CH<sub>2</sub>Cl<sub>2</sub> under nitrogen atmosphere, then, 0.85 mL (8.2 mmol) of 2, 4-dimethyl-1H-pyrrole and 0.6 mL (4.1 mmol) of 2,4,6-trimethylbenzaldehyde were added. The color of the solution was immediately changed to yellow. One drop of trifluoroacetic acid (TFA) was added to initiate the reaction. The resulting mixture was stirred overnight at room temperature. The color of the solution changed to dark brown. Then, 0.90 g (6.791 mmol) of dichlorodicyanobenzoquinone (DDQ) in 20 mL CH<sub>2</sub>Cl<sub>2</sub> was added, and the color immediately changed to purple. The mixture was stirred continuously for 30 min. Then, 8 mL (57 mmol) of trimethylamine and 8 mL (46 mmol) of BF<sub>3</sub>.OEt<sub>2</sub> were added consecutively. The color of the solution became dark purple, and green fluorescence was observed under UV lamp (254 nm). The solution was stirred for another 5 h and the solvent was removed on a rotor evaporator under reduced pressure. The reaction mixture was loaded on the chromatography column filled with silica gel for purification. Chloroform/ hexane (v/v, 100:50) was used as an eluting solvent. The second band was collected. The crude product was purified by column chromatography four times under the same conditions. The final product was

obtained as an orange solid. The purity of the final product was confirmed by TLC. Yield: 47.30%

### 2.3.1. b. Synthesis of PBI<sup>(41, 42)</sup>

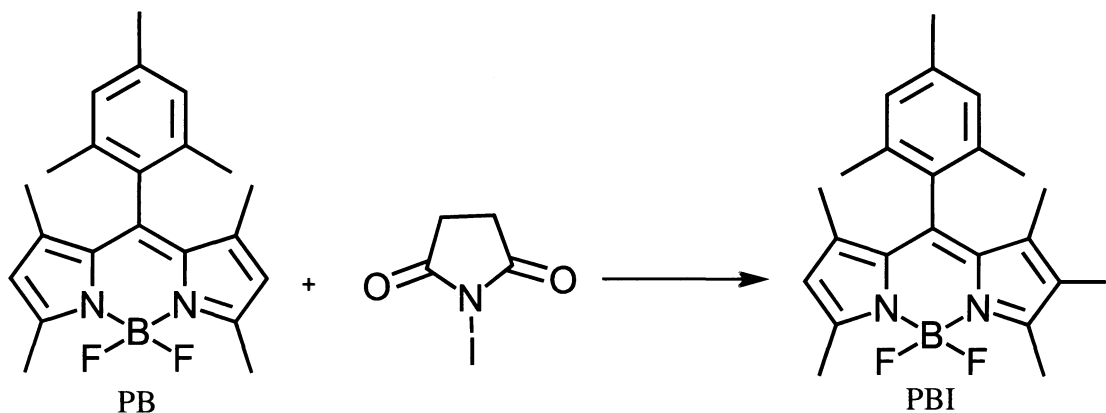


Figure 2.4. Synthesis of PBI

To a 250 mL round- bottom flask was added 100 mL of  $\text{CH}_2\text{Cl}_2$  and 0.340 g (0.93 mmol) of PB at 10-15 °C. Then, 0.280 g (1.24 mmol) of N-iodosuccinimide (NIS) in 20 mL anhydrous  $\text{CH}_2\text{Cl}_2$  was added dropwise into the solution within 1h. After the addition, the reaction mixture was stirred at room temperature for another 1h. The color of the solution changed to red and fluorescence was disappeared. The solvent was then removed on a rotor evaporator under reduced pressure. The reaction mixture was loaded on the chromatography column filled with silica gel for purification. Chloroform/ hexane (v/v, 100:50) was used as an eluting solvent. The second band was collected. The solvent was removed under reduced pressure. Then, a small amount of  $\text{CHCl}_3$  (0.5 mL) was added and the sample was precipitated as orange crystals. Its purity was confirmed by TLC. Yield: 0.243 g, 53.17 %.

### 2.3.1. c. Synthesis of PBI<sub>2</sub><sup>(41)</sup>

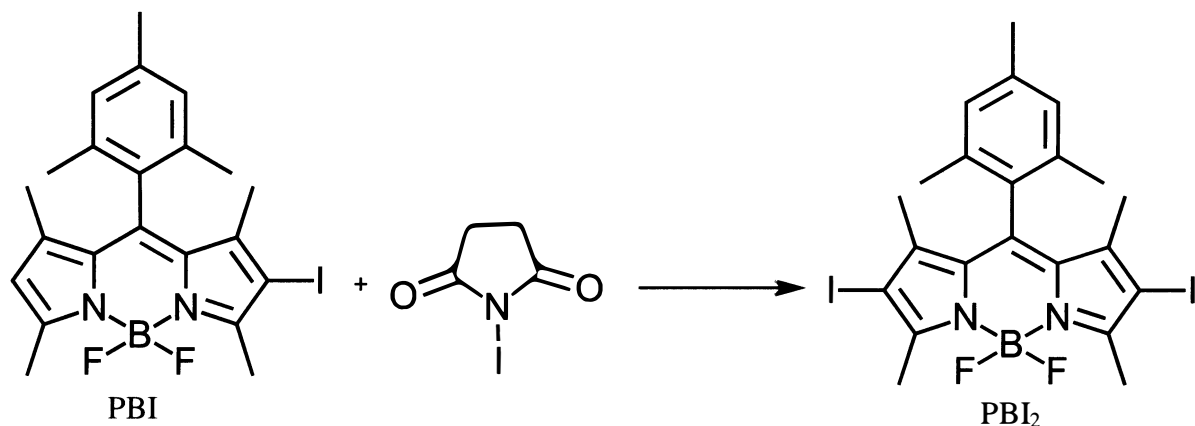


Figure 2.5. Synthesis of PBI<sub>2</sub>

To a 250 mL a round bottom flask was added 50 mL of CH<sub>2</sub>Cl<sub>2</sub> and 0.200 g (0.93 mmol) of PBI at 10-15 °C. Then, 0.0816 g (1.24 mmol) of N-iodosuccinimide (NIS) in 20 mL anhydrous CH<sub>2</sub>Cl<sub>2</sub> was added was added dropwise into the solution within 1h. After the addition, the reaction mixture was stirred at room temperature for another 1h. The color of the solution changed to red and fluorescence was disappeared. The solvent was removed on a rotor evaporator under reduced pressure. The reaction mixture was loaded on the chromatography column filled with silica gel for purification. Chloroform/ hexane (v/v, 100:50) was used as eluting solvent. The first band was collected. The solvent removed under reduced pressure and recrystallized by using pure CHCl<sub>3</sub> to give the product as reddish solid. Its purity was confirmed by TLC. Yield: 0.148 g, 53.47 %.

### 2.3.1. d. Synthesis of DPB<sup>(41, 42)</sup>

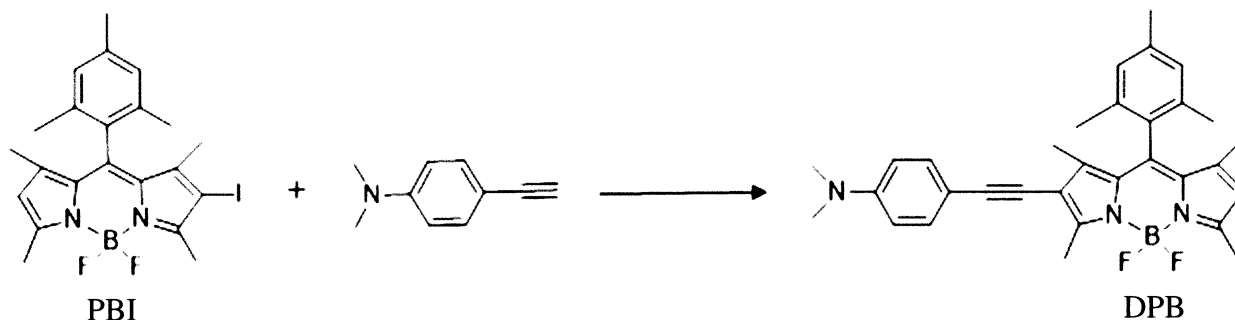


Figure 2.6. Synthesis of DPB

To a 50 mL pressure tube inside a glovebox maintained under an inert atmosphere of nitrogen 0.150 g (0.304 mmol) of PBI, 0.039 g (0.268 mmol) of 4-ethynyl-N, N dimethylaniline, 0.004 g (0.021 mmol) of CuI, 0.033 g (0.028 mmol) of Pd (PPh<sub>3</sub>)<sub>4</sub>, and 2.5 mL (0.017 mmol) of Et<sub>3</sub>N were added and dissolved in 35 mL of THF. Then, the sealed tube was moved out of glovebox and was placed in an oil-bath. The mixture was stirred and heated at 60 °C for 12 h. The color of the solution changed to dark purple. The solvent was removed and the crude product was purified by chromatography column using silica gel. Chloroform/hexane (v/v, 100:50) was used as an eluting solvent. The third band was collected. Then, a small amount of CHCl<sub>3</sub> (0.5 mL) was added and the sample was precipitated as a purple crystal. Yield: 0.080 g, 51.61%.

### 2.3.1. e. Synthesis of DPBI<sup>(41, 42)</sup>

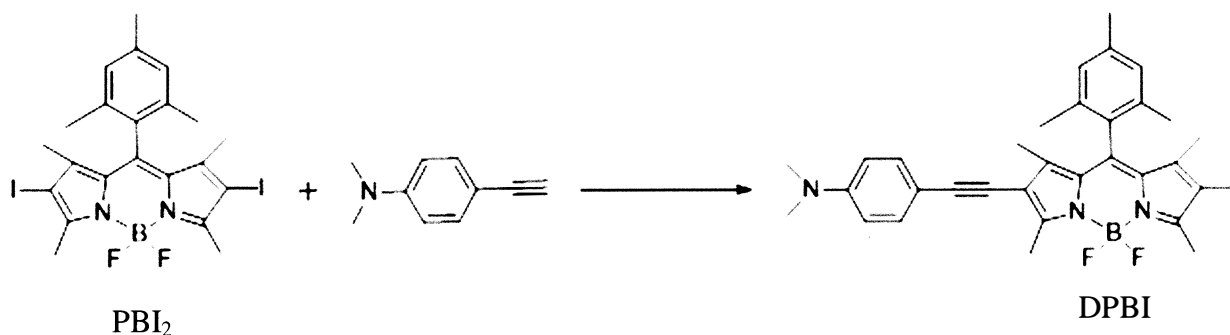


Figure 2.7. Synthesis of DPBI

To a 50 mL pressure tube inside a glovebox maintained under an inert atmosphere of nitrogen 0.092 g (0.148 mmol) of PBI<sub>2</sub>, 0.023 g (0.163 mmol) of 4-ethynyl-N, N-dimethylaniline, 0.004 g (0.021 mmol) of CuI, 0.008 g (0.006 mmol) of Pd (PPh<sub>3</sub>)<sub>4</sub>, were added and dissolved in 25 mL of THF and then 3 mL (0.021 mmol) of Et<sub>3</sub>N was added. The color of the solution changed to dark red immediately. Then, the sealed tube was transferred out of glovebox and was placed in an oil-bath. The mixture was stirred and heated at 60 °C, the color changed to dark red immediately after the addition. The mixture was stirred continuously for 12 h. The color of the solution changed to dark purple. The solvent was removed and the crude product was purified by column chromatography filled with silica gel. Chloroform/hexane (v/v, 100:50) was used as an eluting solvent. The third band was collected. The final product was obtained as purple greenish solid. Yield: 0.011 g, 12.5%.

### 2.3.1. f. Synthesis of HHK1<sup>(41, 42)</sup>

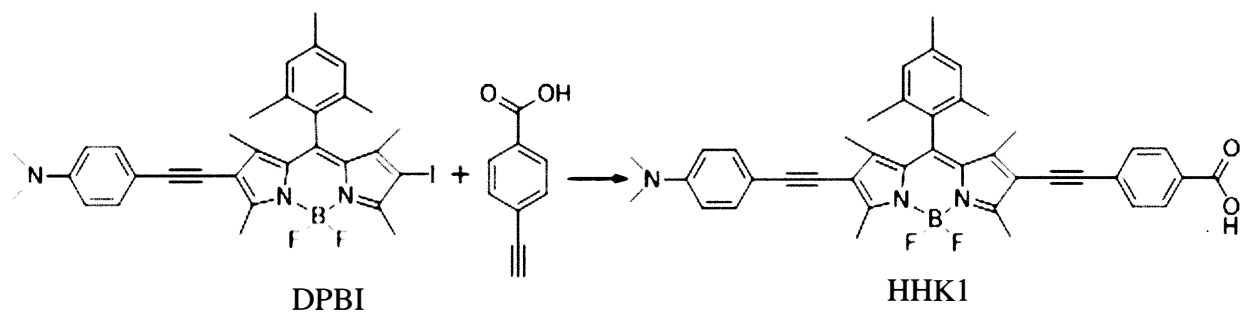


Figure 2.8. Synthesis of HHK1

To a 50 mL pressure tube inside a glovebox maintained under an inert atmosphere of nitrogen 0.100 g (0.153 mmol) of DPBI, 0.069 g (0.472 mmol) of 4-ethynylbenzoic acid (acceptor), 0.027 g (0.023 mmol) of Pd (PPh<sub>3</sub>)<sub>4</sub>, 0.004 g (0.021 mmol) of CuI were dissolved in 35 mL of THF and then 3 mL of triethylamine. The tube was sealed and transferred out of the glovebox.

The tube was placed in an oil-bath and the solution was heated and stirred continuously at 60 °C for 24 h. The color of the solution changed from reddish purple to deep blue. The solvent was then removed under reduced pressure. The crude product was purified by chromatography column filled with silica gel. The chloroform/ methanol (v/v, 100:7) was used as an eluting solvent. The second band was collected, filtered and washed with CH<sub>3</sub>OH to give product as a blue solid with red fluorescence. Yield 0.090 g, 90%.

### 2.3.2 Synthesis of HHK2

The second task was to synthesize dye HHK2 with 2,6-bis(hexyloxy)benzene group in the *meso* position of the BODIPY core. 4-ethynyl-N,N-dimethylbenzamino as a donor and 4-ethynylbenzoic acid as an anchoring group. The chemical structure of this dye was shown in Figure 2.9 and its synthetic route was described in Figure 2.10. The details will be presented in the following sections.

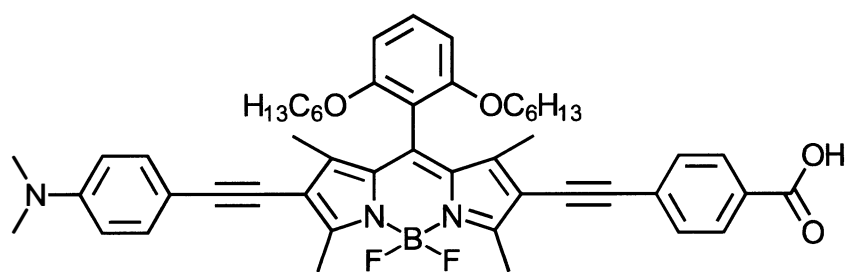


Figure 2.9. The chemical structure of HHK2

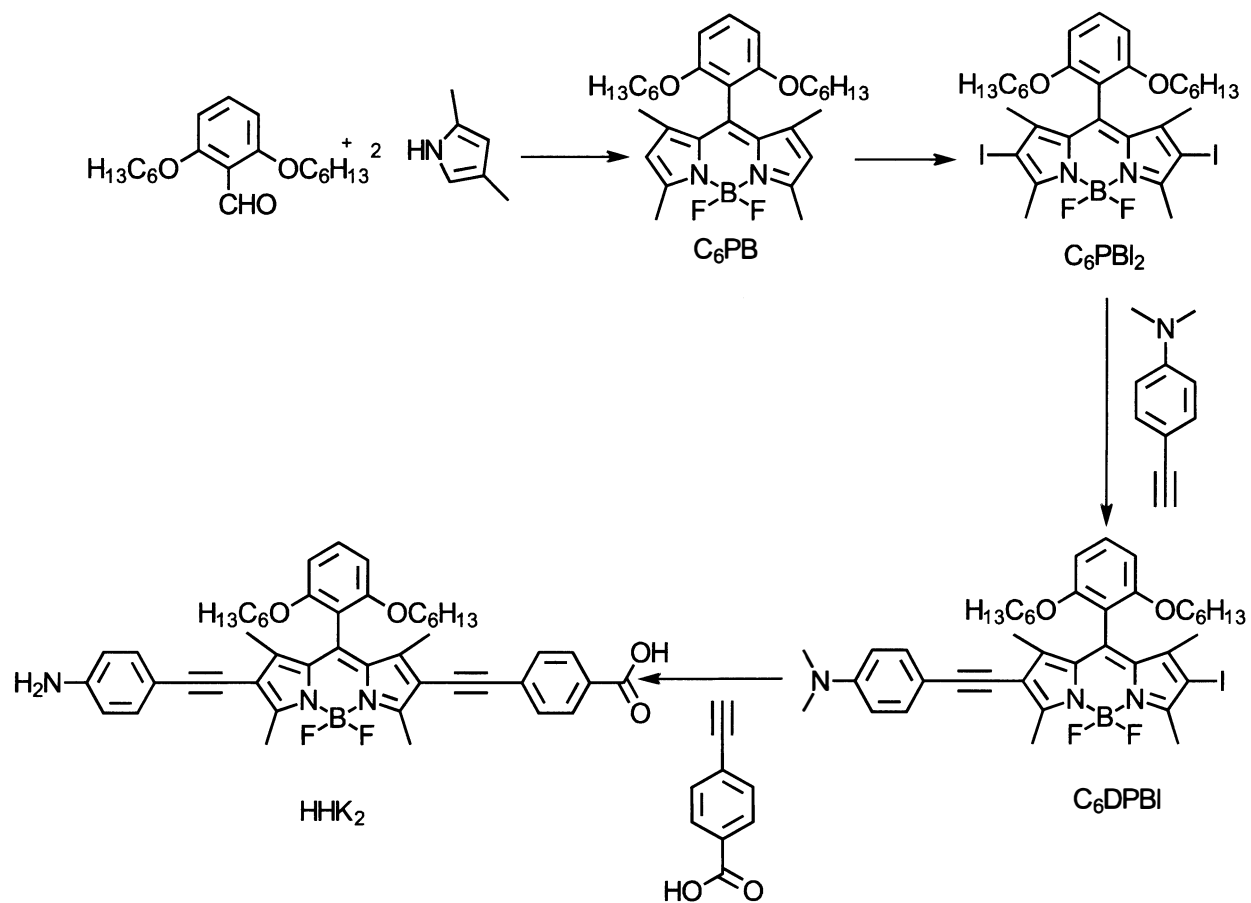


Figure 2.10. Synthetic route for HHK2 dye

### 2.3.2. a. Synthesis of C<sub>6</sub>PB

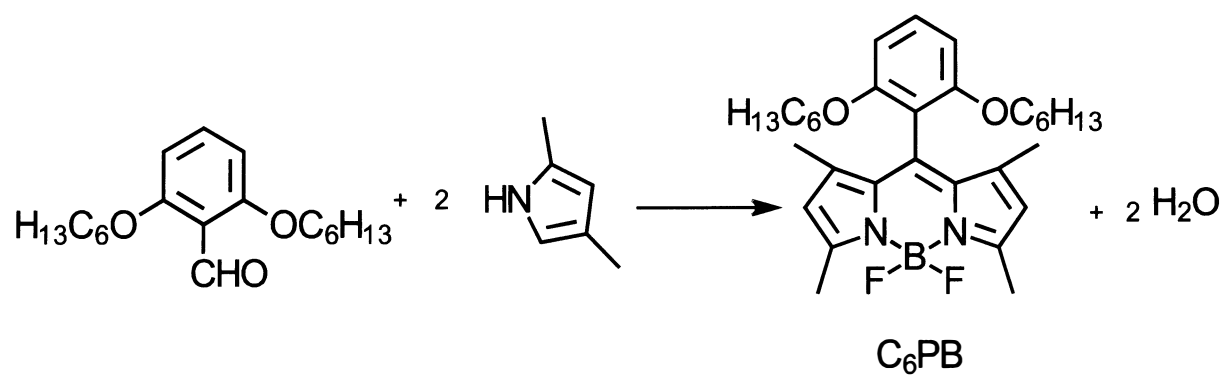


Figure 2.11. Synthesis of C<sub>6</sub>PB



To a 250 mL two neck round bottom flask was added 200 mL of  $\text{CHCl}_3$  under nitrogen atmosphere, then, 1.70 ml (16.4 mmol) of 2, 4-dimethyl-1H-pyrrole and 1.75 ml (8 mmol) of 2,6-bis(hexyloxy)benzaldehyde were added. The color of the solution was immediately changed to yellow. Three drops of  $\text{BF}_3 \cdot \text{OEt}_2$  was added to initiate the reaction. The color changed to dark red and the resulting mixture was stirred overnight at room temperature. The color of the solution changed to dark brown. Then, 1.8 g (13.58 mmol) of 2, 3-dichloro5,6-dicyanobenzoquinone (DDQ) in 20 mL  $\text{CHCl}_3$  was added, the color was immediately changed to purple. The mixture was continuously stirred for 30 min. Then, 16 mL (114 mmol) of trimethylamine and 16 mL (129 mmol) of  $\text{BF}_3 \cdot \text{OEt}_2$  were added consecutively. The color of the solution became dark deep purple, and green fluorescence was observed. The solution was stirred for another 5 h and the solvent was removed on a rotor evaporator under reduced pressure. The reaction mixture was loaded on the chromatography column filled with silica gel for purification. Chloroform/ hexane (v/v, 100:50) was used as an eluting solvent. The second band was collected. The final product was obtained as orange oil. The purity was confirmed with TLC. Yield: 0.387 g, 18.25%

### 2.3.2. b. Synthesis of $\text{C}_6\text{PBI}_2$

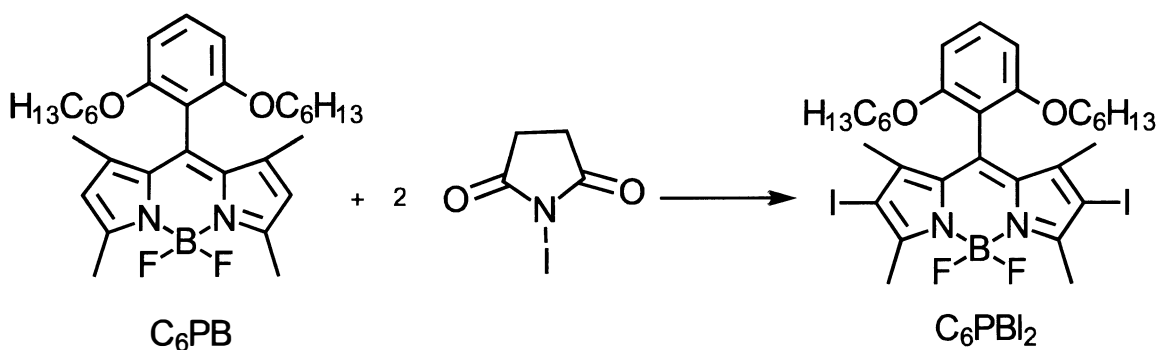


Figure 2.12. Synthesis of  $\text{C}_6\text{PBI}_2$

To a 250 mL a round bottom flask was added 50 mL of  $\text{CH}_2\text{Cl}_2$  at room temperature, then 0.380 g, (0.724 mmol) of  $\text{C}_6\text{PB}$  was added. Then, 0.307 g (1.364 mmol) of  $\text{N}^{\text{succinimide}}$  (NIS) in 25 ml anhydrous  $\text{CH}_2\text{Cl}_2$  was added dropwise into the solution within 1h. After the addition, the reaction mixture was stirred for another 1h. The color of the solution changed to red and fluorescence was disappeared. The solvent was removed on a rotor evaporator under reduced pressure. The reaction mixture was loaded on the chromatography column filled with silica gel for purification. Chloroform/ hexane (v/v, 100:50) was used as an eluting solvent .The first red band was collected. The solvent was removed under reduced pressure and recrystallized by using pure  $\text{CH}_3\text{OH}$  to give the product as a reddish solid. The yield: 0.320 g, 56.93 %.

### 2.3.2. c. Synthesis of $\text{C}_6\text{DPBI}$

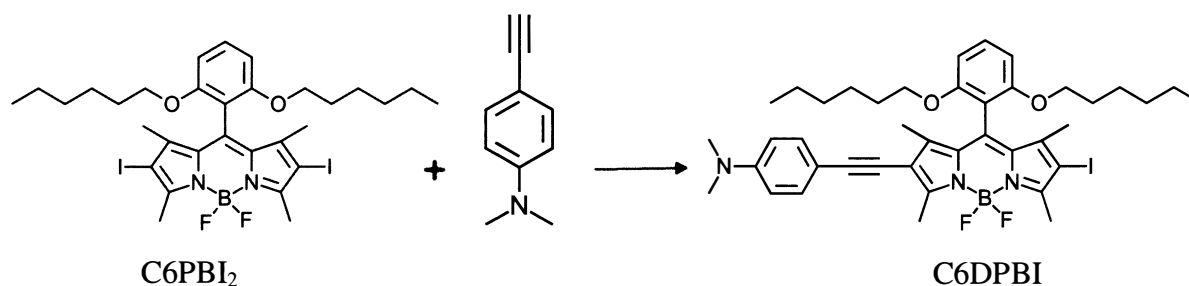


Figure 2.13: Synthesis of  $\text{C}_6\text{DPBI}$

To a 50 mL pressure tube inside a glovebox maintained under an inert atmosphere of nitrogen 0.200 g (0.257 mmol) of  $\text{C}_6\text{PBI}_2$ , 0.037 g (0.254 mmol) of 4-ethynyl-N, N-dimethylaniline, 0.004 g (0.021 mmol) of  $\text{CuI}$ , 0.042 g (0.036 mmol) of  $\text{Pd}(\text{PPh}_3)_4$ , and 3 mL of  $\text{Et}_3\text{N}$  were added. When 25 mL of THF was added, the color of the solution was red and it turned to dark red after the addition of TEA. In an oil-bath, the tube was sealed and the mixture was heated and stirred at  $60\text{ }^\circ\text{C}$  for 12 h; the color of the solution changed to dark purple. The reaction mixture was loaded on the chromatography column filled with silica gel for purification.

Chloroform/ hexane (v/v, 100:50) was used as an eluting solvent. The second band was collected and the solvent was removed under reduced pressure and recrystallized by using pure CH<sub>3</sub>OH to give the product as purple greenish solid. Yield: 0.053 g, 20.94 %.

#### 2.3.2. d. Synthesis of HHK2 <sup>(42)</sup>

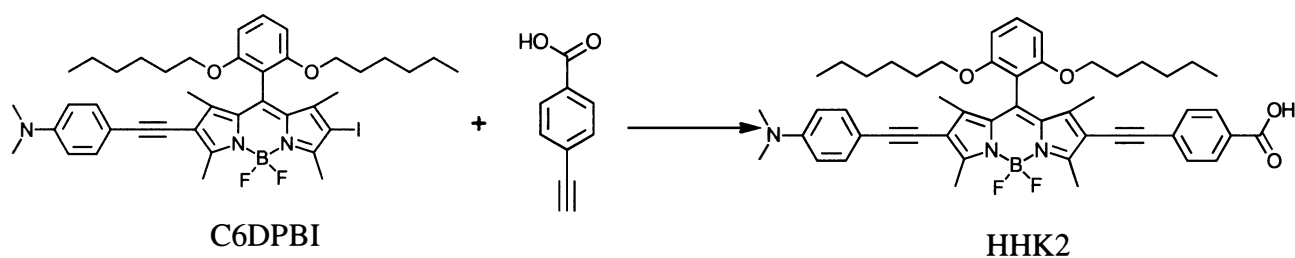


Figure 2.14. Synthesis of HHK2

To a 50 mL pressure tube inside a glovebox maintained under an inert atmosphere of nitrogen, 0.085g (0.107 mmol) of C<sub>6</sub>DPBI, 0.046g (0.314 mmol) of 4-ethynylbenzoic acid, 0.0185g (0.016 mmol) of Pd (PPh<sub>3</sub>)<sub>4</sub>, and 0.004 g (0.021 mmol) of CuI were dissolved in 35 mL of THF, then 4 mL of triethylamine was added. Then, the sealed tube was transferred out of glovebox and was placed in an oil-bath. The mixture was heated and stirred at 60 °C for 24 h. The color of the solution changed from reddish purple to deep blue. The solvent was removed on a rotor evaporator under reduced pressure. The reaction mixture was loaded on the chromatography column filled with silica gel for purification. Dichloromethane/ methanol (v/v, 100:7) was used as eluting solvent. The second band was collected to give product as a blue solid with red fluorescence. Yield was not determined.

## 2.4. Measurements

### 2.4.1. UV-Vis Absorption Spectroscopy in Solution

UV-Vis absorption spectra in solutions were obtained by adding certain volume of stock solution into 3 mL of  $\text{CHCl}_3$  solvent in a 1.0 cm quartz cuvette. The spectra were recorded from 200-800 nm. The concentration of dye in the cuvette ( $C_2$ ) was obtained from the equation:  $C_2V_2 = C_1V_1$ , where  $V_1$  is the volume of the dye stock solution added,  $C_1$  is the concentration of the dye stock solution,  $V_2$  was the total volume of the solution in the cuvette, which was the sum of  $\text{CHCl}_3$  (3 mL) and the volume of stock solution added. The concentration of stock solution was determined by the moles of dye, which was the mass of the dye divided by its molar mass, divided by the total volume of the solution (25 mL). The unit of the concentration was mol/L ( $M$ ). The concentrations of solutions and the final concentrations of each dye were shown in Tables 3.3 and 3.4.

The absorption coefficient ( $\epsilon$ ) of each dye was calculated by using Beer Lambert law:  $A = \epsilon \cdot C \cdot l$ , where  $A$  is absorbance at maximal absorption ( $\lambda_{\text{max}}$ ),  $l$  is the distance of light path (1 cm) and  $C$  is the final concentration of dye in cuvette, which was  $C_2$  in our cases.

### 2.4.2. UV-Vis Absorption Spectroscopy in $\text{TiO}_2$

Absorption spectrum on  $\text{TiO}_2$  film was carried out as described in the following. The microscope glass slide (specimen glass) was cut into small pieces with 2 cm  $\times$  0.9 cm size in order to fit into 1 cm cuvette size as shown in Figure 2.15. Then, it was cleaned with methanol and acetone and air-dried. The edges of the slides were then covered with tape and a layer of nanocrystalline  $\text{TiO}_2$  was doctor-bladed. The resulting film was air-dried for 30 min and sintered at 450 °C for 30 minutes.

After the film was cooled down to room temperature, the TiO<sub>2</sub> slide was immersed into a 1 cm-cuvette containing 3 mL of methanol as shown in Figure 2.15. After a blank spectrum was taken, the slide was taken out, and dried in air for a few minutes. Then, the dried slide was dipped into the dye solution for about 40 seconds. The slide was taken out of the dye solution and flushed with methanol several time to get rid of any physically adsorbed dyes on the TiO<sub>2</sub> nanoparticles. Then, the dye-coated TiO<sub>2</sub> slide was immersed into the cuvette vertically with film facing the incoming light beam and the absorption spectrum was recorded.

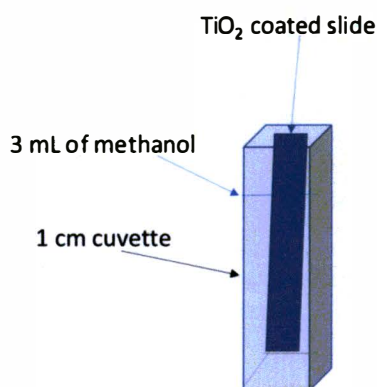


Figure 2.15. TiO<sub>2</sub> coated slide inside a cm cuvette contains 3 mL of methanol

#### 2.4.3. Calibration Curve Measurement

Calibration curves for HHK1 and HHK2 for dye loading density determination were carried out using the following procedure. To a cuvette containing 3 mL of 0.1M of NaOH solution (DMF/H<sub>2</sub>O, v/v, 25:5) was added 100  $\mu$ L of the dye stock solution. The cuvette was then shaken several times. The absorption spectrum was then recorded. Then, another 100  $\mu$ L of dye stock solution was added and spectrum was recorded. This process was repeated several times until 500  $\mu$ L of the dye stock solution was added.

#### 2.4.4. Dye Loading Density on TiO<sub>2</sub>

Dye loading measurements were obtained as the following procedures. On a piece of aluminum foil, doctor-bladed a layer of nanocrystalline TiO<sub>2</sub> paste as described in section 2.4.8. The foil was placed in an oven at 100 °C for overnight. Then, the TiO<sub>2</sub> film was gently peeled off from the aluminum substrate. The resulting free-standing TiO<sub>2</sub> films were usually broken into small pieces during the peeling process. Then, the films were placed on a ceramic plate and sintered at 450 °C for 30 minutes for dye loading.

Dye loading test was carried out according to the following procedures. A piece of sintered free-standing TiO<sub>2</sub> nanoparticles film with a mass about 3 mg was put into a small vial containing 2 mL of the dye solution and 4 mL of methanol and kept overnight. Then, the solution was removed by a pipette and the films were flushed with methanol several times until the solvent was clear. Then, 4 mL of 0.1 M NaOH solution (DMF/H<sub>2</sub>O, v/v, 25: 5) was added to the vial. The dye started to come off the TiO<sub>2</sub> film immediately. When all dyes on the TiO<sub>2</sub> de-adsorbed into the solution, the absorption spectrum of the resulting solution was recorded. The concentration of the solution was determined from the calibration curve and the total number of moles of the dye molecules was obtained by the concentration multiplied by the total volume (0.004 L). The specific area for TiO<sub>2</sub> nanoparticles film used for this study was 760000 cm<sup>2</sup>/g. The total surface area (A) was obtained by the mass of TiO<sub>2</sub> multiplied by 760000 cm<sup>2</sup>/g. The dye-loading density was obtained by the total moles of dye de-adsorbed divided by the total surface area.

#### 2.4.5. Fluorescence Spectroscopy (FL)

The fluorescence spectrophotometer was used to measure dye's steady-state emission spectra at room temperature; excitation wavelength was 375 nm for the starting dyes (PB, PBI,

PBI<sub>2</sub>, DPB, DPBI, C<sub>6</sub>PB, C<sub>6</sub>PBI<sub>2</sub>, C<sub>6</sub>DPBI; however, for the final dyes HHK1 and HHK2 the excitation wavelength was 520 nm. The concentration of the solution that used was the same as the concentration of the absorption measurement, as mentioned in section 2.4.1.

#### 2.4.6. Nuclear Magnetic Resonance (NMR) Spectroscopy

<sup>1</sup>H NMR spectra were recorded on a 400 MHz Bruker NMR spectrometer using the TMS as an internal standard. The solvent that used for NMR solution was CDCl<sub>3</sub> and the amount of sample that used to run the measurements was either 3 or 4 mg depending on the sample. The chemical shifts reported in parts per million (ppm). For split peaks are multiplicities, the following abbreviations were used such as: s, singlet; d, doublet; t, triplet; m, multiplet; b, broad. <sup>13</sup>C NMR spectra were recorded on a 400 MHz Bruker spectrometer using the carbon signal of the deuterated solvent as the internal standard.

#### 2.4.7. Elemental Analysis (EA) & Mass Spectrometry (MS)

The sample of HHK1 was sent to outside provider, NuMega Resonance Labs, for analysis. This measurement was obtained using Electrospray ionization (ESI) technique. This technique is used to determine the molecular mass of the final product and compare it with the calculated molar mass. In the positive ion mode peaks correspond to the protonated or alkali adduct analyte molecules that observed in the mass spectra. However, in the negative ion mode operation peaks correspond to deprotonated analyte molecules will be observed in the mass spectra. In this measurement both the positive ion mode and negative ion mode were used.

#### 2.4.8. Fabrication and Photovoltaic Characterization of DSCs

Before cell fabrications, fluorine-tin-oxide (FTO) glass slides were cleaned in a boiling aqueous soap solution for 30 minutes, then rinsed with distilled water sufficiently. The slides



were washed in distilled water, acetone, and isopropanol for about 30 min at room temperature, respectively. The slides were then flushed with D.I. water and dried in air for next steps.

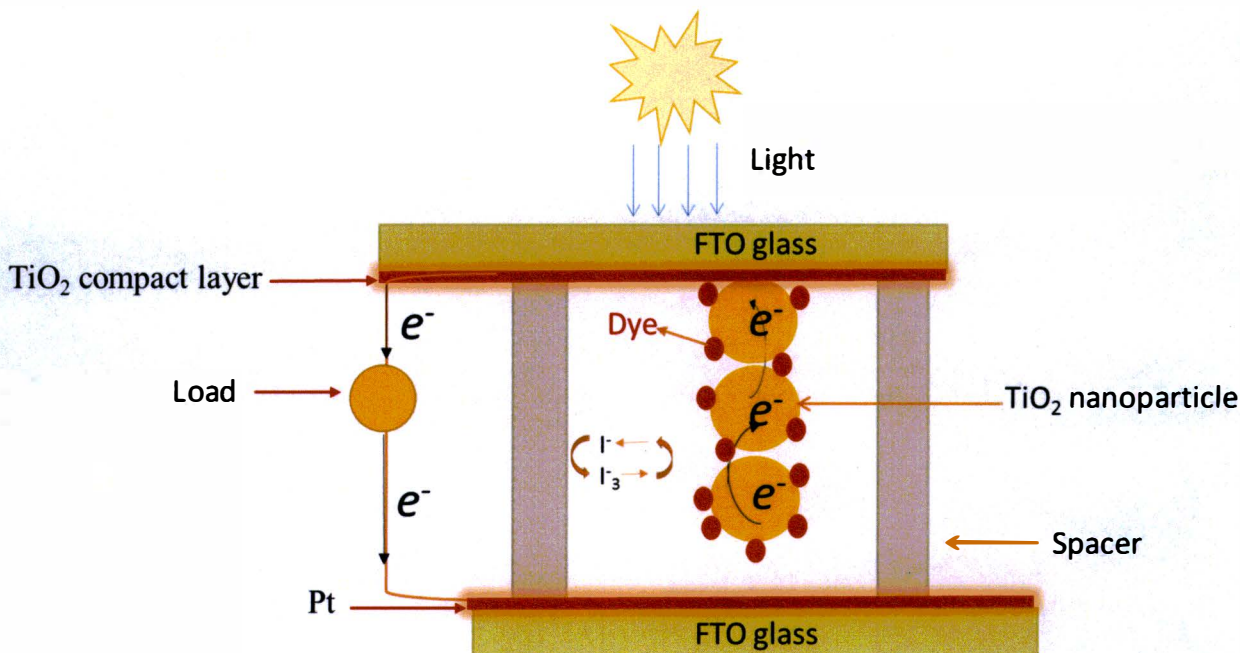


Figure 2.16. A cross-view diagram of DSC

In the first step, a  $\text{TiO}_2$  compact layer was coated on the FTO glass. This was accomplished on a spin-coater. One-half of the FTO glass was covered with 3M magic tape, as shown in Figure 2.17 below. The FTO glass was fixed on the spin-coater. The spin speed was adjusted to 2000 rpm. While the spin-coater was spinning, 0.5 mL of titanium isopropoxide in EtOH was added dropwise into the FTO glass. Then, the sample was removed from the spinner after it was completely stopped. The tape was carefully removed, and the sample placed in the oven for sintering at  $450\text{ }^\circ\text{C}$  for 30 minutes.



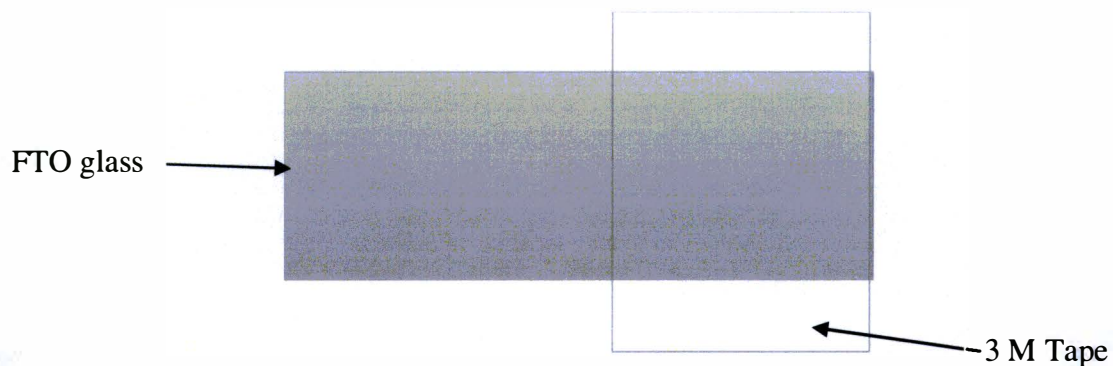


Figure 2.17. Half covered FTO glass with 3 M magic tape

After the sample was cooled down to room temperature, the sample was removed from the oven. Then, a mask made from 3M tape placed on the top of the compact layer. A layer of  $\text{TiO}_2$  nanoparticles with a size of 20 nm was doctor-bladed using a commercial  $\text{TiO}_2$  paste (18 NR-T). The sample was dried for 30 min at room temperature. This process was repeated one more time to make the layer thicker. After this process, the sample was put in an oven and sintered at  $450^\circ\text{C}$  for 30 minutes.

To add one scattering layer, a similar mask made from 3M magic tape was carefully placed on the top of the nanocrystalline layer. Then one layer of  $\text{TiO}_2$  scattering layer (DSL 90-T) was doctor-bladed. The mask was removed and the sample air-dried for 30 min. Then, the sample was sintered again at  $450^\circ\text{C}$  for 30 minutes. In the final step, the sample was dipped into a small vial contain 5 mL of freshly prepared  $\text{TiCl}_4$  solution for 2 h. Then, in this step, only the portion of slide that has  $\text{TiO}_2$  film was immersed into the solution. The film was taken out of the solution and flushed with distilled water for three times. After that, it was sintered at  $450^\circ\text{C}$  for 30 minutes and the film was cooled to  $80^\circ\text{C}$ . The sample then immersed into a 0.2 mM of dye solution was prepared in methanol for 4 hours at room temperature. The sample was then taken out and rinsed with methanol three times and air-dried. This is photoelectrode.

The counter electrode was prepared by adding one drop of  $\text{H}_4\text{PtCl}_6 \cdot 2\text{H}_2\text{O}$  ethanol solution on cleaned FTO glass with two pre-drilled holes. The sample was air-dried for 10 min and sintered at  $450\text{ }^\circ\text{C}$  for 30 minute with the ramping rate  $5\text{ }^\circ\text{C}$  per minute.

To assemble a cell, a mask made from Parafilm was put onto the photoelectrode, and the counterelectrode was placed on its top as shown in Figure 2.18. The assembled device was placed on a hotplate and temperature was maintained  $45\text{ }^\circ\text{C}$ . When the Parafilm started to melt, a pressure was gently applied on the top of the device till two electrode bind tightly. The device was then removed from the hotplate and cooled down to room temperature. The electrolyte (an acetonitrile /valeronitrile (v/v,1:1) solution containing  $0.6\text{ M}$  1-propyl-2,3-dimethylimidazolium iodide,  $0.05\text{ M}$  I<sub>2</sub>,  $0.1\text{ M}$  LiI,  $0.1\text{ M}$  guanidine thiocyanate and  $0.5\text{ M}$  tert-butylpyridine) was injected from one holes in the counter electrode using a syringe, and then the surface was cleaned to remove the extra electrolyte. Two holes were then sealed using 3 M tape. The surface of the photoelectrode was cleaned, and resulting cell was tested.

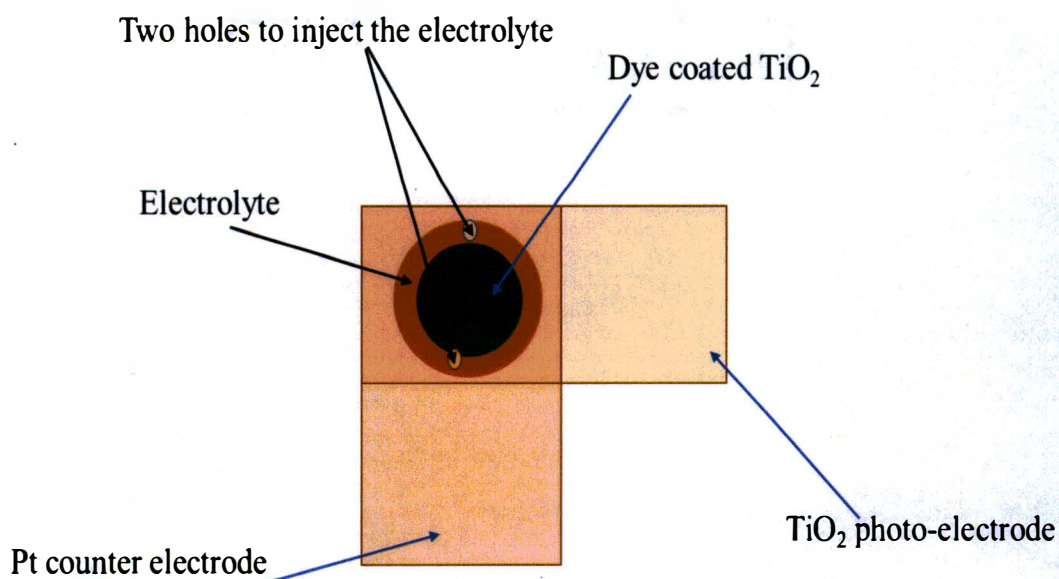


Figure 2.18. Top view of assembled cell

The measurement was carried out on an ORIEL photovoltaic measurements system with a setup as shown in Figure 2.19. Xenon arc lamp with an AM 1.5 filter (LCS-100) was used as a light source. Semiconductor parameter analyzer was used to measure the I-V response of the solar cells. Easy Expert was interfaced to the analyzer to set up the measurement conditions and to obtain the current-voltage and data. Before the measurement, the instrument was turned on and stabilized for 15 min. The system was first calibrated using a standard reference provided by Newport. The sample was scanned from 0 – 1V. After that, the reference was replaced by sample cell and the I-V curves were recorded again. The fill factor (FF) and overall energy conversion efficiency were calculated by  $\eta (\%) = P_{\max} \times 100 / (P_{\text{in}} \times A)$  and  $FF = P_{\max} / (I_{\text{sc}} \times V_{\text{oc}})$ , where  $P_{\max}$  is the maximum output power of cells,  $P_{\text{in}}$  is the power density of the light source ( $100 \text{ mW/cm}^2$ ),  $I_{\text{sc}}$  is the short-circuit current,  $V_{\text{oc}}$  is the open-circuit voltage, and  $A$  is the active area of the cell ( $0.16 \text{ cm}^2$ ).

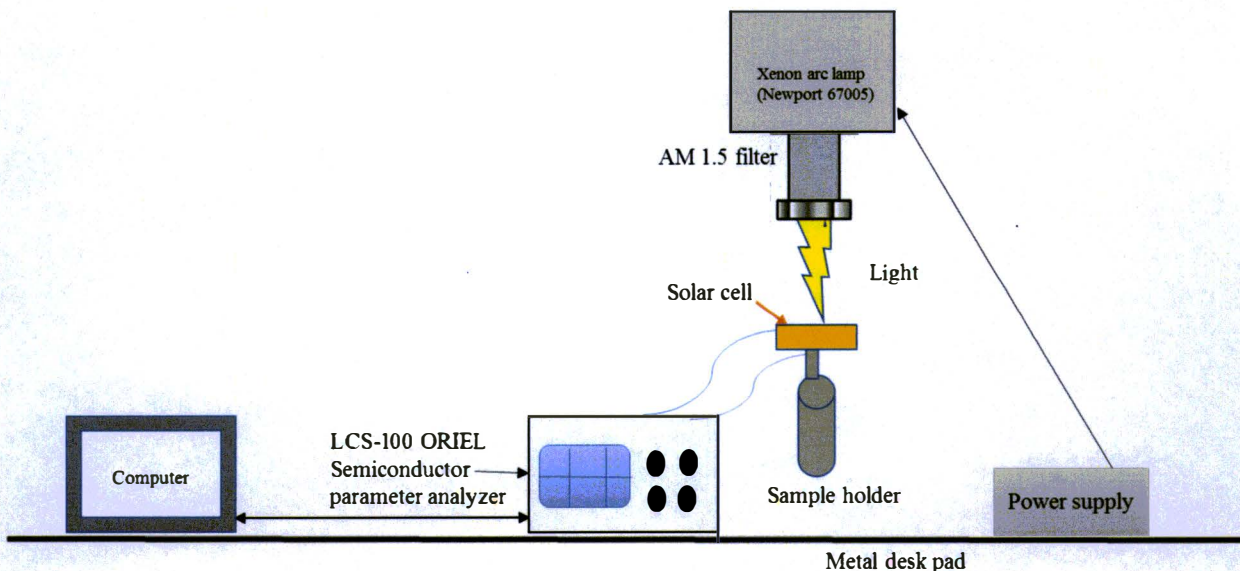


Figure 2.19. Experimental setup of I-V measurement

## CHAPTER 3

### CHARACTERIZATION & PHYSICAL PROPERTIES

#### 3.1. Characterization

The overall yields of BODIPY dyes were 47.30 % for PB, 53.17 % for PBI, 53.47 % for PBI<sub>2</sub>, 51.61 % for DPB, 12.5 % for DPBI, and 90.03% for the final dye HHK1. All BODIPY dyes were soluble in chloroform and dichloromethane; however, most of these dyes showed low solubility in methanol and hexanes. All dyes exhibited very different colors in solid state and in solution. In solid state, PB, PBI, PBI<sub>2</sub>, showed orange color, whereas DPB, DPBI and HHK1 showed purplish color. The samples also showed fluorescence under light illumination. PBI and DPB were characterized by single-crystals X-ray diffraction analysis. All of these dyes were characterized by <sup>1</sup>H and <sup>13</sup>C mass spectroscopy.

The yields for second series dyes were 18.25% for C<sub>6</sub>PB, 56.93 % for C<sub>6</sub>PBI<sub>2</sub>, 20.94 % for C<sub>6</sub>DPBI. The yield was not determined for HHK2. The solubility of these dyes in the organic solvents was quite similar to the first series HHK1 dyes. All products were characterized by <sup>1</sup>H NMR spectra and C<sub>6</sub>PB and C<sub>6</sub>DPB were further ascertained by single-crystal X-ray diffraction analysis.

##### 3.1.1. NMR

###### 3.1.1.a. PB

<sup>1</sup>H NMR (400 MHz, ppm, CDCl<sub>3</sub>): δ 7.26 (solvent, CDCl<sub>3</sub>), 6.94 (s, 2H), 5.95 (s, 2H), 2.55 (s, 6H), 2.33 (s, 3H), 2.09 (s, 6H), 1.38 (s, 6H).

$^{13}\text{C}$  NMR (100 MHz,  $\text{CDCl}_3$ ):  $\delta$  155.08, 142.3, 141.6, 138.5, 134.9, 131.1, 128.9, 120.7, 21.1, 19.4, 14.6, 13.3.

$^1\text{H}$  NMR spectrum of PB was shown in Figure 3.1 in the appendix. It showed seven major peaks. PB has a chemical formula  $\text{C}_{22}\text{H}_{25}\text{BF}_2\text{N}_2$ . Only seven peaks were appeared on the spectrum because of its symmetrical structure. The peak at 7.26 ppm came from the solvent  $\text{CDCl}_3$ . The singlet peak at 6.94 ppm was assigned to two protons in the benzene ring of the mesityl group. The singlet peak at 2.55 ppm (labeled as f) corresponded to six protons and was assigned to two methyl groups in the  $\beta$  position of pyrrole. The third peak, which was observed at 2.33 ppm (labeled as a), has three protons; this peak related to the methyl group in benzene ring of the mesityl group. The singlet peaks at 1.38, 2.09, and 5.95 ppm corresponded to methyl groups in five membrane ring in pyrrole (labeled as d), two methyl groups in benzene ring (labeled as c), and two protons in the pyrrole ring (labeled as e), respectively.  $^{13}\text{C}$  NMR of PB gave twelve peaks shown in Figure 3.2 in the appendix. PB has twenty two carbon atoms, but only twelve were appeared because it is symmetrical.

#### 3.1.1.b. PBI

$^1\text{H}$  NMR spectrum (400 MHz, ppm,  $\text{CDCl}_3$ ):  $\delta$  7.26 (solvent,  $\text{CDCl}_3$ ), 6.95 (s, 2H), 6.02 (s, 1H), 2.63-2.56 (s, 6H), 2.34 (s, 3H), 2.07 (s, 6H), 1.40-1.38 (s, 6H).

$^{13}\text{C}$  NMR (100 MHz,  $\text{CDCl}_3$ ):  $\delta$  157.4, 154.1, 144.3, 142.4, 141.6, 138.9, 134.8, 131.1, 130.9, 130.0, 129.1, 121.8, 21.2, 19.5, 15.8, 15.4.

$^1\text{H}$  NMR of PBI was shown in Figure 3.3 in the appendix. The compound has a chemical formula  $\text{C}_{22}\text{H}_{24}\text{BF}_2\text{IN}_2$ . Ten peaks were observed in the spectrum. The peak at 7.26 ppm came from the solvent  $\text{CDCl}_3$ . The singlet peak at 6.95 ppm labeled as b in the spectrum was assigned to two

protons in benzene ring of the mesityl group. The singlet peak at 2.56 ppm (labeled as f) and 2.63 ppm (labeled as g) were corresponded to six protons of methyl groups in the pyrrole. The peak at 2.34 ppm (a) corresponding to three 3 protons was related to the methyl group in benzene ring of the mesityl group. The singlet peaks at 1.40 and 1.38 ppm corresponded to methyl groups in the five membrane ring in pyrrole (labeled as d and h). The singlet peak at 6.02 ppm was assigned to one proton in pyrrole in C2 position. The peak at 2.34 ppm (labeled as c) was corresponded to two methyl groups in benzene ring.

$^{13}\text{C}$  NMR of PBI gave ten major peaks as shown in Figure 3.4 in the appendix. The extra eight new peaks corresponded to the eight carbons in pyrrole that since the symmetrical condition was gone and resulted to the assigned each carbon on BODIPY as a unique peak with a unique chemical shift.

### 3.1.1.c. PBI<sub>2</sub>

$^1\text{H}$  NMR (400 MHz, ppm,  $\text{CDCl}_3$ ):  $\delta$  7.26 (solvent,  $\text{CDCl}_3$ ), 6.96 (s, 2H), 2.64 (s, 6H), 2.34 (s, 3H), 2.05 (s, 6H), 1.53-1.50 (s, 6H).

$^1\text{H}$  NMR spectrum of PBI<sub>2</sub> was shown in Figure 3.5 in the appendix. PBI<sub>2</sub> has a  $\text{C}_{22}\text{H}_{23}\text{BF}_2\text{I}_2\text{N}_2$  chemical formula and only six peaks appeared on the spectrum due to its symmetrical structure. The peak at 7.26 ppm was corresponded to the solvent  $\text{CDCl}_3$ . The singlet peak at 6.96 ppm, labeled as b in the spectrum, was assigned to two protons in benzene ring. The singlet peak at 2.34 ppm, labeled as a in the spectrum was assigned to three protons in the methyl group (*para* position) in mesityl group. The singlet peaks at 2.64, 1.50, and 2.05 ppm were corresponded to six protons in two methyl groups in pyrrole (labeled as in d and e), six protons in two methyl groups in mesityl (*ortho* position) (labeled as c,) respectively. These peaks indicated that the



compound was symmetrical. The other small peaks that appeared might come from generating water or some impurity.

#### 3.1.1.d. DPB

$^1\text{H}$  NMR (400 MHz, ppm,  $\text{CDCl}_3$ ):  $\delta$  7.26 (solvent,  $\text{CDCl}_3$ ),  $\delta$  1.56 (s, 3H),  $\delta$  2.09 (s, 6H),  $\delta$  2.34 (s, 3H),  $\delta$  2.57 (s, 3H),  $\delta$  2.69 (s, 3H),  $\delta$  2.96 (s, 6H),  $\delta$  5.97 (s, 1H),  $\delta$  6.62-6.64 (d,  $J=8$ , 2H),  $\delta$  6.95 (s, 2H),  $\delta$  7.32-7.34 (d,  $J=8$ , 2H).

$^{13}\text{C}$  NMR (100 MHz,  $\text{CDCl}_3$ ):  $\delta$  156.7, 156.3, 149.9, 143.1, 141.8, 141.5, 138.7, 134.9, 132.4, 131.3, 130.9, 129.5, 129.0, 121.2, 115.8, 111.8, 110.4, 96.9, 79.5, 40.2, 21.2, 19.4, 14.7, 13.6, 13.5, 12.2.

$^1\text{H}$  NMR spectrum of DPB was shown in Figure 3.6 in the appendix. DPB has a  $\text{C}_{32}\text{H}_{34}\text{BF}_2\text{N}_3$  chemical formula and only 14 peaks appeared in the spectrum due to the symmetry of the molecule. The peak at 0.00 came from TMS internal standard and peak and peak at 7.26 ppm is the solvent peak ( $\text{CDCl}_3$ ). The two doublet peaks at 7.34 and 7.32 ppm and 6.64 and 6.62 ppm labeled j and I in the spectrum, were assigned to the four protons in the benzene ring in the donor. A new singlet peak at 2.97 ppm was assigned to the six protons in the two methyl groups that were attached to the nitrogen atom in the donor, which were labeled as l and k in the spectrum. the other peaks at 6.95, 5.97, 2.69, 2.69, 2.34, 2.57, 1.56, and 2.09 labeled as (b, e, f, g, c, a, h and d) in the spectrum, were assigned to the two protons in the benzene ring, one proton in the pyrrole, six protons in the two methyl groups in the pyrrole rings (C3 position), six protons in two methyl groups in the pyrrole (C1 position), three protons in the one methyl group in the mesityl group (*para* position), and six protons in the methyl groups in the mesityl groups (*ortho* position), respectively.

There were only ten major peaks were observed in its  $^{13}\text{C}$  NMR spectrum as shown in Figure 3.7. This might be due to the low concentration of the sample and short acquisition time.

#### 3.1.1.e. DPBI

$^1\text{H}$  NMR (400 MHz, ppm,  $\text{CDCl}_3$ ):  $\delta$  7.26 (solvent,  $\text{CDCl}_3$ ),  $\delta$  1.46(s, 3H),  $\delta$  1.42 (s, 3H)  $\delta$  1.99 (s, 6H),  $\delta$  2.62 (s, 3H),  $\delta$  2.56 (s, 3H),  $\delta$  2.27 (s, 3H),  $\delta$  2.90 (s, 6H),  $\delta$  6.56-6.54 (d,  $J=8$ , 2H),  $\delta$  6.89 (s, 2H),  $\delta$  7.24-7.18 (d,  $J=8$ , 2H).

$^{13}\text{C}$  NMR (100 MHz,  $\text{CDCl}_3$ ):  $\delta$  167.77, 167.69, 149.08, 143.23, 141.83, 138.72, 134.91, 132.63, 132.46, 132.38, 130.92, 130.89, 129.05, 128.85, 128.81, 121.32, 111.98, 111.41, 96.84, 79.33, 71.80, 68.16, 65.58, 38.74, 30.58, 30.43, 30.37, 28.93, 27.73, 23.75, 22.99, 21.22, 19.49, 19.17, 14.72, 14.06, 13.74, 13.60, 13.51, 12.37, 12.20, 10.97.

$^1\text{H}$  NMR spectrum of DPBI was shown in Figure 3.8 in the appendix. DPBI has a  $\text{C}_{32}\text{H}_{33}\text{BF}_2\text{IN}_3$  chemical formula. The peak at 7.26 ppm came from the solvent. The two doublet peaks at 7.24 and 7.18 ppm and 6.56 and 6.54 ppm was assigned to four protons in the benzene ring in the donor. The singlet peak at 6.89 ppm was assigned to two protons in the mesityl group. The singlet peak at 2.27 ppm was related to the three protons in methyl group in the mesityl group. The singlet peak at 2.90 ppm was assigned to the six protons in two methyl groups that were attached to the nitrogen atom in the donor. The singlet peaks at 2.62, 2.56, 1.46, and 1.42 ppm were assigned to twelve protons in methyl groups in the pyrrole rings, which were labeled as g, e, d, and f in the spectrum.

The  $^{13}\text{C}$  NMR spectrum shown in Figure 3.9 exhibited 32 major peaks that were corresponded to all carbon atoms in the compound. Several minor peaks were also observed. They might be linked to the impurity in the sample.



### 3.1.1.f. HHK1

<sup>1</sup>H NMR (400 MHz, ppm, CDCl<sub>3</sub>): δ 7.23 (solvent, CDCl<sub>3</sub>), δ 2.34 (s, 3H), δ 1.51-1.50 (s, *J*= 4, 6H), δ 2.07 (s, 6H), δ 2.69 (s, 6H), δ 2.95 (s, 6H), δ 6.96 (s, 2H), δ 6.62-6.60 (d, *J*=8, 2H), δ 6.95 (s, 2H), δ 7.32-7.29 (d, *J*= 12, 2H), δ 7.50-7.48 (d, *J*= 8, 2H), δ 8.02-8.00 (d, *J*= 8, 2H).

<sup>1</sup>H NMR spectrum of HHK1 was shown in Figure 3.10 in the appendix. HHK1 has a C<sub>41</sub>H<sub>34</sub>BF<sub>2</sub>N<sub>3</sub>O<sub>2</sub> chemical formula and twelve major peaks appeared in the spectrum. The peak at 0.0 ppm came from TMS reference peak and the peak at 7.23 ppm came from the solvent (CDCl<sub>3</sub>) peak. That leaves ten major peaks. The four doublet peaks at 8.02 and 8.00, 7.50 and 7.49, 7.48 and 7.32, and 6.62 and 6.60 ppm were corresponded to eight protons in the benzene rings in the donor and acceptor as shown in the spectrum. They were labeled as (f, e, j and k in the spectrum). The singlet peak at 2.95 ppm was assigned to the methyl group in the benzene ring in the donor. The singlet peaks at 2.69, 2.34, 2.07, 1.51-1.50 ppm were assigned to 21 protons in two methyl groups in pyrrole rings, three methyl groups in meistyl group, two methyl groups in pyrrole rings. They were labeled as i, g, a, c, d, h in the spectrum, respectively.

### 3.1.1.g. C<sub>6</sub>PBI<sub>2</sub>

<sup>1</sup>H NMR (400 MHz, ppm, CDCl<sub>3</sub>): δ 7.32 (solvent, CDCl<sub>3</sub>), δ 0.80-0.78 (t, 6H), δ 1.16-1.10 (m, 12H), δ 1.51 (m, 4H), δ 2.60 (s, 6H), δ 2.63 (s, 6H), δ 3.92-3.89 (t, 4H), δ 6.61-6.59 (d, *J*= 8, 2H), δ 7.33-7.33 (t, 1H).

<sup>1</sup>H NMR spectrum of C<sub>6</sub>PBI<sub>2</sub> was shown in Figure 3.11 in the appendix. The peak at 7.32 came from the solvent. This compound has a symmetrical structure. The triplet peaks 7.38 and 7.34 ppm were corresponded to one proton in the benzene ring in the *meso* position of the BODIPY core. It was labeled as a in the spectrum. The doublet peaks with chemical shifts between 6.61

and 6.59 ppm were assigned to two protons in the benzene ring, which was labeled as b in the spectrum. The triplet peaks between 3.92 and 3.89 ppm, labeled as c in the spectrum, were related to the two -CH<sub>2</sub> groups that were attached to oxygen atom in 2,6-bis(hexyloxy)benzene ring. It shifted downfield because it is attached to an oxygen atom. Peaks labeled as (d, e, f, g, and h) 1.54, 1.66-1.09, 0.81-0.78, and 2.24 ppm were assigned to 22 protons in (-CH<sub>2</sub> and -CH<sub>3</sub>) groups in the hexloxy groups. The peaks at 2.63 and 2.60 ppm, which were assigned as j and i in the spectrum, were related to the four methyl groups that were attached to the pyrrole rings.

#### 3.1.1.h. C<sub>6</sub>DPBI

<sup>1</sup>H NMR (400 MHz, ppm, CDCl<sub>3</sub>): δ 7.32 (solvent, CDCl<sub>3</sub>), δ 0.80-0.78 (t, 6H), δ 1.16-1.12 (m, 12H), δ 1.51 (m, 4H), δ 2.62 (s, 3H), δ 2.68 (s, 3H), δ 2.9 (s, 6H), δ 3.48 (s, 3H), δ 3.50 (s, 3H), δ 3.92-3.89 (t, 4H), δ 6.61-6.59 (d, *J*= 8, 2H), δ 6.64-6.62 (d, *J*= 8, 2H), δ 7.33-7.33 (t, 1H), δ 7.37-7.35 (d, *J*= 8, 2H).

<sup>1</sup>H NMR spectrum of C<sub>6</sub>DPBI was shown in Figure 3.12 in the appendix. Twelve peaks are observed in the spectrum. The peak at 7.32 ppm came from the solvent. Peaks a, b, c, d, e, f, g, h, i, j, k, l in the spectrum remained the same as observed in C<sub>6</sub>PBI<sub>2</sub>; however, their chemical shifts shifted slightly downfield to 7.35-7.33 (triplet), 6.61-6.59 (doublet), 3.92-3.89 (triplet), 1.63-1.51 (multiplet), 1.16-1.12 (triplet), 0.81-0.78 (triplet), 2.68, 2.62 (singlet), and 3.50, 3.48 (singlet) ppm, respectively. The peaks assigned as a and b in the spectrum were related to three protons in the benzene ring, the peaks labeled as c, d, e, f, g, and h were assigned to 26 protons in the hexloxy group, whereas peaks labeled as i, j, k, and l in the spectrum were assigned to four methyl groups that were attached to pyrroles rings, respectively. Two doublet peaks at 6.64 and

6.62 and 7.37 and 7.35 ppm were related to four protons in the benzene ring in the donor group, which labeled as m and n, respectively. Moreover, one new singlet peak with a chemical shift of 2.97 ppm was observed and was assigned to the methyl groups that were attached to the nitrogen atom in the donor. It was labeled as o and p in the spectrum.

### 3.1.1.i. HHK2

$^1\text{H}$  NMR (400 MHz, ppm,  $\text{CDCl}_3$ ):  $\delta$  7.31 (solvent,  $\text{CDCl}_3$ ),  $\delta$  0.80-0.76 (t, 6H),  $\delta$  1.14-1.12 (m, 12H),  $\delta$  1.51 (m, 4H),  $\delta$  2.00 (s, 3H),  $\delta$  2.32 (s, 3H),  $\delta$  2.96 (s, 3H),  $\delta$  2.96 (s, 6H),  $\delta$  3.92-3.89 (t, 4H),  $\delta$  6.62-6.60 (d,  $J=8$ , 2H),  $\delta$  6.64-6.62 (d,  $J=8$ , 2H),  $\delta$  7.33-7.31 (t, 1H),  $\delta$  7.37-7.35 (d,  $J=8$ , 2H),  $\delta$  7.51-7.49 (d,  $J=8$ , 2H),  $\delta$  8.02-8.00 (d,  $J=8$ , 2H).

$^1\text{H}$  NMR spectrum of the final compound HHK2 was shown in Figure 3.13 in the appendix.

HHK2 has a  $\text{C}_{50}\text{H}_{56}\text{BF}_2\text{N}_3\text{O}_4$  chemical formula and 14 peaks were observed in the spectrum. The peak at 7.31 ppm came from the solvent. The two doublet peaks observed at (7.51 and 7.49 and 8.02 and 8.00) ppm were assigned to four protons in the benzene ring in the donor (labeled as m, n, q and r in the spectrum) and other peaks that appeared were similar to those observed in  $\text{C}_6\text{DPBI}$ . The singlet peak at 2.96 ppm was corresponded to the methyl groups that were attached to the nitrogen atom in the donor. The triplet peak between at 3.92-3.89 ppm were assigned to the  $(-\text{CH}_2)$  groups that were attached to oxygen atoms in the hexyloxy chain. The singlet peaks at (2.69, 2.32, 2.00, and 1.65) ppm were assigned to four methyl groups attached to pyrroles rings, respectively. The multiplet and triplet peaks between 1.56 and 1.12, and between 0.80 and - 0.76 ppm were assigned to 22 protons in  $(-\text{CH}_2$  and  $-\text{CH}_3)$  groups in the long chain (labeled as d, e, f, g, and h in the spectrum) respectively.

### 3.1.2. Elemental Analysis (EA) & Mass Spectrometry (MS)

Figure 3.14 showed the mass spectra of HHK1. The HHK1 has a molecular formula  $C_{41}H_{38}BF_2N_3O_2$  with a molar mass of 653.57 g/mol. In the mass spectrum with a negative mode, one major peak at 652.6 was observed, which was corresponded to the M-1 species. In Figure 3.15 showed the mass spectrum of HHK1 in positive mode. Two major peaks were appeared. The first main peak at 676.5 corresponded to the molar mass of HHK1 with one Na ( $653.57 + 22.9 = 676.45$ ). The Na ion may come from container for the sample. The second main peak was found at 654.6, which was related to  $653.57 + 1 = 654.57 \sim 654.6$  [M+1].

The elemental analysis of HHK1 showed 74.21% of carbon atoms, 6.84% of hydrogen atoms, and 6.46% of nitrogen atoms, which were closed to the calculated values 75.35%, 5.86%, and 6.43%, respectively.

Printing Date: Tuesday, April 07, 2015  
Polarity/Scan Type: Negative Q1 Scan

Sample Name: DPBA 1501EILU.766A

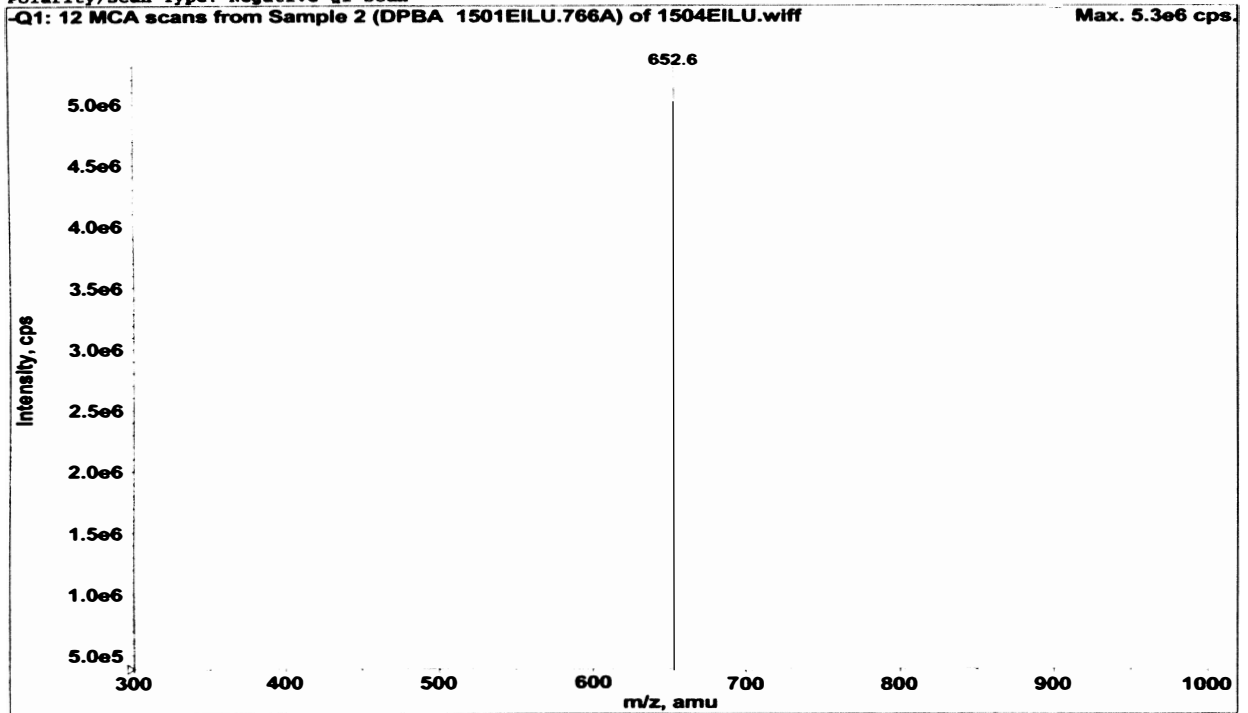


Figure 3.14. Mass spectra of HHK1 in the negative ion mode

Printing Date: Tuesday, April 07, 2015  
Polarity/Scan Type: Positive Q1 Scan

Sample Name: DPBA 1501EILU.766A

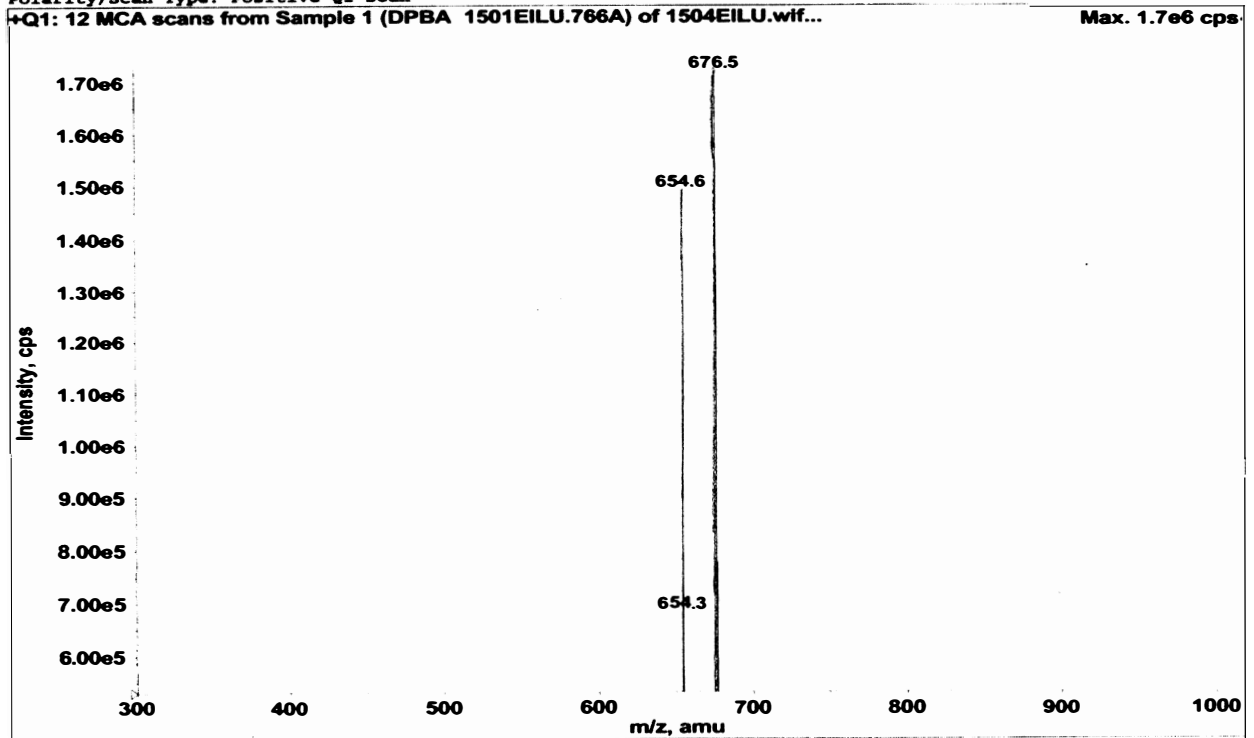


Figure 3.15. Mass spectra of HHK1 in the positive ion mode

### 3.1.3. Single Crystal X-ray Diffraction Analysis

Single-crystal X-ray diffraction analysis were obtained on a CCD-based commercial X-ray diffractometer using Cu-K  $\alpha$  radiation ( $\lambda = 1.54178 \text{ \AA}$ ) the crystals were mounted on glass fibers for data collection. The frames were collected at 100 K. The different measurement device type was Bruker APEXII CCD. The data were corrected for absorption using APEX2. The data were corrected for absorption using SADABS (Bruker, 2012) program. Computing data reduction was performed by using SAINT (Bruker, 2010) and XPREP (Bruker, 2010) also the computing structure solution was completed by using SHELXL-2014 (Sheldrick, 2014). The detailed results of the bond lengths and bond angles of PBI, DPB, C6PBI<sub>2</sub>, and C6PBI were listed in Table 3.1.

Figure 3.16 shows the ORTEP diagram of single-crystal structure of PBI that was crystallized from CHCl<sub>3</sub>. The boron B adopted a tetrahedral geometry with two N atoms and two F atom surrounding it. The BODIPY unit exhibited a planar geometry, and it was almost perpendicular to the mesityl unit. The detailed bond lengths and bond angles were listed in Table 3.2.

Single crystals of DPB were obtained from slow evaporation of the solvent of a CHCl<sub>3</sub> solution, at room temperature. The single-crystal structure of DPB was shown in Figure 3.17. It had very similar features to PBI. The boron adopted a tetrahedral geometry according to the bond angles as shown in Table 3.2. They very close similar to the theoretical bond angle of the tetrahedral geometry (109.5°). Moreover, the BODIPY core was also almost perpendicular to the mesityl unit. In addition, the BODIPY core did not fall in a plane with the donor group; instead both were with an angle 177.06° and 179.91°, respectively.

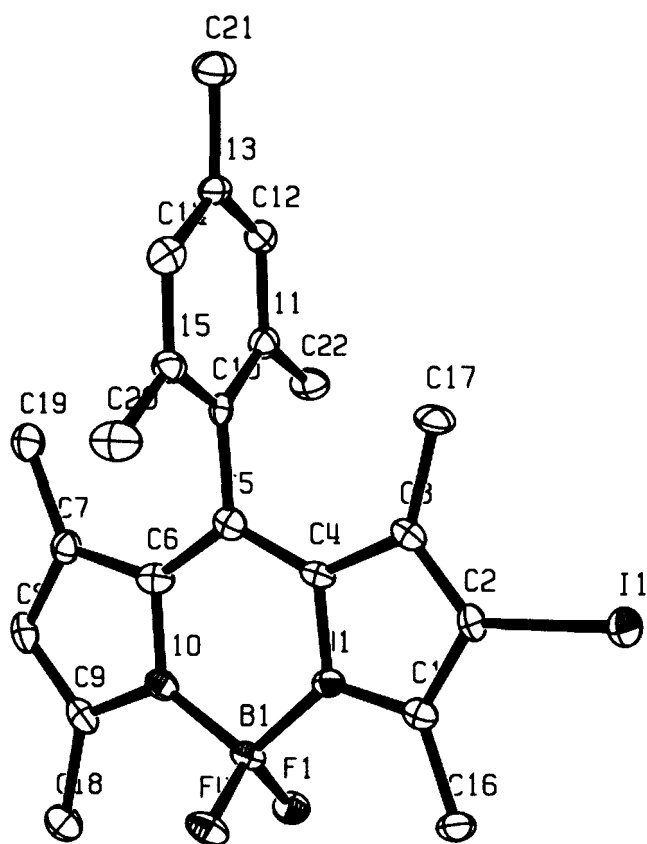


Figure 3.16. ORTEP diagram of PBI with 50% thermal ellipsoid probability. Hydrogen atoms were omitted for clarity.

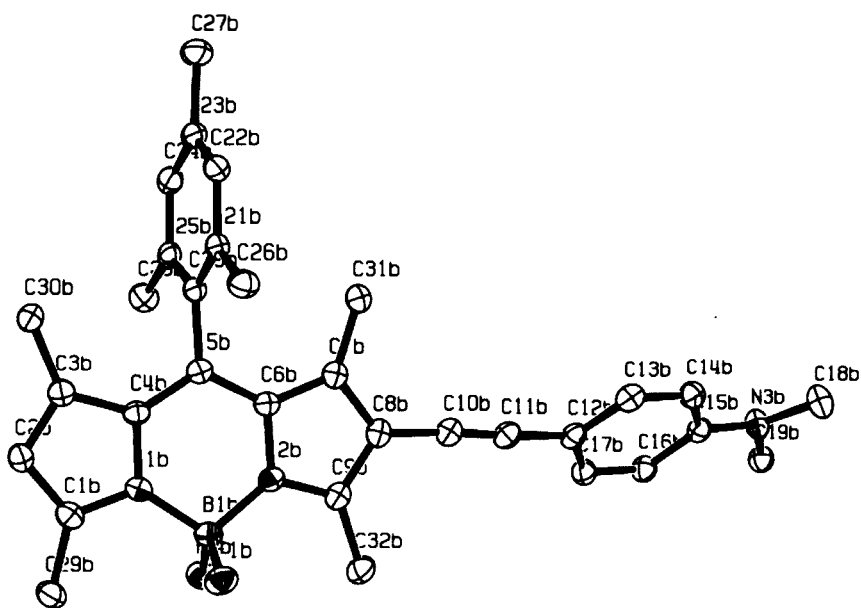
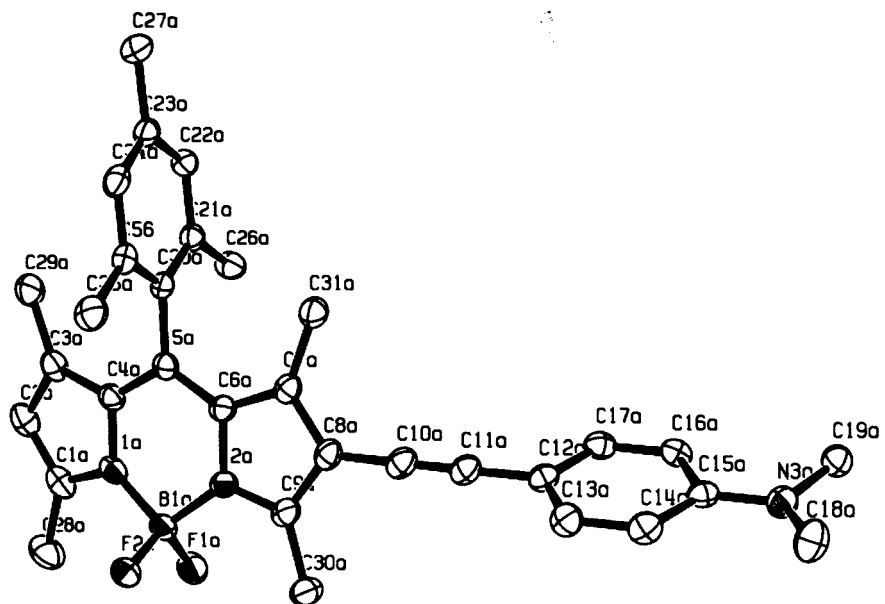


Figure 3.17 ORTEP diagrams of DPB with 50% thermal ellipsoid probability. Two molecules are existed in one asymmetric unit. Hydrogen atoms were omitted for clarity



The single crystals of C<sub>6</sub>PBI<sub>2</sub> were obtained from a methanol solution. Its ORTEP diagram was as shown in Figure 3.18. The boron has a tetrahedral geometry as the same as in PBI and DPB; this observation matched the observation in 8-HHQ-BODIPY molecules.<sup>(43)</sup> The BODIPY unit was perpendicular to benzene group in its *meso* position.

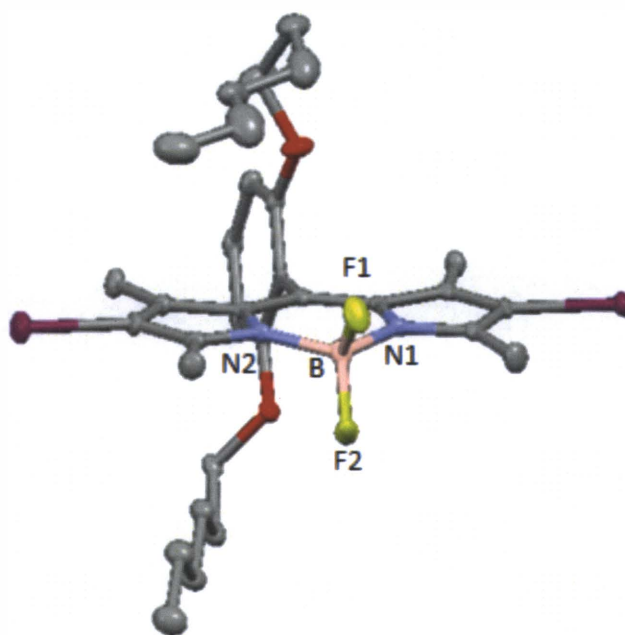


Figure 3.18. ORTEP diagram of C<sub>6</sub>PBI<sub>2</sub> with 50% thermal ellipsoid probability. Hydrogen atoms were omitted for clarity

Figure 3.19 showed the ORTEP diagram of the single-crystal structure of C<sub>6</sub>DPBI. The crystals were crystallized from a chloroform/methanol solution. The bond angle of the boron B has a tetrahedral geometry with BODIPY unit and perpendicular to benzene unit. The selected bond lengths were detailed in Table 3.2. The most interesting result in this molecule was that the BODIPY core and the donor group were almost in the same plane. The crystallographic data of PBI, DPB, C<sub>6</sub>PBI<sub>2</sub>, and C<sub>6</sub>DPBI are listed in Table 3.2.

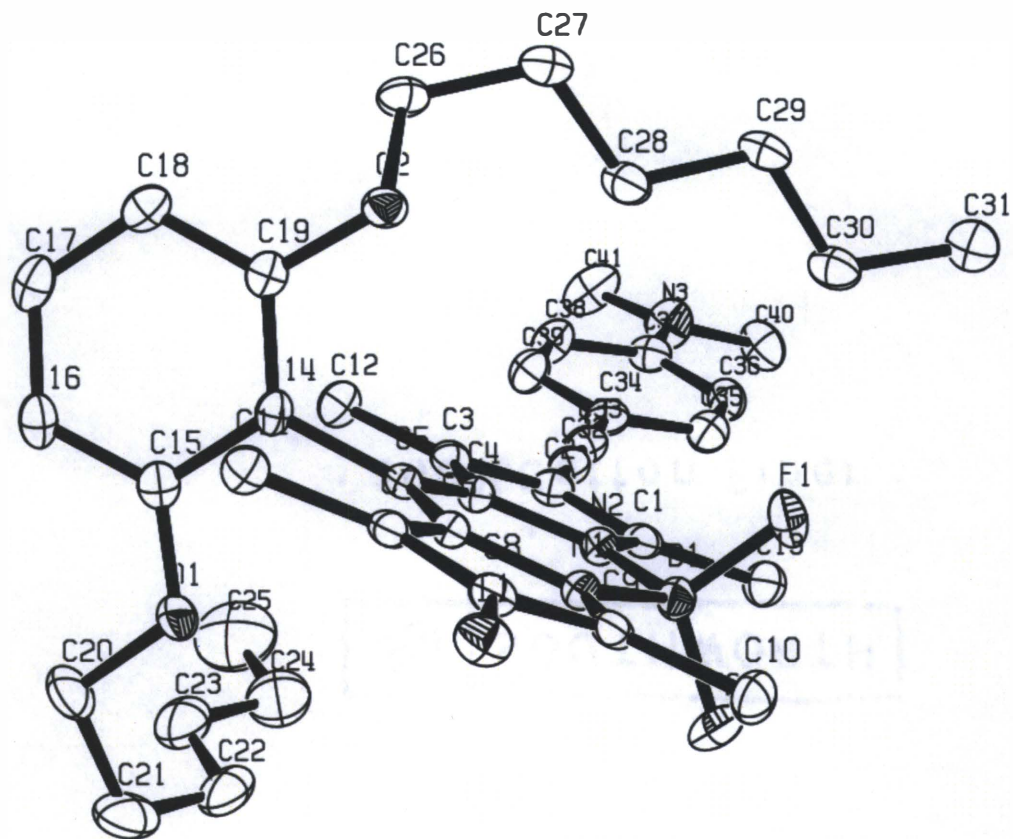


Figure 3.19. ORTEP diagram of C<sub>6</sub>DPBI with 50% thermal ellipsoid probability. Hydrogen atoms were omitted for clarity

Table 3.1. Structural parameters for PBI, DPB, C<sub>6</sub>PBI<sub>2</sub>, and C<sub>6</sub>DPBI

	PBI	DPB	C <sub>6</sub> PBI <sub>2</sub>	C <sub>6</sub> DPBI
Chemical Formula	C <sub>22</sub> H <sub>24</sub> B F <sub>2</sub> I N <sub>2</sub>	C <sub>32</sub> H <sub>34</sub> B F <sub>2</sub> N <sub>3</sub>	C <sub>31</sub> H <sub>41</sub> B F <sub>2</sub> I <sub>2</sub> N <sub>2</sub> O <sub>2</sub>	C <sub>41</sub> H <sub>51</sub> B F <sub>2</sub> I N <sub>3</sub> O <sub>2</sub>
Formula Weight	492.14	509.43	776.27	793.55
Crystal color	Orange	Red	Red-orange	Purple
T/K	100(2)	100(2)	100(2)	100(2)
$\lambda/\text{\AA}^{\circ}$	1.54178	1.54178	1.54178	1.54178
Z	4	4	2	2
F(000)	984	1080	772	820
Space group	P n a 21 P 2c -2n	P -1 -P 1	P -1 -P 1	P -1 -P 1
Crystal System	Orthorhombic	Triclinic	Triclinic	Triclinic
Cell dimensions				
a/ $\text{\AA}$	15.9793(3)	8.1527(3)	9.6794(2)	9.4191(4)
b/ $\text{\AA}$	12.1975(3)	15.3925(5)	10.3912(3)	10.4719(4)
c/ $\text{\AA}$	10.7613(2)	22.0290(7)	16.8611(4)	21.6589(8)
$\alpha(^{\circ})$	90	86.567(2)	87.899(1)	76.224(2)
$\beta(^{\circ})$	90	86.084(2)	82.009(1)	87.060(2)
$\gamma(^{\circ})$	90	77.629(2)	68.776(1)	67.692(2)
Volume/ $\text{\AA}^3$	2097.46(8)	2691.03(16)	1565.35(7)	1917.78(13)
Refl. Collected/independent	3350/3097	9626/8357	5614/5225	6867/6564
R <sub>int</sub>	0.0367	0.0355	0.0388	0.0387
Data/restraints/parameters	3349/1/260	9626/0/703	5614/0/367	6867/0/459
Goodness-of-fit on F <sup>2</sup>	1.026	1.051	1.073	1.100
Final R indices [I>2s(1)]	R <sub>1</sub> =0.0365 wR <sub>2</sub> =0.0938	R <sub>1</sub> =0.0424 wR <sub>2</sub> =0.0980	R <sub>1</sub> =0.0366 wR <sub>2</sub> =0.0751	R <sub>1</sub> =0.0259 wR <sub>2</sub> =0.0660
R indices (all data)	R <sub>1</sub> =0.0421 wR <sub>2</sub> =0.0980	R <sub>1</sub> =0.0365 wR <sub>2</sub> =0.0938	R <sub>1</sub> =0.0281 wR <sub>2</sub> =0.0706	R <sub>1</sub> =0.0241 wR <sub>2</sub> =0.0614

Table 3.2. Selected bond length and bond angles for PBI, DPB, C<sub>6</sub>PBI<sub>2</sub>, and C<sub>6</sub>DPBI

Dye		Bond length Å		Bond angle Å
PBI	B-F1	1.383	N2-B-F1	110.52
	B-F2	1.399	N1-B-F2	109.08
DPB	B-F1	1.384	N2-B-F1	110.45
	B-F2	1.390	N1-B-F2	110.70
C <sub>6</sub> PBI <sub>2</sub>	B-F1	1.379	N2-B-F1	110.37
	B-F2	1.383	N1-B-F2	109.92
C <sub>6</sub> DPBI	B-F1	1.385	N2-B-F1	110.11
	B-F2	1.390	N2-B-F1	109.62

## 3.2. Photophysical Properties

### 3.2.1. UV-Vis Absorption Spectra in Solution

UV-visible absorption spectra of synthesized dyes PB, PBI, PBI<sub>2</sub>, DPBI, and HHK1 were obtained in CHCl<sub>3</sub>. They are shown in Figure 3.20. All the five dyes exhibited strong absorption bands between 450 and 650 nm; however, how the absorption coefficients and broadness of the spectra were dependent upon the substituents on the BODIPY core. PB dye without any substituent exhibited a strong and narrow band at 503 nm. When I atoms or a donor group were added to 2 and (or) 6 positions, the spectra red-shifted and became broader. The wavelengths with maximal absorption of PBI, PBI<sub>2</sub>, and DPBI were at 517, 535, and 555 nm, respectively. When the acceptor was added the absorption was red-shifted further and the absorption band became much broader. This is a good indication that this dye might be a good BODIPY dye for DSCs. The absorption coefficient or the maximal absorption wavelength spectra of second series of dyes with 2, 6-bis (hexyloxy) benzene group was increased slightly farther than the first task dyes. The increasing of the absorption coefficient increased in this order of C<sub>6</sub>PB (508 nm) < C<sub>6</sub>PBI<sub>2</sub> (538 nm) < C<sub>6</sub>DPBI (554 nm) < (HHK2 (576 nm)). By comparing the absorption spectra of first series with the second series, the second series dyes exhibited much broader absorption. For examples, the absorption wavelength of PB is 503 while that for the C<sub>6</sub>PB is 508 nm. The similar trend was also observed in other corresponding dyes as shown in Table 3.3. However, the absorption wavelength was slightly blue-shifted in BODIPY when the mesityl group was replaced by 2,6-bis(hexyloxy)benzene as shown in Figure 3.21.



### 3.2.1.a. UV-Vis Absorption in Solution of HHK1 Dyes

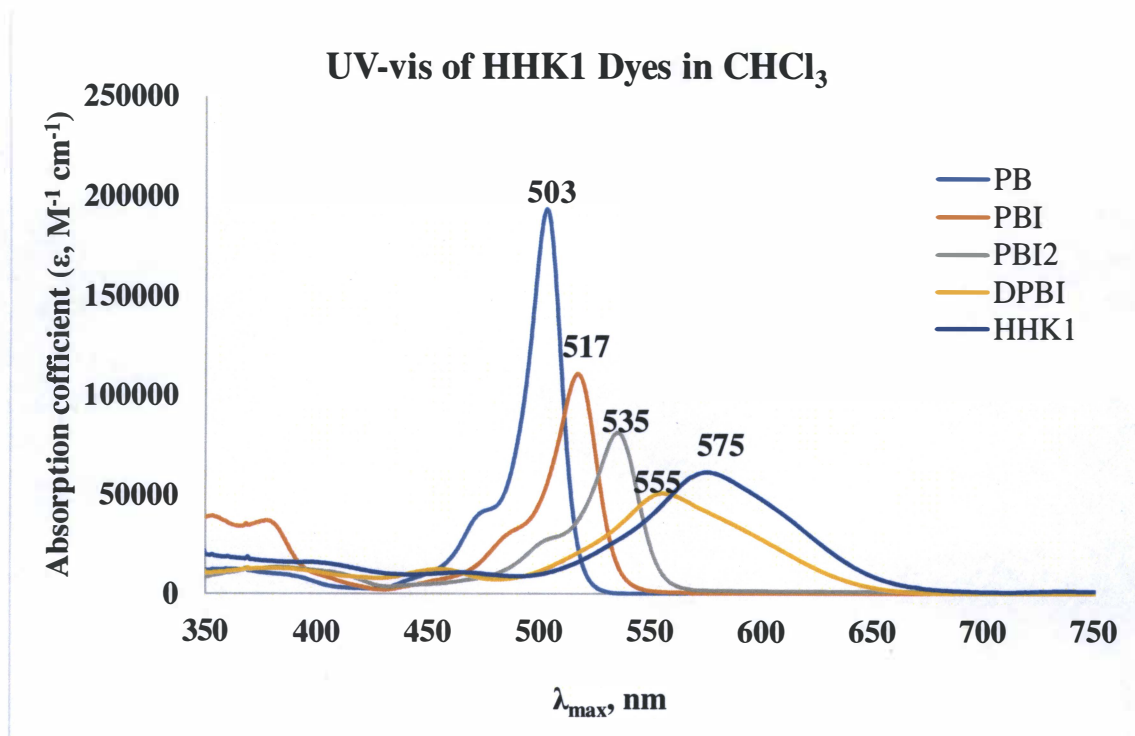


Figure 3.20. Absorption spectra of PB, PBI, PBI<sub>2</sub>, DPBI, and HHK1 dyes in CHCl<sub>3</sub> solution at room temperature.

Table 3.3. The concentrations, volume, absorption maximum and absorption coefficients of dyes PB, PBI, PBI<sub>2</sub>, DPBI, and HHK1 in CHCl<sub>3</sub> at room temperature

Dye	Volume (μL) of dye added in the cuvette	Absorbance at λ <sub>max</sub>	C1 (mol/L <sup>-1</sup> )	C2 (mol/L <sup>-1</sup> )	λ <sub>max</sub> (nm, ε, M <sup>-1</sup> cm <sup>-1</sup> )
PB	40	0.8	3.2 × 10 <sup>-4</sup>	4.2 × 10 <sup>-6</sup>	503 (1.9 × 10 <sup>5</sup> )
PBI	50	0.4	2.4 × 10 <sup>-4</sup>	3.9 × 10 <sup>-6</sup>	517 (1.0 × 10 <sup>5</sup> )
PBI <sub>2</sub>	60	0.3	2.1 × 10 <sup>-4</sup>	4.1 × 10 <sup>-6</sup>	535 (7.3 × 10 <sup>4</sup> )
DPBI	80	0.3	1.9 × 10 <sup>-4</sup>	4.9 × 10 <sup>-6</sup>	555 (6.1 × 10 <sup>4</sup> )
HHK1	100	0.2	1.2 × 10 <sup>-4</sup>	3.8 × 10 <sup>-6</sup>	575 (5.3 × 10 <sup>4</sup> )

3.2.1.b. UV-Vis Absorption in Solution of C<sub>6</sub>PB, C<sub>6</sub>PBI<sub>2</sub>, C<sub>6</sub>DPBI and HHK2 dyes in CHCl<sub>3</sub>

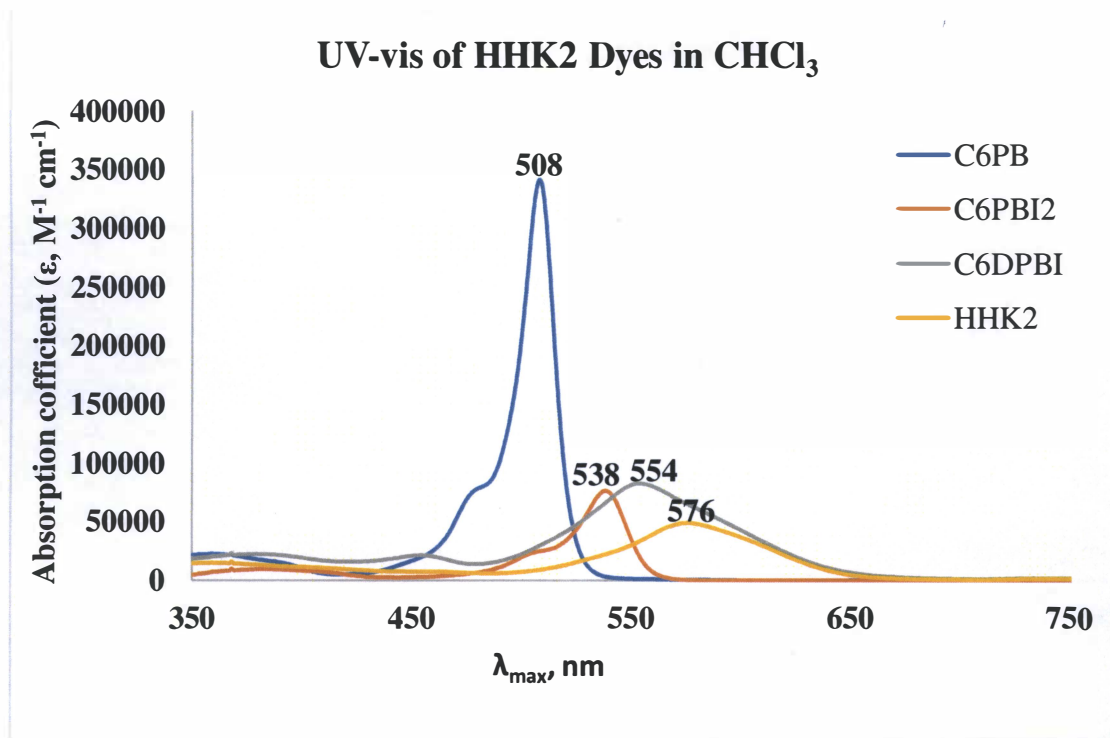


Figure 3.21. Absorption spectra of C<sub>6</sub>PB, C<sub>6</sub>PBI<sub>2</sub>, C<sub>6</sub>DPBI, and HHK2 in CHCl<sub>3</sub> solution at room temperature

Table 3.4. The concentrations, volume, absorption maximum and absorption coefficient data of dyes C<sub>6</sub>PB, C<sub>6</sub>PBI<sub>2</sub>, C<sub>6</sub>DPBI and HHK2 in CHCl<sub>3</sub> at room temperature

Dye	Volume (μL) of dye added in the cuvette	Absorbance at (λ <sub>max</sub> )	C1 (mol/L <sup>-1</sup> )	C2 (mol L <sup>-1</sup> )	λ <sub>max</sub> (ε, M <sup>-1</sup> cm <sup>-1</sup> )
C <sub>6</sub> PB	40	0.9	2.1×10 <sup>-4</sup>	2.8×10 <sup>-6</sup>	508 (3.4 ×10 <sup>5</sup> )
C <sub>6</sub> PBI <sub>2</sub>	60	0.2	1.5 ×10 <sup>-4</sup>	2.9×10 <sup>-6</sup>	538 (6.8 ×10 <sup>4</sup> )
C <sub>6</sub> DPBI	50	0.2	1.5 ×10 <sup>-4</sup>	2.5×10 <sup>-6</sup>	554 (8.0 ×10 <sup>4</sup> )
HHK2	100	0.1	9.3 ×10 <sup>-5</sup>	3.0×10 <sup>-6</sup>	576 (3.3 ×10 <sup>4</sup> )

### 3.2.2. UV-Vis Absorption on TiO<sub>2</sub> Film

Absorption spectra of HHK1 and HHK2 on TiO<sub>2</sub> films were shown in Figures 3.22 and 3.23. The absorption peaks were blue-shifted and become narrower than their respective absorption spectra in solution. This phenomenon was interpreted as being probably due to the aggregation of the dyes on TiO<sub>2</sub> surface.

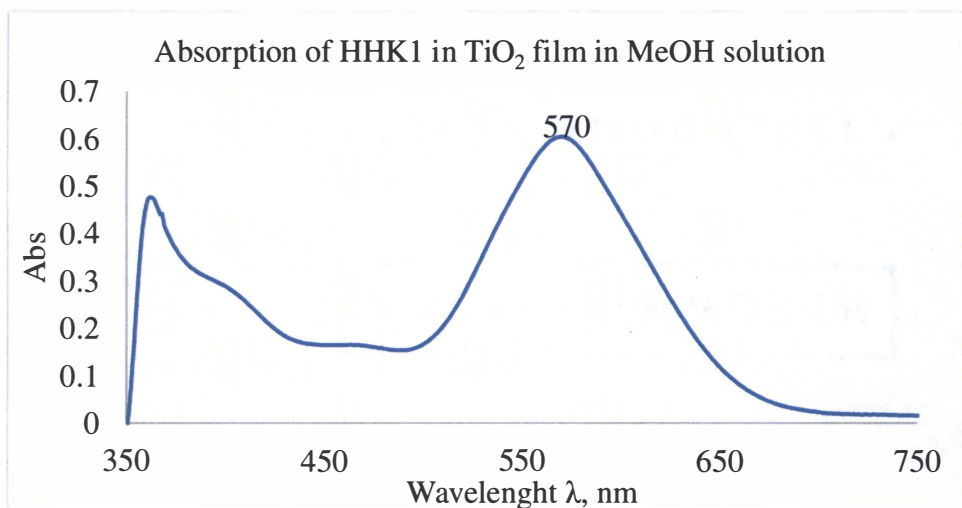


Figure 3.22. Absorption spectrum of HHK1 on TiO<sub>2</sub> film

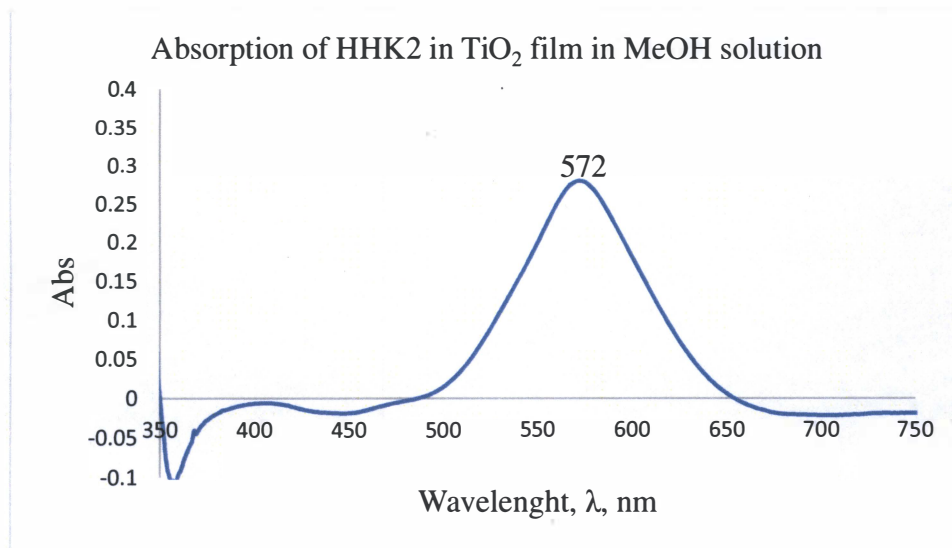


Figure 3.23. Absorption spectrum of HHK2 on TiO<sub>2</sub> film



### 3.2.3. Calibration Curve

In order to determine the dye-loading density of HHK1 and HHK2 on TiO<sub>2</sub> nanoparticle films, calibration curves in 0.1 M NaOH solution (DMF/H<sub>2</sub>O, v/v 25:5) were obtained. As shown in Figure 3.24 and Figure 3.25, linear fitting of experimental data gave two formulas  $y=6159x+0.063$  and  $y=96946x-0.0781$  for HHK1 and HHK2, respectively. The formula will be used to determine the concentration of de-adsorbed dye in 0.1M NaOH solution.

Table 3.5. Concentration, volume and maximum wavelength data of standard solutions of HHK1 in 0.1M NaOH solutions ((DMF/H<sub>2</sub>O, v/v 25:5)

Volume (μL) of HHK1 added in cuvette.	$\lambda_{\max}$ (nm)	Absorbance @582 nm	HHK1 concentration in (M)
100	583	0.27	$3.81 \times 10^{-6}$
200	582	0.55	$7.37 \times 10^{-6}$
300	582	0.72	$1.07 \times 10^{-5}$
400	582	0.88	$1.38 \times 10^{-5}$
500	582	1.11	$1.68 \times 10^{-5}$

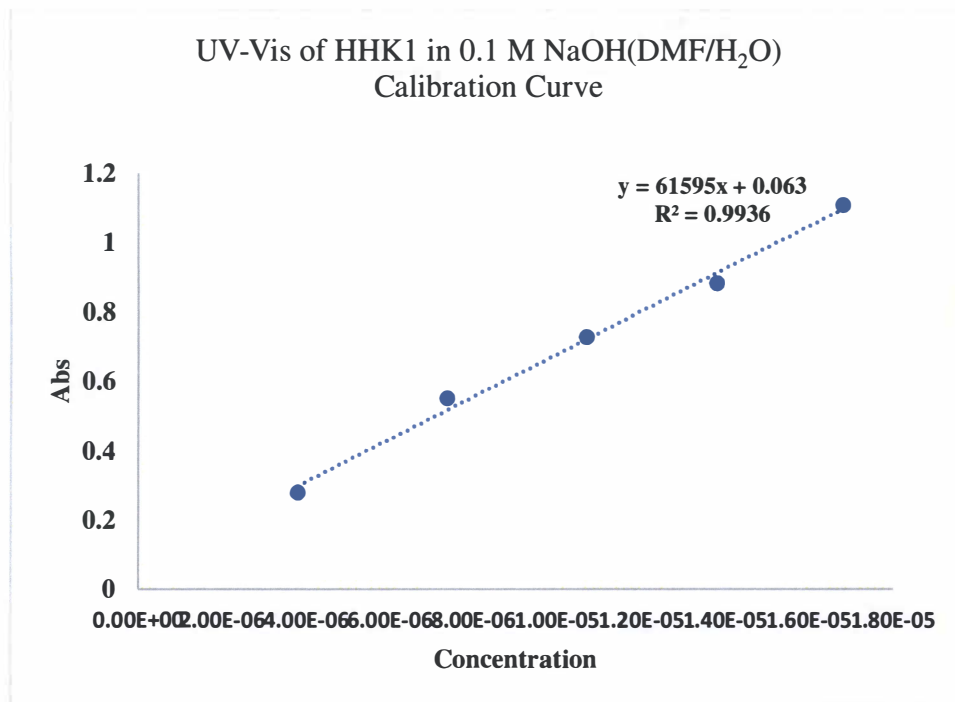


Figure 3.24. Calibration curve of HHK1 in 0.1 M NaOH (DMF/H<sub>2</sub>O,v/v 25:5) solution

Table 3.6. Concentration, volume and maximum wavelength for HHK2 in 0.1M NaOH solution  
(DMF/H<sub>2</sub>O, v/v 25:5)

Volume ( $\mu$ L) of HHK2 added in the cuvette	$\lambda_{\max}$ (nm)	Absorbance @ 581 nm	HHK2 concentration in (M)
100	582	0.22	$2.98 \times 10^{-6}$
200	581	0.47	$5.77 \times 10^{-6}$
300	581	0.72	$8.40 \times 10^{-5}$
400	581	0.95	$1.08 \times 10^{-5}$
500	581	1.22	$1.32 \times 10^{-5}$

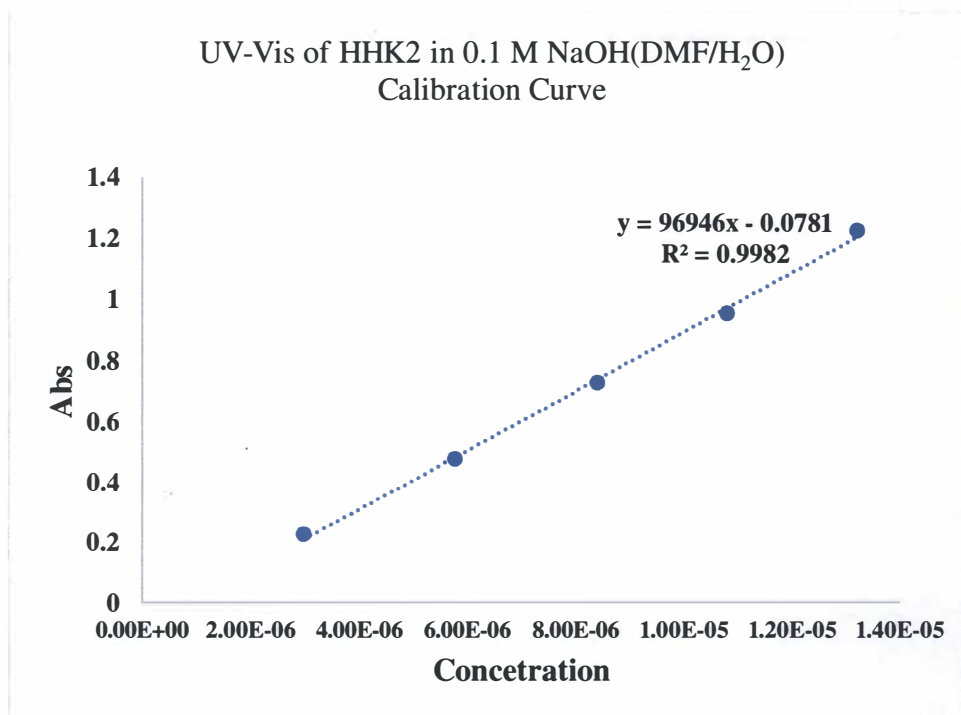


Figure 3.25. Calibration curve of HHK2 in 0.1 M NaOH (DMF/H<sub>2</sub>O, v/v 25:5) solution

#### 3.2.4. Dye-loading Density in TiO<sub>2</sub>

The adsorbed dye on the TiO<sub>2</sub> films came off the TiO<sub>2</sub> nanoparticles quickly after the films were immersed in 0.1M NaOH solution. The color of the solution was deep purple, which was quite similar to those in chloroform. The resulting solution was used directly for the measurement of absorption without dilution. Figure 3.26 and Figure 3.27 show the absorption spectra of de-adsorbed HHK1 and HHK2 in 0.1M NaOH solution. The spectra are very similar to those in CHCl<sub>3</sub>, however the peak positions shifted to longer wavelengths. This is probably due to the formation of ionic salt of HHK1 and HHK2 in the presence of NaOH. Table 3.7 shows the absorbance of the solution (abs @581 nm), concentrations calculated using calibration curves (c) the mass of TiO<sub>2</sub> used ( $m_{\text{TiO}_2}$ ), and the dye-loading density (d). In the calculation, the specific surface area of TiO<sub>2</sub> nanoparticles was 760000 cm<sup>2</sup>/g. It was found that HHK1 had higher dye loading density than HHK2. This finding was in consistent with different size of HHK1 and HHK2. In HHK1, the substituent in the meso position is a mesityl group, whereas in HHK2 it is a 2,6-bis(hexoxy)benzene group. As their single-crystal structures show that two hexoxy groups were located on the two sides of the BODIPY core and occupied much large space than mesityl group, as a result, HHK2 exhibited a larger footprint than HHK1. Therefore, the number of molecules adsorbed on the TiO<sub>2</sub> will be less.

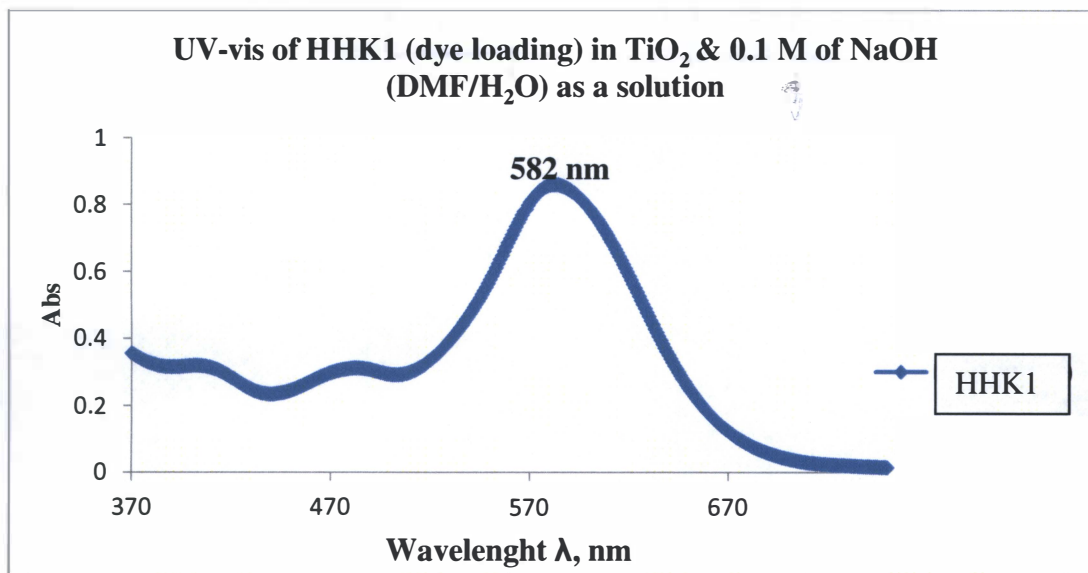


Figure 3.26. Absorption of HHK1 in 0.1 M of NaOH (DMF/H<sub>2</sub>O, v/v, 25:5)

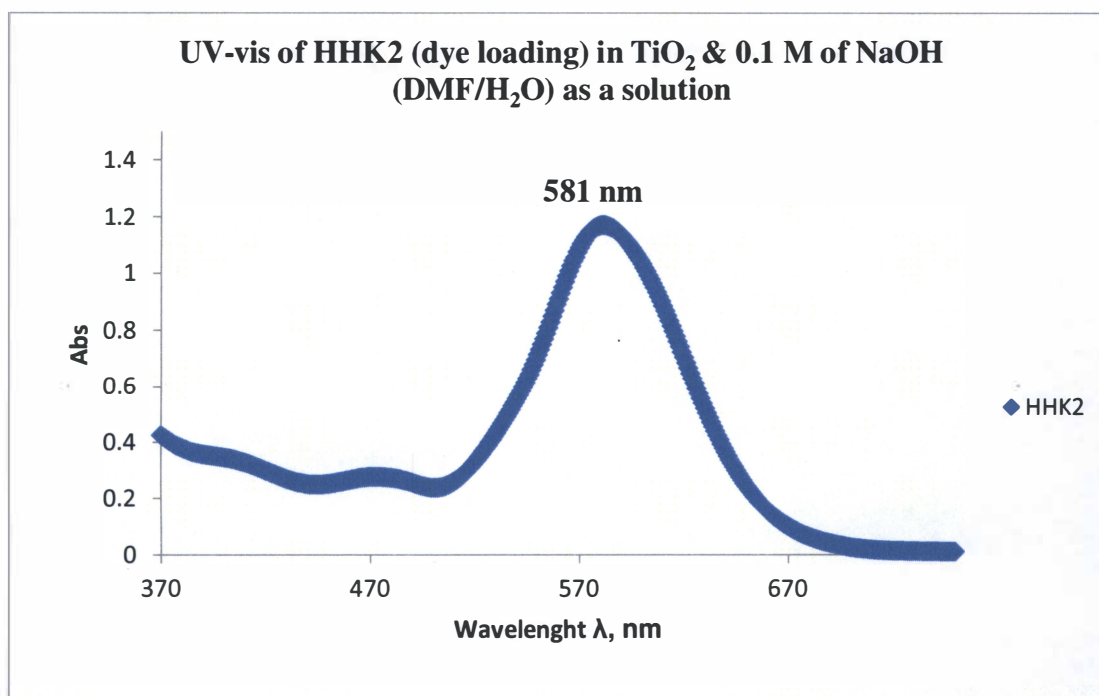


Figure 3.27. Absorption of HHK2 in 0.1 M of NaOH (DMF/H<sub>2</sub>O, v/v 25:5)

Table 3.7. The results of dye loading density measurement

Dye name	$m_{\text{TiO}_2}$ (g)	$A_{\text{TiO}_2}$ ( $\text{cm}^2$ )	Abs ( $\lambda_{\text{max}}$ )	$C_{\text{Dye}}$ (mol/L)	Total # of dye (mol)	$V_{\text{total}}$ (L)	D ( $\text{mol}/\text{cm}^2$ )
HHK1	0.00175	760000	0.85	$1.29393 \times 10^{-5}$	$5.17572 \times 10^{-8}$	0.004	$3.89152 \times 10^{-11}$
HHK2	0.00218	760000	1.16	$1.28711 \times 10^{-5}$	$5.14844 \times 10^{-8}$	0.004	$3.10746 \times 10^{-11}$

### 3.2.5. Fluorescence (FL)

The fluorescence data of PB, PBI, PB I<sub>2</sub>, DPBI, HHK1 and C6PB, C6PBI<sub>2</sub>, C6DPBI, and HHK2 dyes were shown in Table 3.3 and 3.4. PB and C6PB gave strong fluorescence, and the peaks were narrow. Adding two iodine atoms to PB and C6PB increased  $\lambda_{\text{em}}$  and decreased the intensity. When the donor group introduced to DPBI and C6DPBI the fluorescence of the dyes were almost completely quenched because the heavy-metal atom effect.<sup>(44)</sup> The fluorescence spectra of the final compounds HHK1 and HHK2 were shown in Figures 3.28 and 3.29. For HHK1, the maximal emission peak was at 592 nm. The maximal emission peaks were shifted toward longer wavelength at 670 nm in HHK2 and it was broader than HHK1 peak. The data were summarized in Tables 3.8

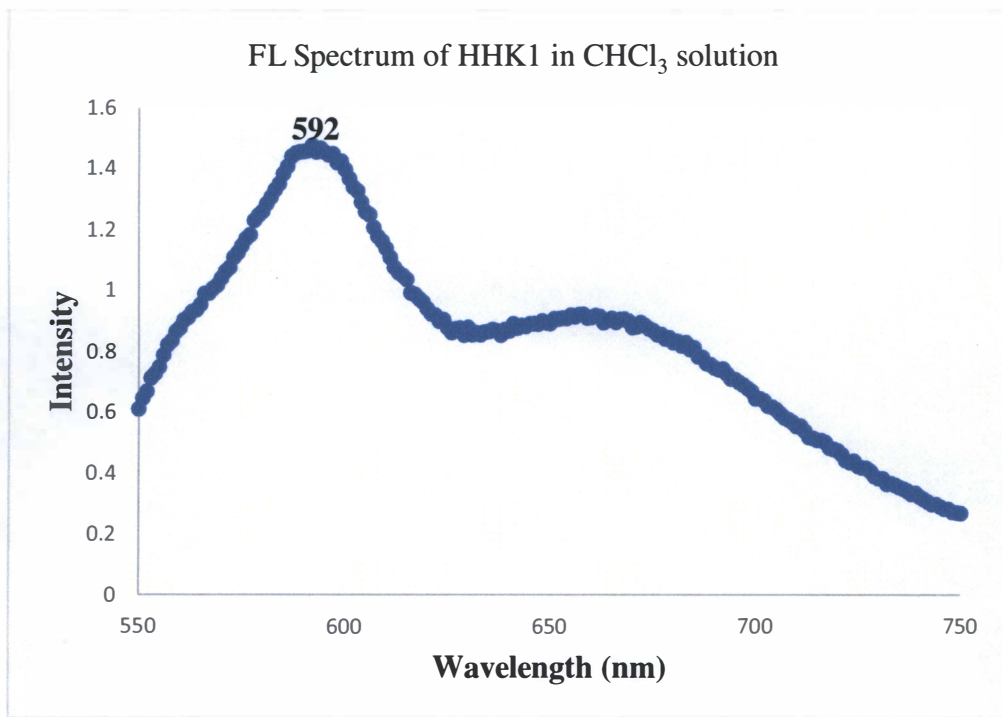


Figure 3.28. Fluorescence Spectrum of HHK1 in CHCl<sub>3</sub> solution

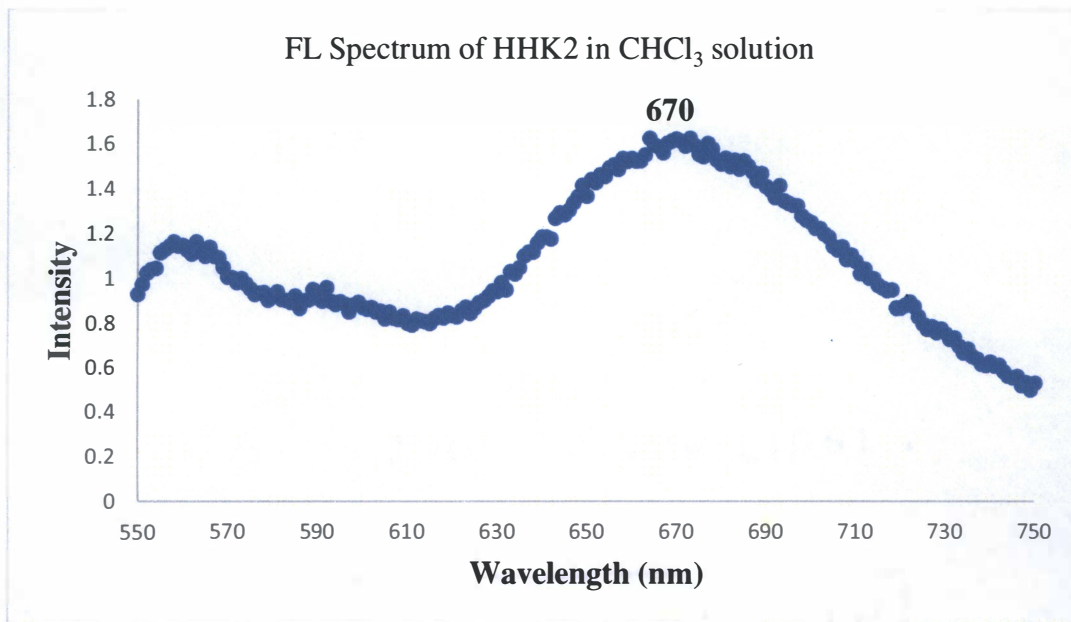


Figure 3.29. Fluorescence Spectrum of HHK2 in CHCl<sub>3</sub> solution



Table 3.8. The fluorescence data of the synthesized BODIPY dyes in CHCl<sub>3</sub>

Dye	$\lambda_{em}$ (nm)	$\lambda_{ex}$ (nm)	Dye	$\lambda_{em}$ (nm)	$\lambda_{ex}$ (nm)
PB	526	375	C <sub>6</sub> PB	548	375
PBI	530	375	C <sub>6</sub> PBI		
PBI <sub>2</sub>	550	375	C <sub>6</sub> PBI <sub>2</sub>	549	375
DPBI	536	375	C <sub>6</sub> DPBI	522	375
HHK1	592	575	HHK2	670	375



## CHAPTER 4

### PHOTOVOLTAIC PROPERTIES

#### 4.1. J-V Curves

Grätzel type dye-sensitized solar cells were fabricated and tested under AM1.5 condition. The thickness of the TiO<sub>2</sub> film was not measured due to the limitation of instrumentation; however, the thickness was estimated to be around 17 μm since we were following the same procedure reported by He *et al.* <sup>(41)</sup> The prepared TiO<sub>2</sub> films were examined under a stereo microscopy. The film was opal and the surface was smooth. Some cracks were also observed. After the films were immersed in dye solution for four hours, the TiO<sub>2</sub> films exhibited a deep purple color as shown in Figure 4.1. The electrolyte was completely inside the chamber of cell.

Figures 4.2 and 4.3 showed the *J-V* curves of two devices. The photovoltaic data were summarized in Table 4.1. The J<sub>SC</sub> of HHK1 was greater than that of HHK2. The V<sub>OC</sub> were quite similar, although it was slightly higher in HHK1 (0.55 V) than (0.53 V). Although the HHK2 sensitized cell gave higher FF than HHK1 sensitized cell, the over performance of HHK1 was better than HHK2. HHK1 cell showed an efficiency value at 0.87% compared with 0.57% of HHK2. The efficiency of HHK1 and HHK2 was quite low compared to several other BODIPY dyes with a D-π-A configuration in the literature. <sup>(16)</sup> This is an indication that other factors may play a role. For example, the FTO glass may not be cleaned thoroughly, the sintering process may not optimal and dye loading process may also not optimized. Although both dyes showed low efficiency, but, surprisingly, the efficiency of HHK1 was slightly higher than HHK2, which indicated that the long hexyloxy groups in HHK2 did not prevent the aggregation of the dye. The data of the absorption in TiO<sub>2</sub> film showed the peaks of

HHK1 and HHK2, which indicated the aggregation of HHK1 and HHK2 in TiO<sub>2</sub> surface. Thus, adding long chain enhanced the absorption wavelengths of the dyes, but not improved the efficiency in our cases.

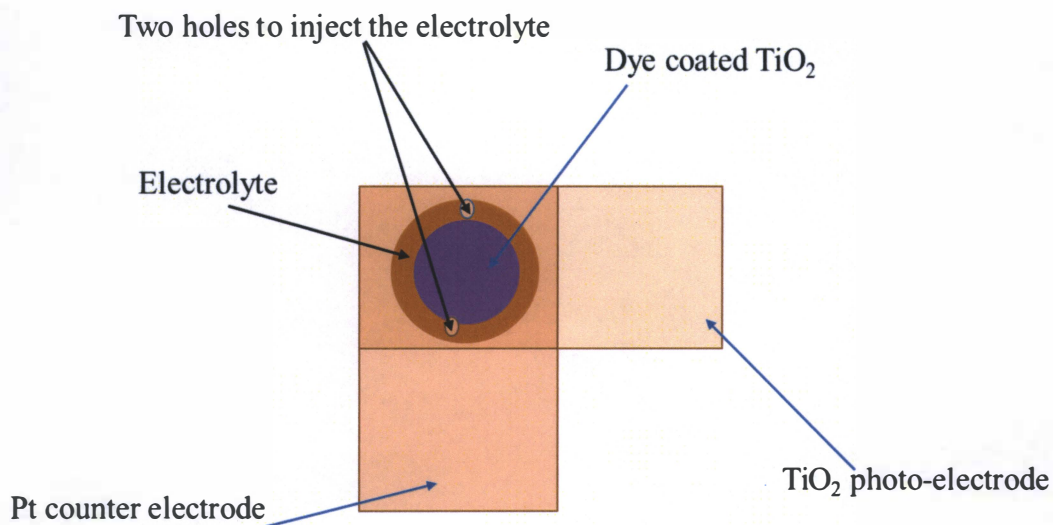


Figure 4.1. Optical image of dye-coated TiO<sub>2</sub> film and assembled DSCs.

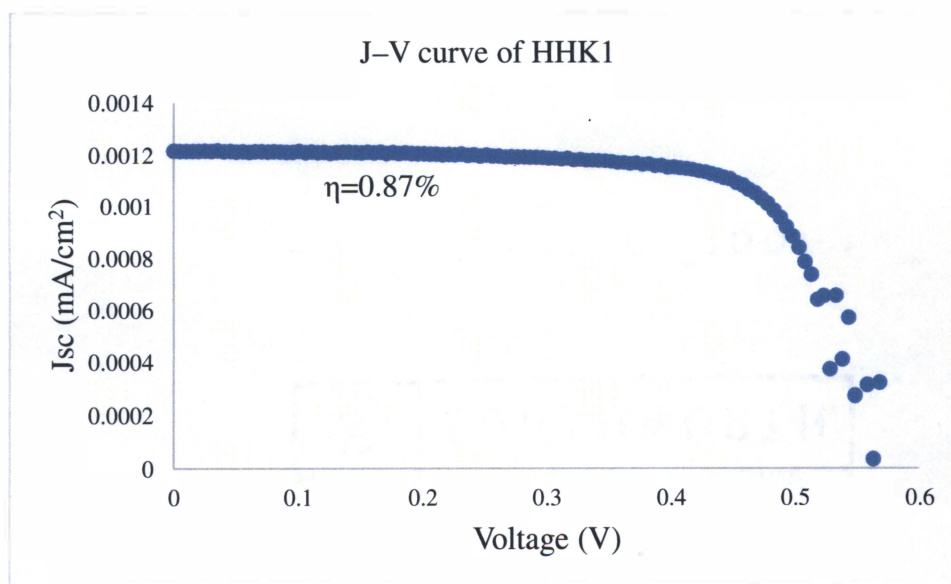


Figure 4.2. J-V curve of HHK1 sensitized solar cells

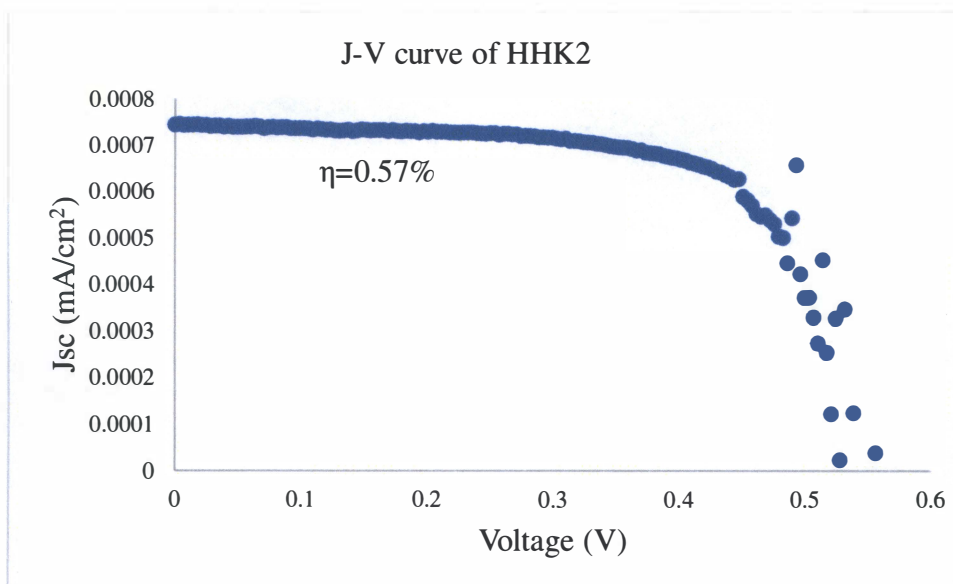


Figure 4.3. J–V curve of HHK2 sensitized solar cells

Table 4.1. Photovoltaic data of HHK1 and HHK2 dyes sensitized solar cells (dye loading time 4h)

Dye	$J_{sc}$ (mA/cm <sup>2</sup> )	Voc(V)	FF %	$\eta$ %
HHK1	2.16	0.55	72.54	0.87
HHK2	1.32	0.53	80.75	0.57

## CHAPTER 5

### CONCLUSION

The sun is an attractive energy resource that could meet world energy demands. The availability and renewability of solar energy make solar cells a promising alternative to other energy resources. Solar energy can be converted into electricity using solar cells. Dye-sensitized solar cells (DSCs) are of importance for the efficient conversion of solar energy to electricity. However, it is challenging to make the process more efficiency and low-cost. Inorganic semiconductors including CdS and Cu<sub>2</sub>S have been studied for solar cells, however, the high toxicity and degradation of these materials at higher humidity makes these materials less desirable. Organic solar cells including dye-sensitized solar cells have been studied widely because of their low-cost thin film and flexibility. Ruthenium (Ru) based dyes have been investigated extensively because it has shown above 11% of energy conversion efficiency of light to electricity. However, the environmental issue and the limited resources for ruthenium since it is a rare metal open the gate for organic dyes as a replacement of ruthenium. Organic dyes, such as porphyrin dyes are low-cost and easy to prepare. Many organic dyes based on donor-( $\pi$ -spacer)-acceptor system have been studied to find a replacement for metal complex dyes. Porphyrin dyes have been reached an energy conversion efficiency of greater than 12% using donor - $\pi$ - acceptor.

BODIPY dyes have emerged as potential dyes for DCS for several reasons: strong absorption in the visible to near-IR range with high extinction coefficients, large quantum yields, good solubility in organic solvents, and photostability. Therefore, of the BODIPY dyes show greater promise than many proposed sensitizers. Researchers have investigated, and synthesized novel BODIPY dyes for DSCs. Studies on *meso* substituted BODIPY dyes showed poor

photovoltaic performance. Several studies have shown the promise of 2 or 6-position substituted BODIPY dyes for high-performance DSCs. However, there is a need for developing new BODIPY dyes with broader light absorption capability and stronger binding strength on the TiO<sub>2</sub> surface for efficient and stable DSCs.

In this study, two dyes with a donor- $\pi$ -spacer-acceptor configuration were synthesized and tested in dyes-sensitized solar cells. HHK1 with mesityl group showed higher efficiency than HHK2, with a 2,6-bis (hexyloxy) benzene group. The later was thought to be a good replacement for mesityl group to prevent the aggregation. However, this research results showed the opposite. HHK2 did not prevent dye aggregation on TiO<sub>2</sub> surface as expected. This would be explained by the planner geometry of the dye C6DPBI's crystal structure. Moreover, the absorption on TiO<sub>2</sub> was blue- shifts for both dyes. The conclusion of this work is that replacing mesityl group by hexyloxy groups did increase the absorption wavelength; however, it did not improve the dye binding capability on TiO<sub>2</sub> surface. The absorption spectra of HHK1 and HHK2 (final dyes) were broad and shifted to the red region to 575 nm and 576 nm respectively. Moreover, the maximal emission was increased to larger wavelengths for HHK2. However, it did not improve the photovoltaic performance of dyes.

## REFERENCES

1. P. A. Lynn, *Electricity from sunlight*. **2010**
2. History of Solar Energy in California - Go Solar California. (n.d.). Retrieved from <http://www.gosolarcalifornia.ca.gov/about/gosolar/california.php>.
3. A. Hagfeldt, G. Boschloo, L. Sun, L. Kloo and H. Pettersson, *Chem. Rev.*, **2010**, *110*, 6595–6663.
4. B. O'Regan and M. Grätzel, *Nature*, **1991**, *353*, 737-740.
5. Z. Yao; M. Zhang; R. Li.; L. Yang; Y. Qiao and P. Wang. *Angew. Chem. Int. Ed.*. **2015**, DOI: 10.1002/anie.201502497.
6. L. Si and H. He; *J. Phys. Chem. A*, **2014**, *118*, 3410–3418
7. S. Mathew; A. Yella; P. Gao; R. Humphry-Baker; F. E. Curchod Basile; N. Ashari-Astani; I. Tavernelli; U. Rothlisberger; M. K. Nazeeruddin and M. Grätzel. *Nat. Chem.* **2014**, *6*, 242-247.
8. J. Yang; P. Ganesan; J. Teuscher; T. Moehl; Y. Kim; C. Yi; P. K. Pei; T. W. Holcombe; M. K. Nazeeruddin; J. Hua; S. M. Zakeeruddin; H. Tian and M. Grätzel. *J. Am. Chem. Soc.* **2014**. *136*, 5722-5724.
9. P. Qin; S. Paek; M. Dar; N. Pellet; J. Ko; M. Grätzel and M. K. Nazeeruddin. *J. Am. Chem. Soc.*, **2014**, *136*, 8516–8519
10. P. Wang, S. M. Zakeeruddin, J. E. Moser and M. K. Nazeeruddin. *Adv. Mater.* **2004**, *16*, 1806–1811.
11. R. Y. Ogura; S. Nakane; M. Morooka; M. Orihashi; Y. Suzuki and K. Noda. *Appl. Phys. Lett.* **2009**, *94*, 073308-1 – 0733083
12. A. Treibs and F. H. Kreuzer *Justus Liebigs Ann. Chem.* **1968**, *718*, 208.

13. M. Shrestha; L. Si; C. W. Chang; H. He; A. Sykes; C. Y. Lin and E. W. G. Diau, *J. Phys. Chem. C*, **2012**, *116*, 10451–10460
14. H. He; A. Gurung; L. Si and A. G. Sykes; *Chem. Comm.*, **2012**, *48*, 7619-7621
15. K.C. Kim, C. Y. Lee, D. Fairen-Jimenez, S. T. Nguyen, J. T. Hupp, and Lee, C. She, N. C. Jeong and J. T. Hupp, *Chem. Commun.* **2010**, *46*, 6090 - 6092.
16. P. S. Surya and G. Thumuganti, *Eur. J. Org. Chem.* **2014**, 4689–4707
17. M. K. Nazeeruddin; P. Pe'chy; T. Renouard; S. M. Zakeeruddin; G. B. Deacon; C. A. Bignozzi and M. Grätzel. *J. Am. Chem. Soc.* **2001**, *123*, 1613-1624.
18. Y. L. Chang and J. T. Hupp. *Langmuir*, **2010**, *26*, 3760–3765
19. T. Bessho; S. Zakeeruddin; C. Y. Yeh; E. G. Diau and M. Grätzel *Angew. Chem. Int. Ed.* **2010**, *49*, 6646-6649.
20. L. Si; H. He and K. Zhu, *New J. Chem.* **2014**, *38*, 1565-1572.
21. S. Mathew; A. Yella; P. Gao; R. Humphry-Baker; F. E. Curchod Basile; Ashari-Astani, N.; Tavernelli, I.; Rothlisberger, U.; M. K. Nazeeruddin and M. Grätzel, *Nat. Chem.* **2014**, *6*, 242-247.
22. W. M. Campbell; K. W. Jolley; P. Wagner; K. Wagner; P. J. Walsh; K. C. Gordon; L. Schmidt-Mende; M. K. Nazeeruddin; Q. Wang; M. Grätzel; and D. L. Officer. *J. Phys. Chem. C*, **2007**, *111* (32), pp 11760–11762
23. M. Maheshwar; L. Si; C-W Chang, H. He; A. Sykes; C. Lin and E. W. Diau. *J. Phys. Chem. C*, **2012**, *116*, 10451–10460
24. M. M. Zhang; C., Xi, L. Yao and G., Wu. *J. Phys. Chem.* **2015**, *117*, 28-36.
25. S. S. Prakash and G. Thumuganti. *Eur. J. Org. Chem.* **2014**, *22*, 4689-4707

26. M. Zhang; X. Lin; G. Wu, D., Yong; L. Xiu-Lin. Yong and S. Qin-Hua. *Org. Elect.* **2014**, *15*, 2079-2090.
27. A. Yella; H.-W. Lee; H. N. Tsao; C. Yi; A. K. Chandiran; M. K. Nazeeruddin; E. W.-G. Diao; C.-Y. Yeh; S. M. Zakeeruddin and M. Grätzel, *Science*, **2011**, *334*, 629-634
28. C. Jacky; H. Yim; and S. L. Laurel. *J. Org. Chem.* **2014**, *22*, 4689-4707.
29. M. Gouterman, *J. Mol. Spectrosc.* **1961**, *6*, 138-163.
30. H. Imahori; S. Hayyashi; H. Hayashi; A. Oguro; S. Eu; T. Umeyama and Y. Matano, *J. Phys. Chem. C* **2009**, *113*, 18406-18413.
31. R. K. Lammi; A. Ambroise; T. Balasubramanian; R. W. Wagner and D. F. Bocian. *J. Phys. Chem. B* **2001**, *105*, 5341-5352.
32. L. Luo; C. F. Lo; C. Y. Lin; I. J. Chang and E. W.G. Diao, *J. Phys. Chem. B* **2005**, *110*, 410-419.
33. M. Pastore and F. D. Angelis, *ACS Nano*, **2009**, *4*, 556-562
34. A. Loudet and K. Burgess, *Chem. Rev.*, **2007**, *107*, 4891-4932.
35. S. Erten-Ela; D. Yilmaz; B. Icli; Y. Dede; S. Icli and E. U. Akkaya, *Org. Lett.* **2008**, *10*, 3299-3302.
36. S. Hattori; K. Ohkubo; Y. Urano; H. Sunahara; T. Nagano; Y. Wada; N. V. Tkachenko; H. Lemmetyinen and S. Fukuzumi, *J. Phys. Chem. B* **2005**, *109*, 15638-15375.



37. S. Kolemen; O. A. Bozdemir; Y. Cakmak; G. Barin; S. Erten-Ela; M. Marszalek; J. H. Yum; S. M. Zakeeruddin; M. K. Na-zeeruddin; M. Grätzel and E. U. Akkaya, *Chem. Sci.* **2011**, *2*, 949–954.
38. S. Kolemen; Y. Cakmak; S. Erten-Ela; Y. Altay; J. Brendel; M. Thelakkat and E. U. Akkaya, *Org. Lett.* **2010**, *12*, 3812–3815.
39. M. Mao; J. Wang; Z. Xiao; S. Dai and Q. Song, *Dyes Pigm.* **2012**, *94*, 224–232.
40. Y. Kubo; D. Eguchi; A. Matsumoto; R. Nishiyabu; H. Yakush-iji; K. Shigaki and M. Kaneko, *J. Mater. Chem. A*, **2014**, *50*, 5258-5260.
41. L.Huang; J.Zhao; S. Guo; C.Zhang and J. Ma.*J. Org.Chem.*, **2013**,*78*, 5627–5637.
42. W. Wu; Sh. Ji; W. Wu; J. Shao;H. Guo and T. D. James. *J. Org. Chem.* **2011**, *76*, 7056-7064.
43. Y. Zhong; L. Si; H. He and S. G. Andrew, *RSC Advances.* **2011**, *40*, 11389–11395.
44. J. Zhao; W. Wu; J. Sun and S. Guo. *Chem. Soc. Rev.* **2013**, *42*, 532.

# APPENDIX

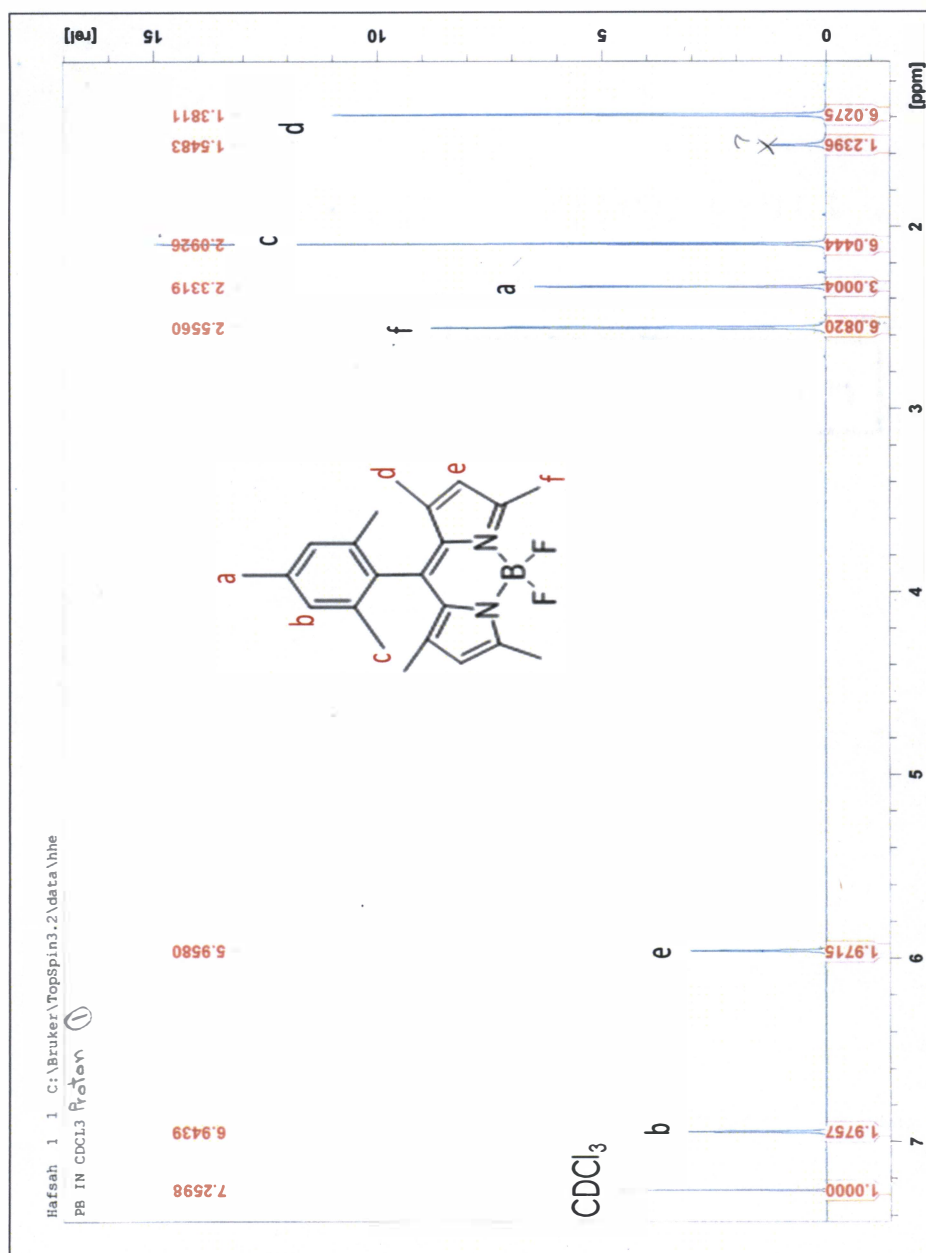


Figure 3.1. <sup>1</sup>H NMR spectrum of PB in CDCl<sub>3</sub>

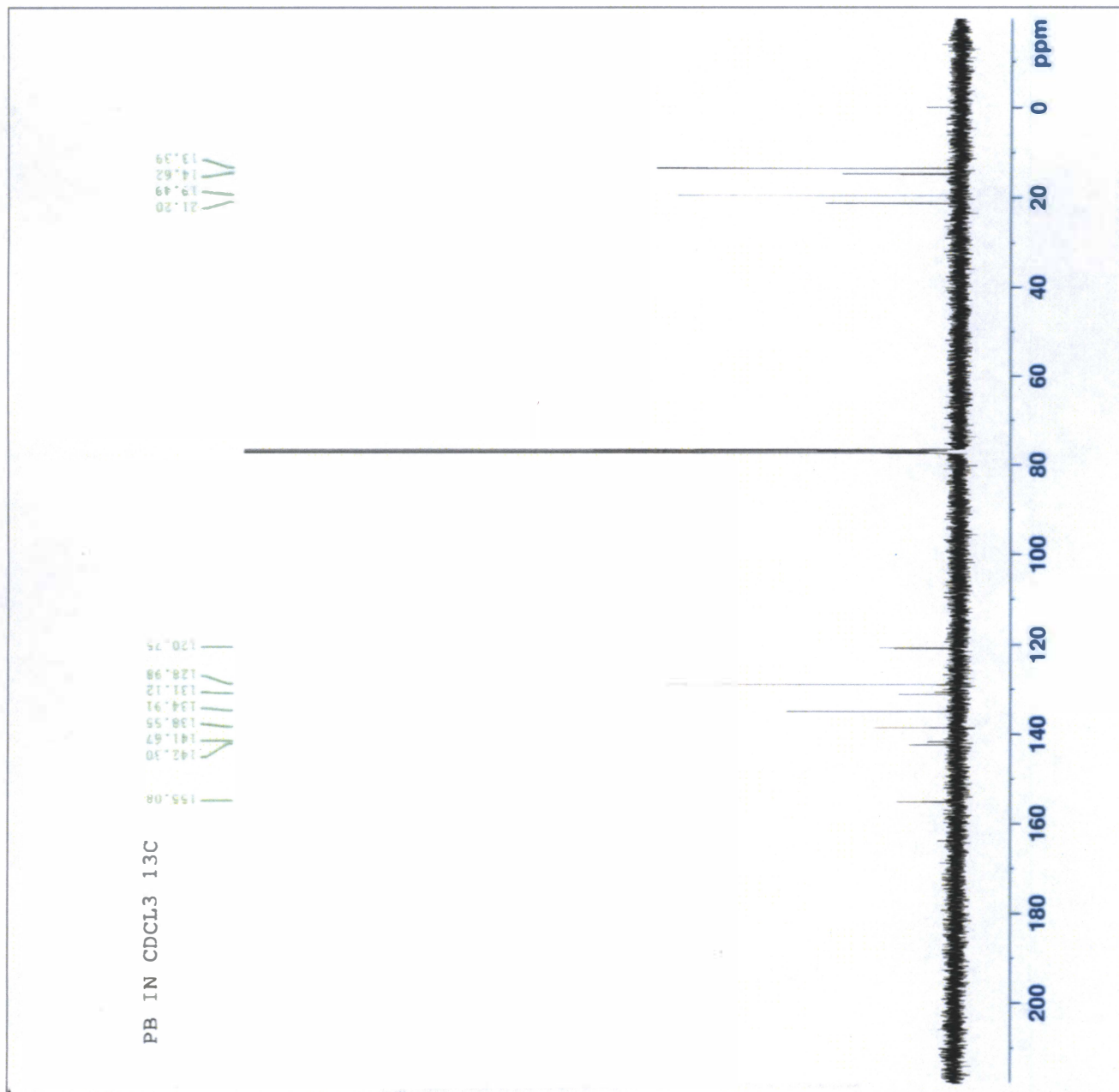


Figure 3.2. <sup>13</sup>C NMR spectrum of PB in CDCl<sub>3</sub>

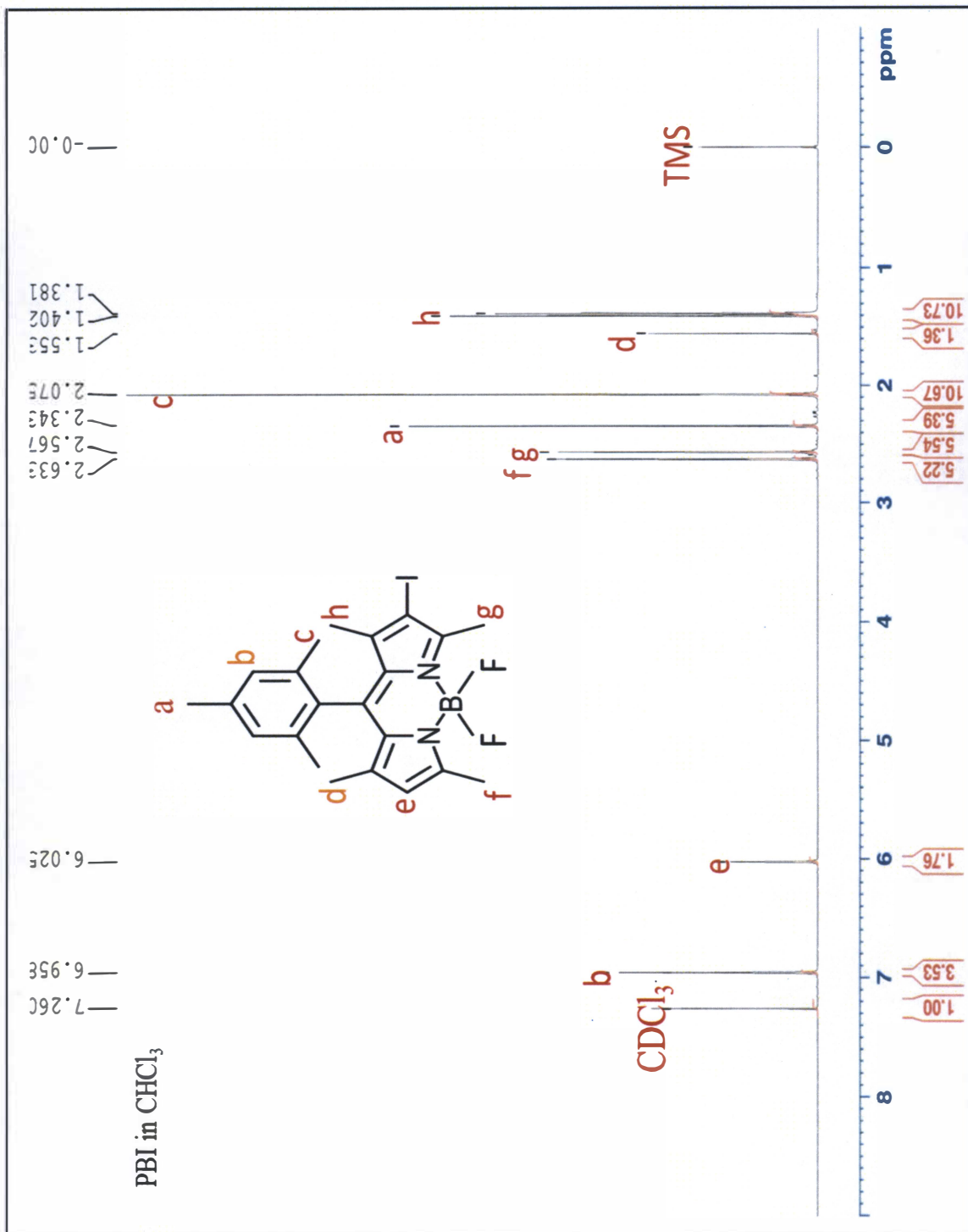


Figure 3.3. <sup>1</sup>H NMR spectrum of PBI in CDCl<sub>3</sub>

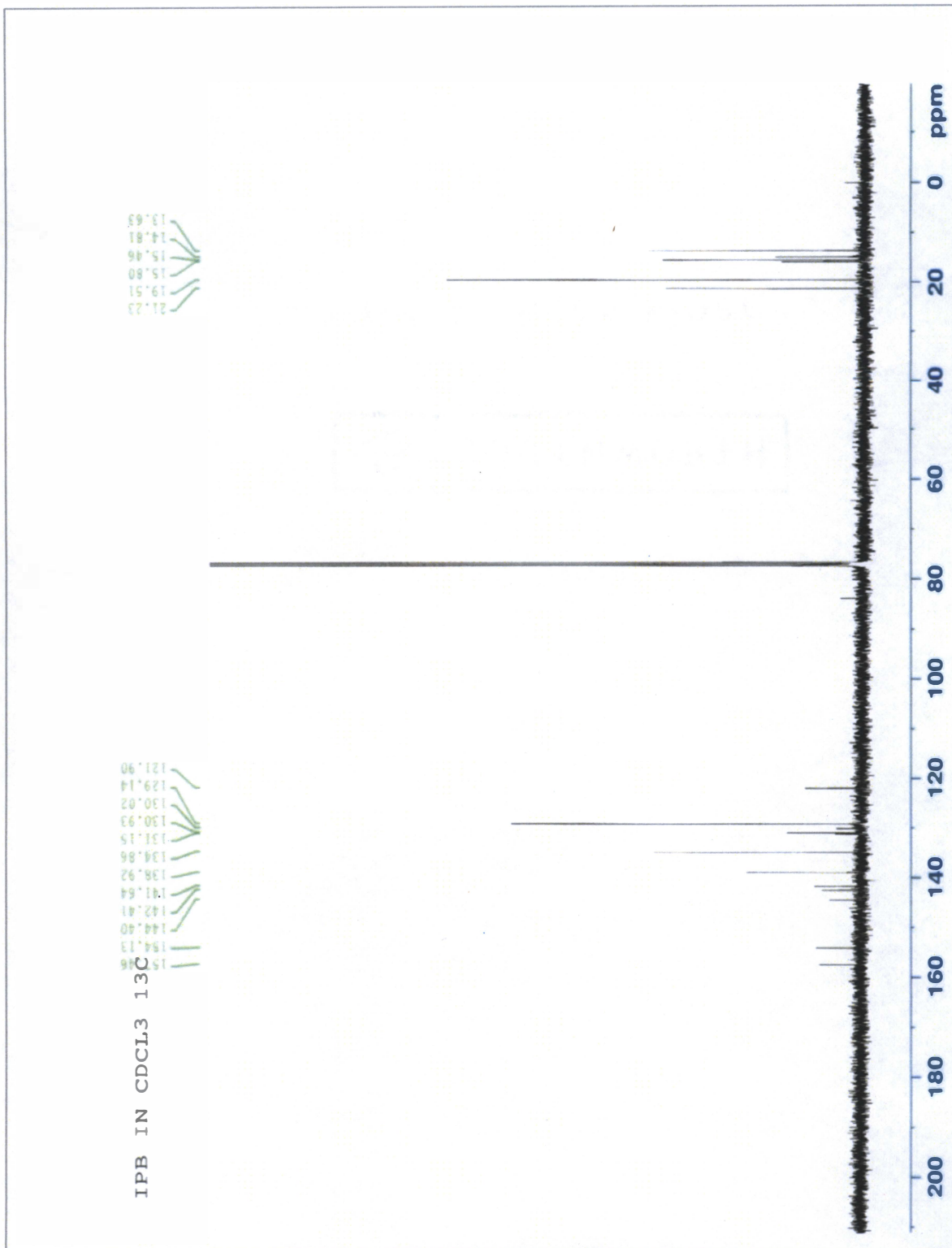


Figure 3.4.  $^{13}\text{C}$  NMR spectrum of PBI in  $\text{CDCl}_3$

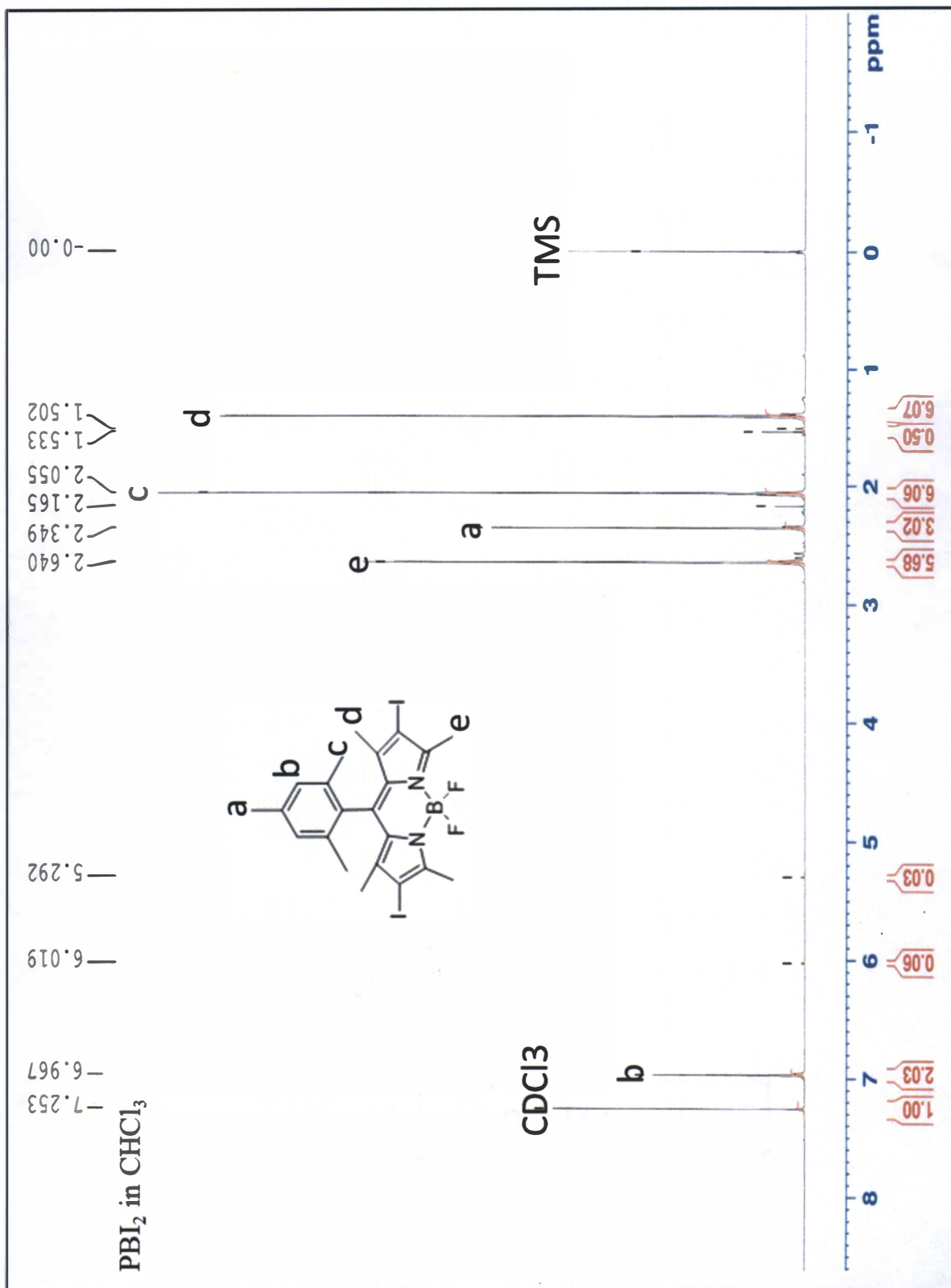


Figure 3.4. <sup>1</sup>H NMR spectrum of PBI<sub>2</sub> in CDCl<sub>3</sub>

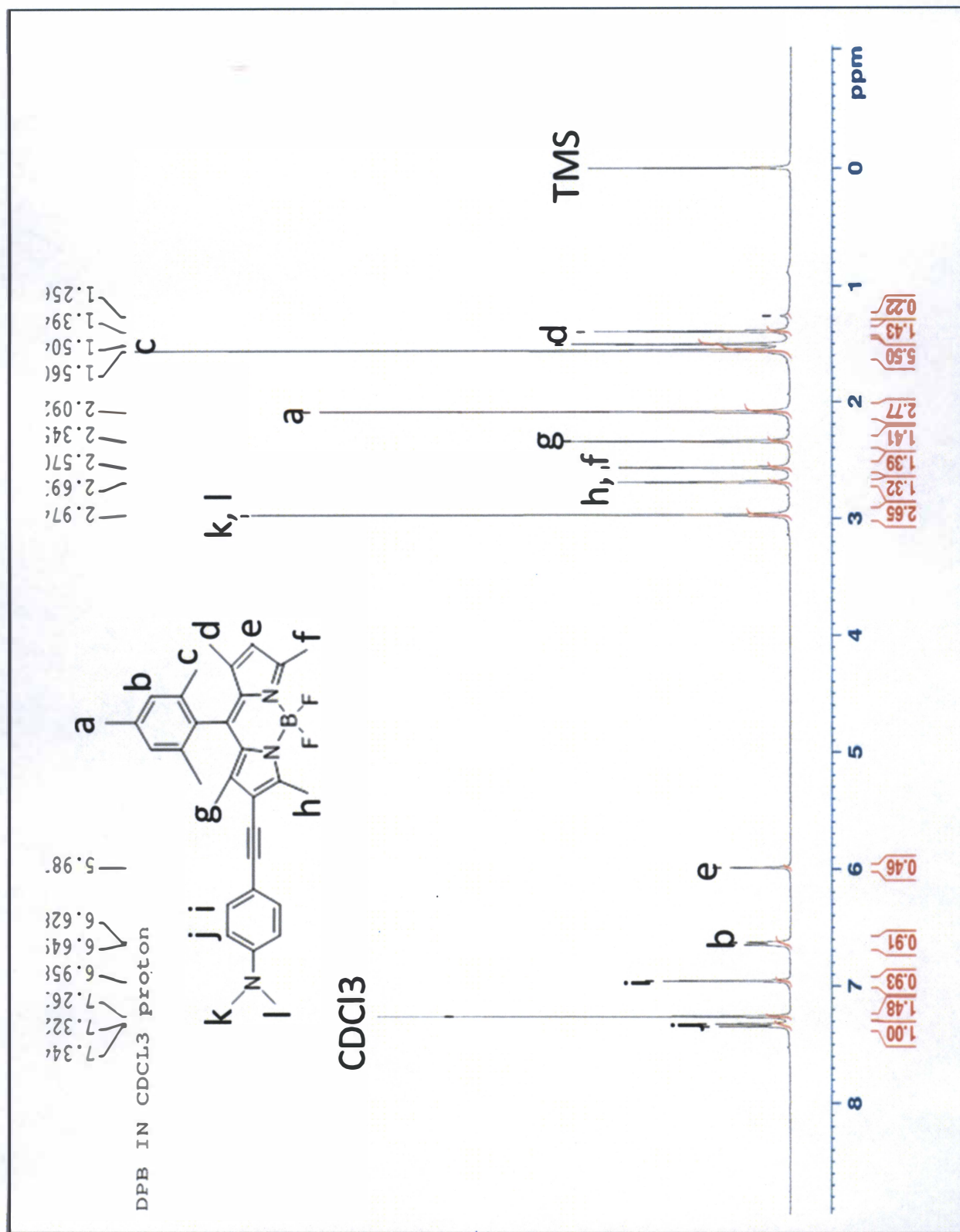


Figure 3.6. <sup>1</sup>H NMR spectrum of DPB in CDCl<sub>3</sub>



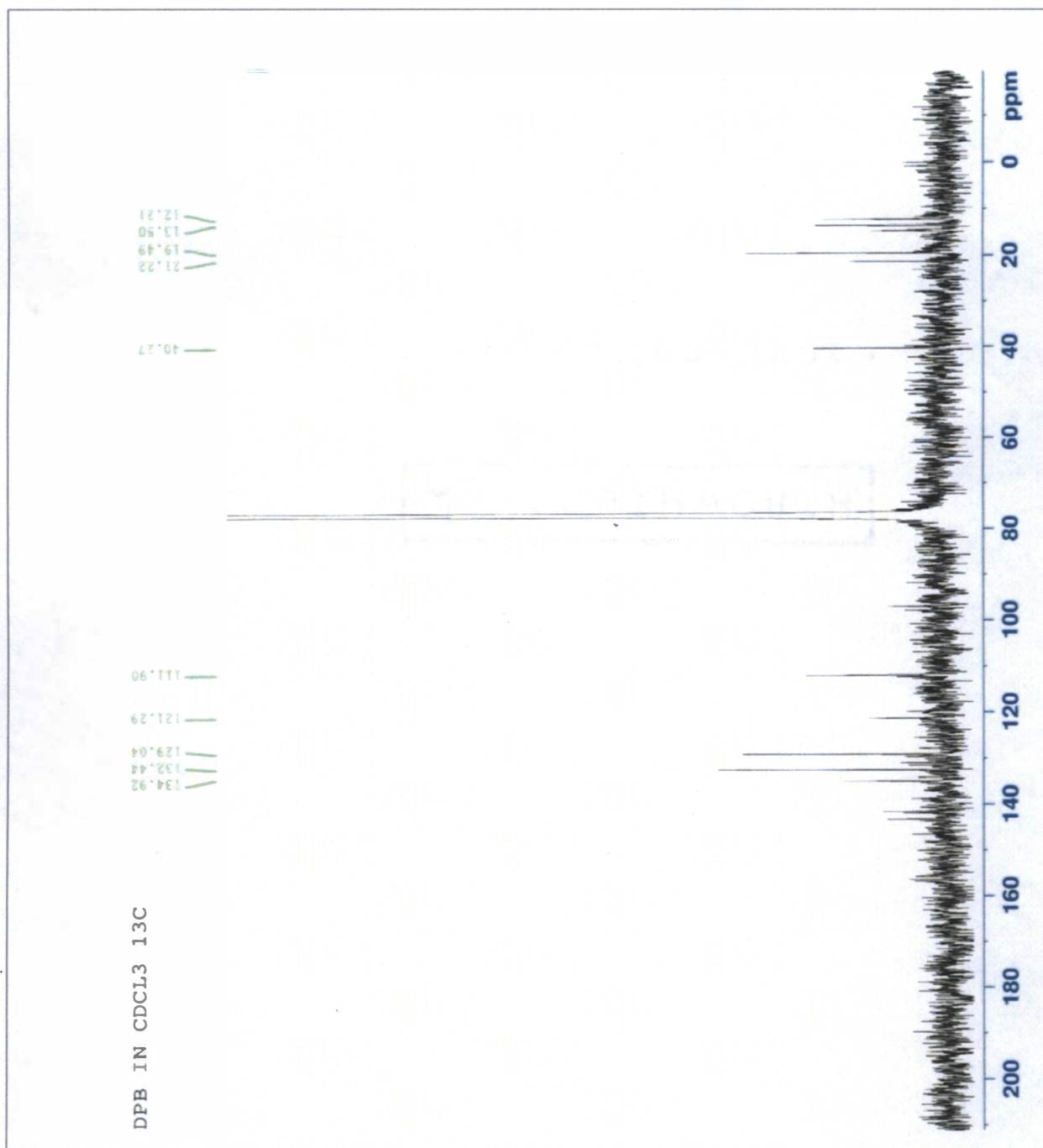


Figure 3.7.  $^{13}\text{C}$  NMR spectrum of DPB in  $\text{CDCl}_3$



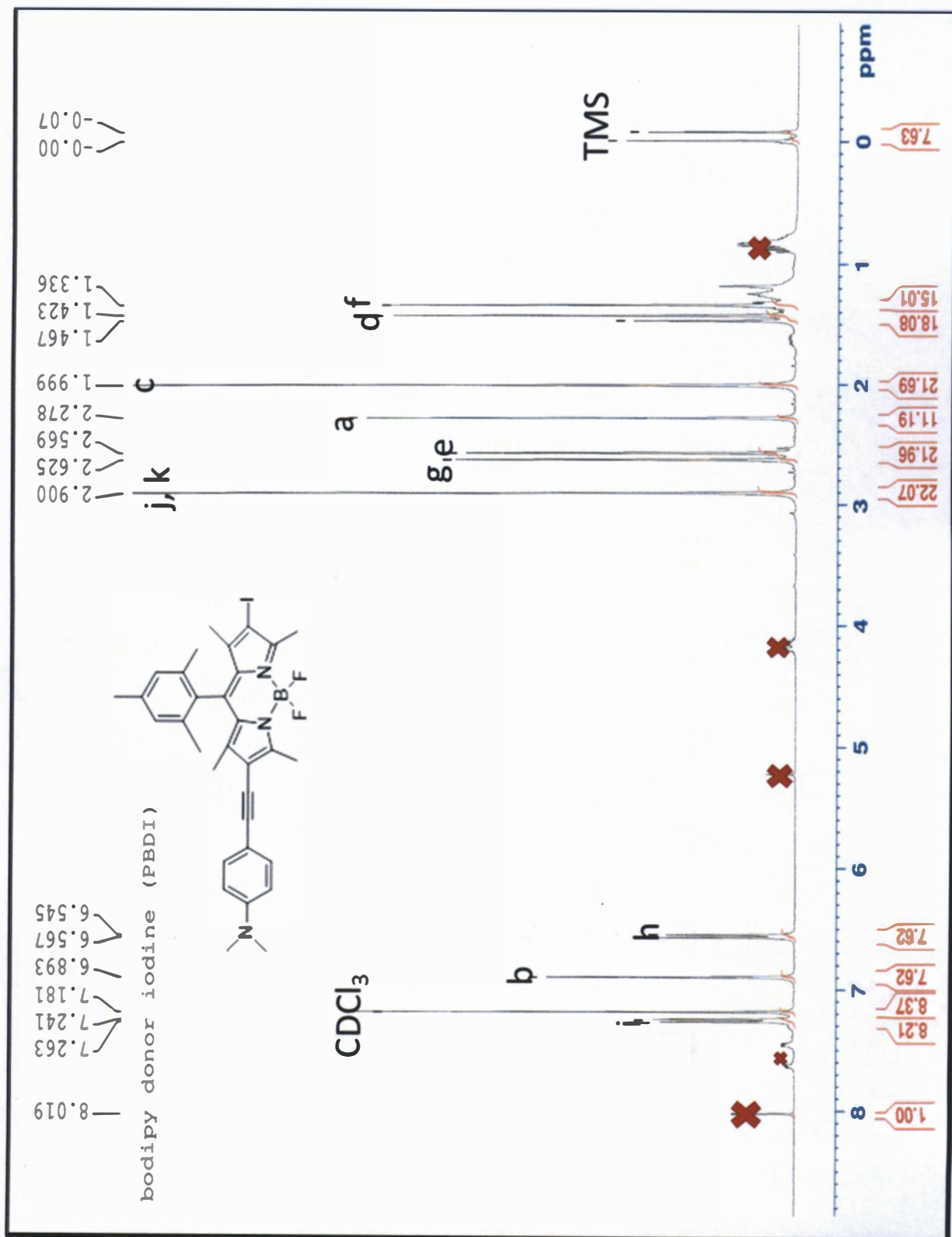


Figure 3.8. <sup>1</sup>H NMR spectrum of DPBI in CDCl<sub>3</sub>

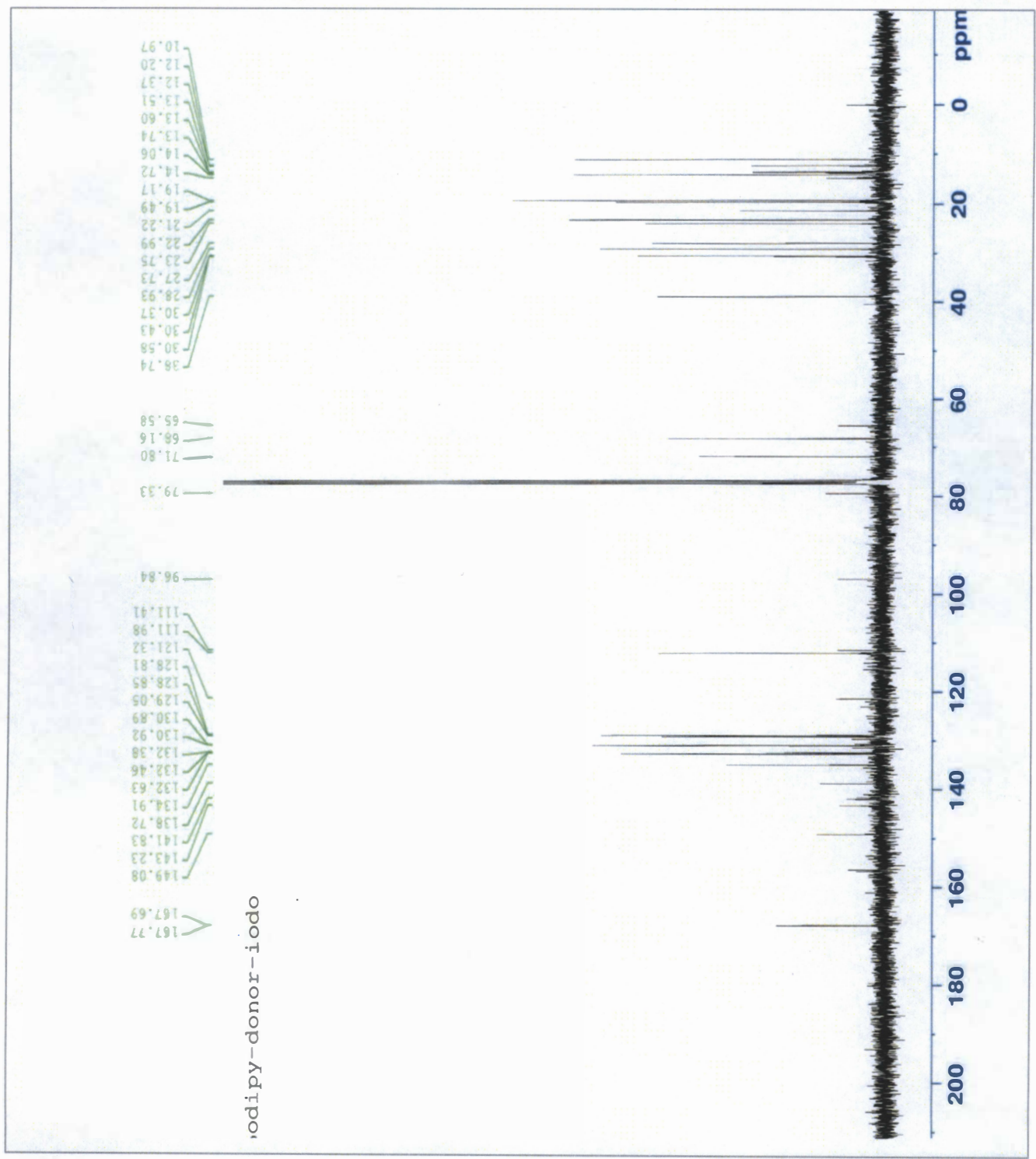


Figure 3.9. <sup>13</sup>C NMR spectrum of DPBI in CDCl<sub>3</sub>

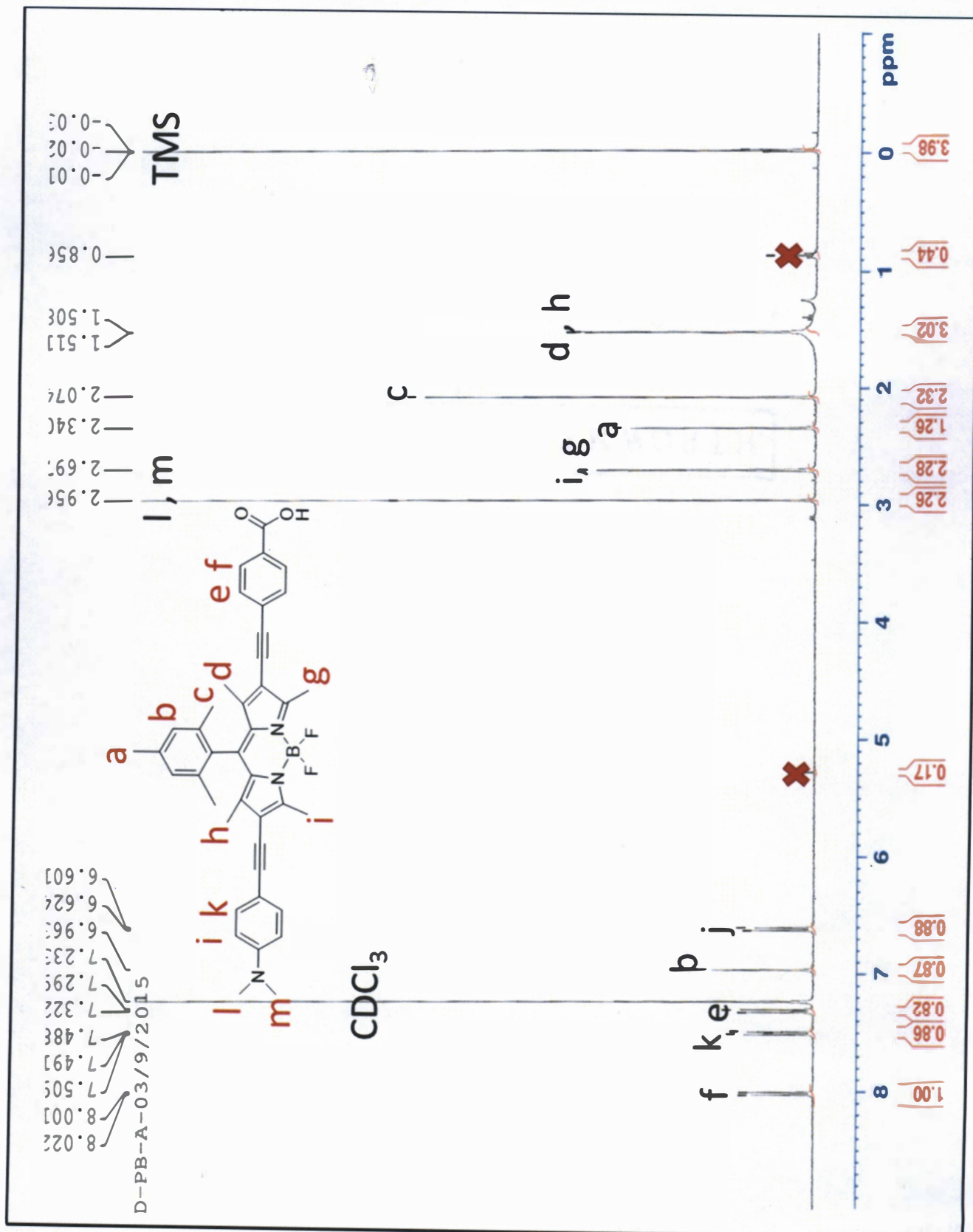


Figure 3.10. <sup>1</sup>H NMR spectrum of HHK1 in CDCl<sub>3</sub>

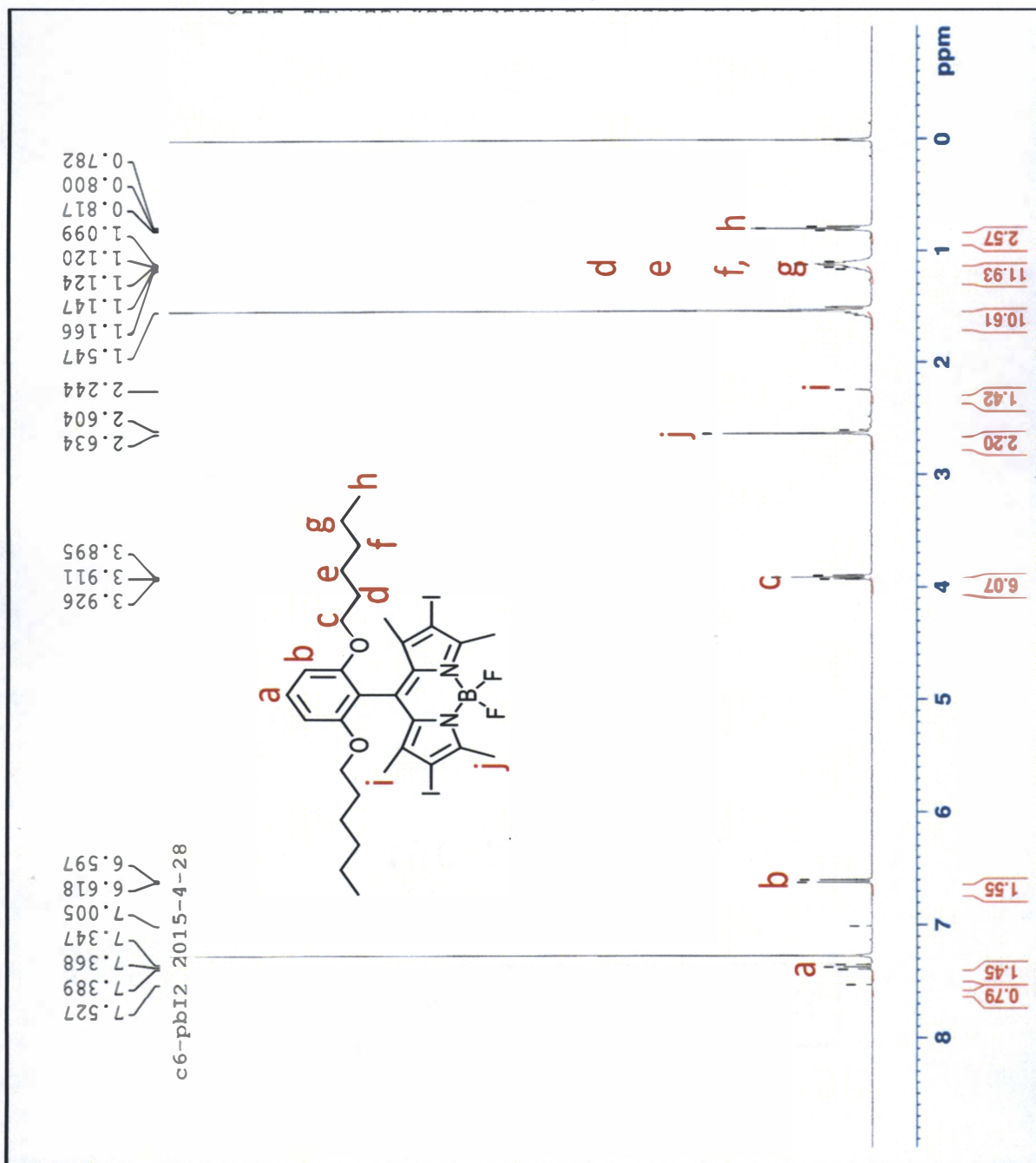
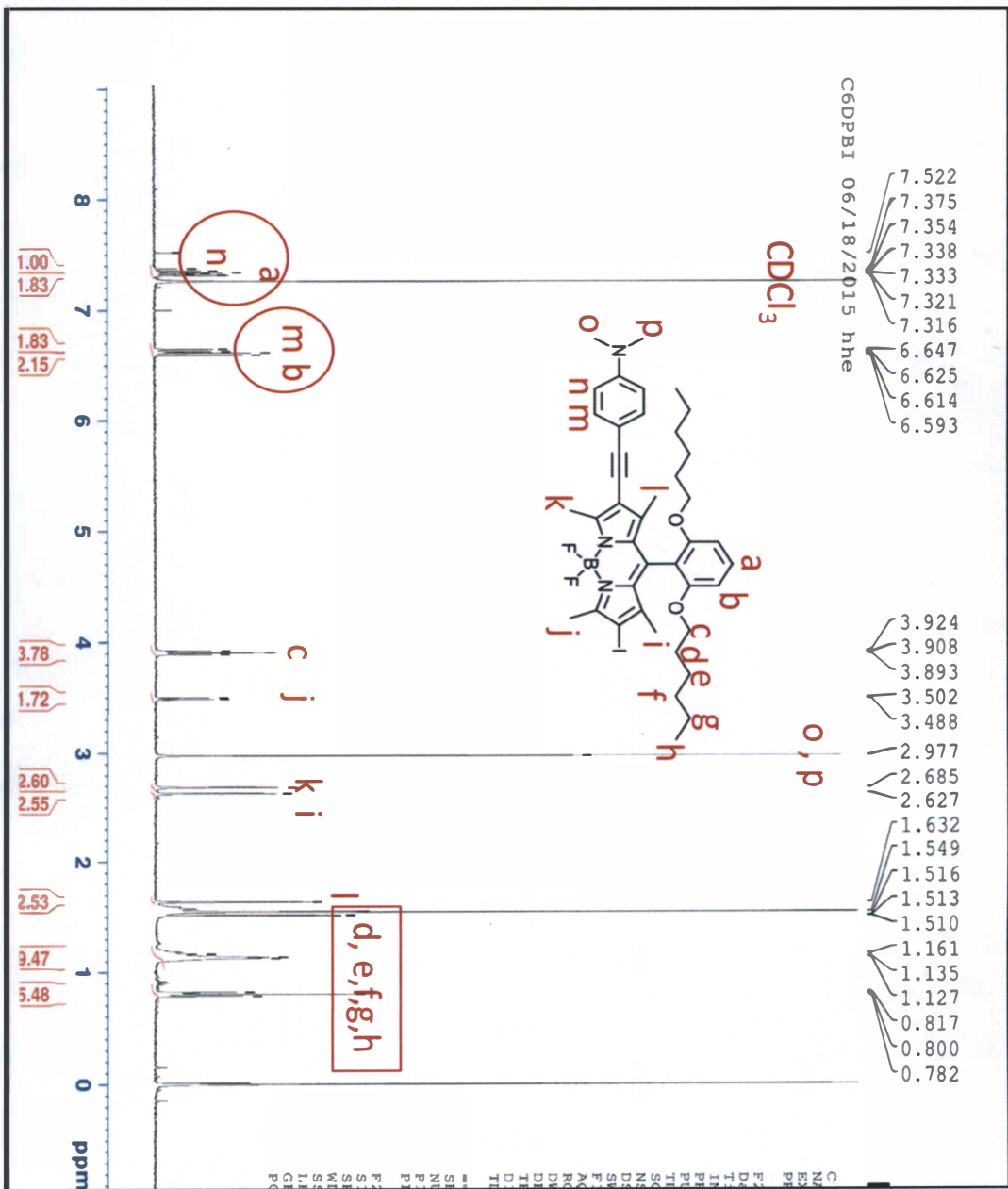


Figure 3.11. <sup>1</sup>H NMR spectrum of C<sub>6</sub>PBI<sub>2</sub> in CDCl<sub>3</sub>

Figure 3.12. <sup>1</sup>H NMR spectrum of C<sub>6</sub>DPBI in CDCl<sub>3</sub>



MSD



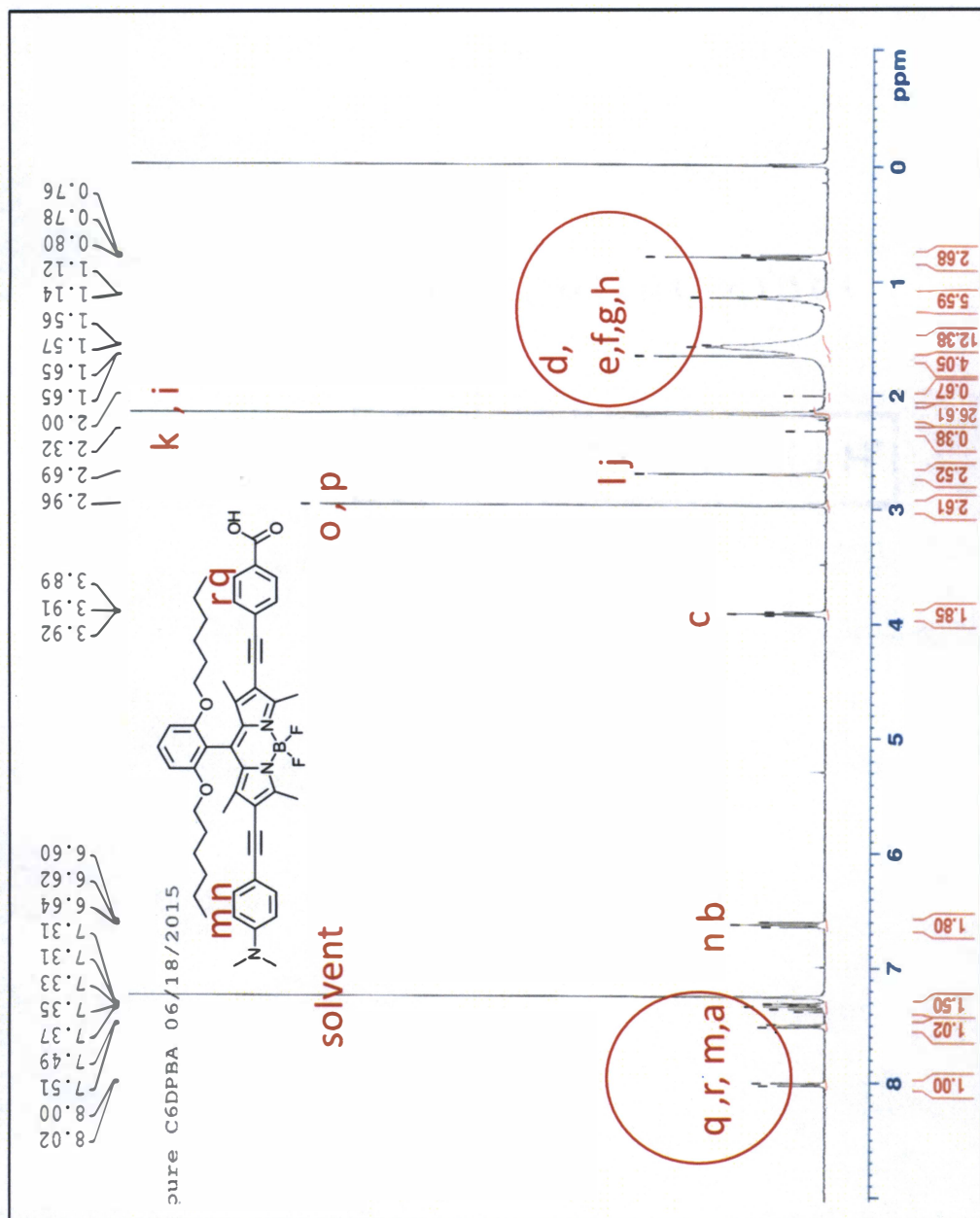


Figure 3.13.  $^1\text{H}$  NMR spectrum of HHK2 in  $\text{CDCl}_3$